Applied Physics Reviews

Bandgap engineering in III-nitrides with boron and group V elements: Toward applications in ultraviolet emitters

Cite as: Appl. Phys. Rev. **7**, 041314 (2020); https://doi.org/10.1063/5.0025371
Submitted: 14 August 2020 • Accepted: 11 November 2020 • Published Online: 09 December 2020

Robert Kudrawiec and Detlef Hommel

Applied Physics Reviews REVIEW scitation.org/journal/are

Bandgap engineering in III-nitrides with boron and group V elements: Toward applications in ultraviolet emitters

Cite as: Appl. Phys. Rev. **7**, 041314 (2020); doi: 10.1063/5.0025371
Submitted: 14 August 2020 · Accepted: 11 November 2020 ·
Published Online: 9 December 2020

Robert Kudrawiec[1,2,a)] and Detlef Hommel[1,3]

AFFILIATIONS

[1]LUKASIEWICZ Research Network, PORT Polish Center for Technology Development, Stablowicka 147, 54-066 Wroclaw, Poland
[2]Department of Semiconductor Materials Engineering, Wroclaw University of Science and Technology, Wybrzeże Wyspiańskiego 27, 50-370 Wroclaw, Poland
[3]Institute of Experimental Physics, University of Wroclaw, Pl. Maxa Borna 9, 50-204 Wroclaw, Poland

[a)]Author to whom correspondence should be addressed: robert.kudrawiec@pwr.wroc.pl

ABSTRACT

A key material system for opto- and high-power electronics are III-nitrides. Their functionality can be expanded when bandgap engineering is extended beyond common materials such as AlN, GaN, and InN. Combining these three compounds with boron nitride and other III–V compounds (GaP, GaAs, GaSb, InP, etc.) is an intuitive method of expanding bandgap engineering in semiconductor devices. This may allow improvement of current devices for which performances are limited by the intrinsic properties of common III-nitride alloys, as well as the creation of novel devices. A comprehensive review of this activity is presented in this article, including an up-to-date compilation of material parameters for wurtzite boron nitride; its alloying with other III-nitrides, including structural and optical characterization; the band anti-crossing model for III-nitrides diluted with group V atoms; their synthesis and structural and optical characterization; and examples of applications of III-nitrides containing boron and group V atoms in semiconductor devices. It is shown to be very beneficial for ultraviolet emitters to incorporate alloying of III-nitrides with BN, as these compounds have lattice constants much smaller than that of AlN, offering unique possibilities in strain engineering. It is shown that the incorporation of P, As, Sb, and Bi in GaN is low when the material is deposited at this temperature, which is optimal for the host. Lowering the growth temperature significantly enhances the incorporation of isovalent dopants, but deteriorates the optical quality of the material. The obtained changes in the electronic band structure can be beneficial in many applications, including water splitting or shifting emission toward longer wavelengths.

TABLE OF CONTENTS

I. INTRODUCTION

Over the last three decades, wurtzite (WZ) III-nitrides (III-N) have been investigated intensively, leading to a breakthrough in lighting technology.[1–3] They are currently widely used in both optoelectronic and electronic devices, such as light-emitting diodes (LEDs), laser diodes (LDs), ultraviolet (UV) detectors, solar cells, surface acoustic wave devices, high-temperature and high-frequency field-effect transistors, heterojunction bipolar transistors, etc.[4–10] However, the performances of many of these devices are still unsatisfactory for various reasons, including the poor structural quality of the epitaxial layers. In general, the quality and applicability of III-N heterostructures are closely associated with the growth conditions, underling substrate, and post-growth treatment. However, the performance of a device can be also limited by the intrinsic properties of the AlN, GaN, and InN compounds. As these intrinsic properties cannot be improved by optimization of the growth conditions, etc., other solutions, such as alloying with other III–V compounds, is needed for further development of many III-N devices.

For example, the current AlGaN UV devices cannot address urgent and severe socio-economic demands, such as disinfection of water and air, in a satisfactory manner. According to UNESCO data, over 660×10^6 people have no access to clean water. This problem can be solved using cheap UV-LEDs. To kill bacteria and viruses efficiently, a light source emitting in the range of 240–260 nm (UV-C) with an output power of >50 mW is needed. Unfortunately, the output powers of available UV-LEDs decrease dramatically when going from 360 nm (135 mW at 350 mA) down to 310 nm (15 mW at 20 mA).[11] The values obtained in the required UV-C range are as low as 0.2–2.0 at 20 mA, with external quantum efficiencies (EQEs) below 1%. In this case, an improvement in material quality is required, but it is also understood that the intrinsic properties of $Al_xGa_{1-x}N$ can strongly limit the performances of UV LEDs. Therefore, it is proposed that the necessary improvement in the intrinsic properties of III-N compounds (i.e., a broader tuning of the lattice constant, bandgap, and other properties) can be realized by including BN in the bandgap engineering. The general idea of including BN in bandgap engineering in III-N compounds has been explored for many years,[12] but no critical review on this subject can be found in the literature. Therefore, one of the aims of this review is to fill this gap. The other aim is to review existing knowledge of engineering III-N semiconductors with group V elements (P, As, Sb, and Bi) in the diluted regime. It is shown that this approach can also significantly improve the functionalities of III-N compounds and their utilization in semiconductor devices.

However, it is also worth noting that many III-N devices are very well developed and dominate the market (white LEDs, LDs operating at 405 nm, high-power transistors, etc.). Moreover, the quality of III-N heterostructures is being systematically improved and hence the performances of other III-N-based devices are becoming increasingly better. Hence, it is expected that an increasing number of semiconductor devices will be based on III-N compounds; however, the bandgap engineering within the three fundamental compounds (AlN, GaN, and InN) strongly limits the functionalities of this material system. Therefore, the further modification of III-N devices that are well developed can in many cases be associated with the bandgap engineering of III-N with B and group V elements. The present review addresses this issue as well, and is organized as follows.

Section II is devoted to III-N bandgap engineering with B, i.e., alloying BN with other III-N compounds (AlN, GaN, and InN). Initially, this alloying is motivated by the context of applications of III-N compounds in UV emitters. In addition, the different phases of BN are discussed, with particular attention given to wurtzite BN (*w*-BN). The remainder of this section is divided between specific alloys: BAlN, BGaN, BInN, and (B, Al, Ga, In)N lattices matched to AlN and GaN. In each of these subsections, theoretical predictions for a given alloy are reviewed, the applied growth methods and conditions are then discussed, and finally, studies of the structural, electrical, and optical properties of the given alloy are summarized.

Section III is devoted to III-N bandgap engineering with other group V elements. Initially, the main differences between III-N and other III–V compounds (GaP, GaAs, GaSb, etc.) are discussed and the motivation for alloying these compounds in the diluted regime is presented. Next, the general ideas of highly mismatched alloys (HMAs) and the band anticrossing model, which is able to describe the electronic band structure of HMAs, are introduced. The growth conditions and structural, electrical, and optical properties of specific alloys are subsequently reviewed and discussed in separate subsections.

The application of the discussed alloys in semiconductor devices is reviewed in Sec. IV. Section V summarizes this paper and suggests further perspectives for bandgap engineering in III-N with B and group V elements.

II. (B, III)-N

As mentioned previously, the combination of III-N (AlN, GaN, and InN) with BN is mainly motivated by the application of (B, III)N alloys in UV emitters. Further development of the current LEDs and LDs operating in the short-wavelength region is very challenging due to the serious limitations of their component materials, which are difficult to solve for the current (Al, Ga)N ternary system. The most significant limitations, and thus challenges, of UV emitters appear to be

(i) Inefficient light extraction from LEDs operating in the UV-C range due to the dominant transverse magnetic (TM) polarization instead of the desired transverse electric (TE) polarization for Al-rich AlGaN quantum wells (QWs) grown along the c-axis;
(ii) Inefficient carrier injection into the active region, which is related to doping problems for a high Al content in general, and p-type doping in particular, as well as transparent p-type electric contacts with low resistance;
(iii) Non-radiative recombination and inefficient heat dissipation, associated with high concentration of threading dislocations and point defects.

A proper solution to these problems is critical for the further development of UV LEDs and LDs, to enable their advantages to be applied to practical use. In our opinion, this will be difficult, if not impossible, for the "classical" III-N, i.e., (Al, Ga, In)N alloys. The scale of the problem can be illustrated by the fact that, despite the many prospective applications and potential market for UV LEDs and LDs, no breakthroughs in the field of LEDs operating in the UV-C and LDs operating in the UV-B and UV-C ranges have been reported in recent years.[12] From reviewing and analyzing papers in this area, the main problem appears to lie in the fundamental limits of (Al, Ga)N heterostructures. Therefore, it is obvious that further development of LEDs and LDs operating in the deeper UV range will require novel material solutions.

Considering the relationship between band gaps and lattice constants (see Fig. 1), adding *w*-BN to well-developed III-N semiconductors (AlN, GaN, and their combinations) appears to be a good approach to improve the functionality of the III-N compounds for deep-UV emitters. However, this approach has not yet been extensively explored, as the growth of *w*-B(Al)N structures is very challenging. Therefore, the existing data for alloys/heterostructures composed of these elements are predominantly theoretical.[13–35] To date, only a few publications have described experimental approaches to grow *w*-B(Al)N structures.[36–63] Both theoretical and experimental studies are discussed later in this article. Based on these reports, it is rather obvious that *w*-B(Al)N structures can be the future of UV emitters, and that further work could finally result in a breakthrough in this newly emerging field.

Regarding LEDs and LDs operating in the visible range, and other devices containing GaN-rich alloys, a B incorporation in such structures also appears very interesting because of bandgap engineering in a broader spectral range. For example, the built-in strain in InGaN QWs grown on a GaN substrate limits the tuning of emission wavelengths, and therefore it is difficult to achieve red emission from such QWs. The incorporation of B in GaInN QWs reduces the built-in strain and thereby can shift emission to longer wavelengths, as shown in Fig. 1. However, the growth of high-quality BGaInN/GaN QWs can be a challenge because of difficulties in incorporating B into the GaInN host. To summarize, there is strong motivation for alloying III-N with BN, but the growth of high-quality (B, III)N alloys is not a simple task because of the different phases of BN and significant mismatch between the lattice constant of *w*-BN and those of the remaining III-N compounds.

A. Boron nitride

B and N, the neighbors of C in the periodic table (see Fig. 1), form BN compounds, which are isoelectronic and isostructural to the polymorphs of C. Graphite-like sp^2-bonded hexagonal BN (α-BN,

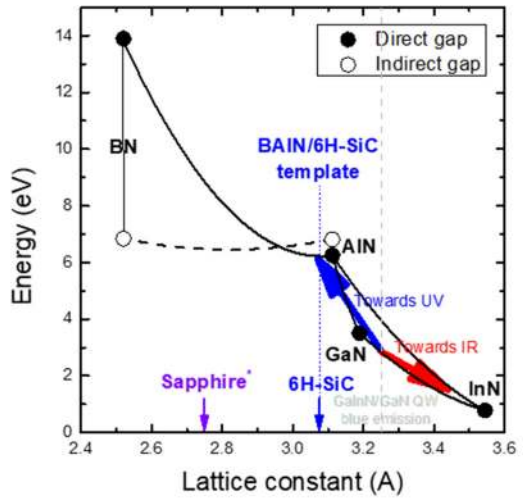

III	IV	V
B 2.04	C 2.55	N 3.04
Al 1.61	Si 1.90	P 2.19
Ga 1.81	Ge 2.01	As 2.18
In 1.78	Sn 1.96	Sb 2.05
Ti 1.62	Pb 2.33	Bi 2.02

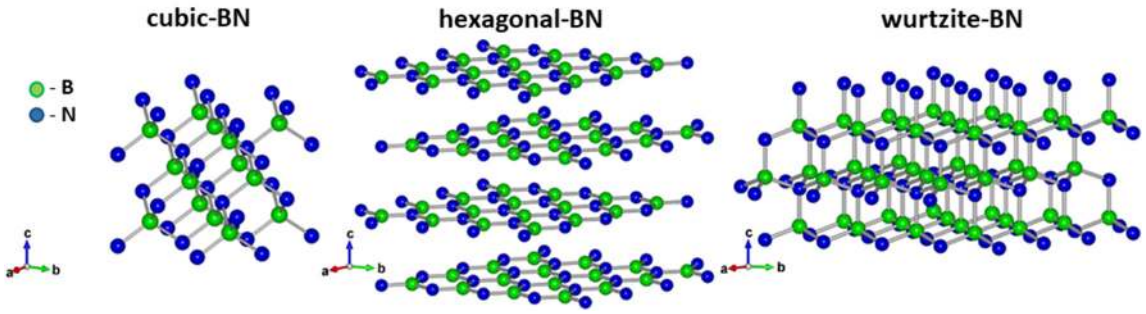

FIG. 1. Relation between the bandgap and the lattice constant for WZ III-N semiconductors. Fragment of the periodic table with electronegativity of atoms. Atom arrangement in cubic, hexagonal, and *w*-BN.

usually called *h*-BN) is a soft material, whereas the diamond-like sp^3-bonded phase is hard cubic BN [β-BN, usually called *c*-BN, which is a zinc blende (ZB) semiconductor]. Both *h*-BN and *c*-BN are stable forms of BN. The metastable sp^3-bonded modification of BN is *w*-BN, which is the focus of this review. The atom configurations in the three phases of BN are shown in Fig. 1. In addition to the three phases, BN can also be present in the forms of amorphous (*a*-BN), turbostratic (*t*-BN), and rhombohedral (*r*-BN) phases.[64–66] To date, BN has been the subject of only a few review papers,[67–70] one of which is devoted to *w*-BN.[67] In this subsection, only the *w*-BN phase is discussed as it is the complementary compound for alloying with WZ AlN, GaN, and InN.

The phase diagram of BN is shown in Fig. 2. According to this diagram, a *w*-BN crystal cannot be obtained under the equilibrium growth conditions, and therefore, *w*-BN crystals are difficult to fabricate using common growth methods close to thermodynamic equilibrium. However, it is surely worth attempting a method to grow *w*-BN crystals under non-equilibrium growth conditions (e.g., by epitaxial methods).

Figure 3 shows the calculated total energy per BN molecule as a function of volume for three phases of BN: *c*-BN, *h*-BN, and *w*-BN.[13] It is clearly visible that the energy difference between the cubic and WZ phases is not very large. When BN is grown epitaxially on a proper WZ substrate (AlN or SiC), the substrate is expected to force the hexagonal phase to grow. In contrast, the cubic phase is more favorable from the perspective of total energy per BN molecule; see Fig. 3. Therefore, competition between the two phases can be expected in the epitaxial growth of BN on AlN or SiC. This competition can be tuned by the growth conditions, and this is a very interesting topic to explore. Considering the above arguments, the growth of *w*-BN on AlN and SiC holds great prospects.

To date, the growth of *w*-BN has only been reported in a few papers,[36–40,56,57,61] but macro crystals of *w*-BN were realized for the first time quite recently by Deura *et al.*[56] These crystals were obtained by direct conversion of *h*-BN bulk crystals, which were grown for

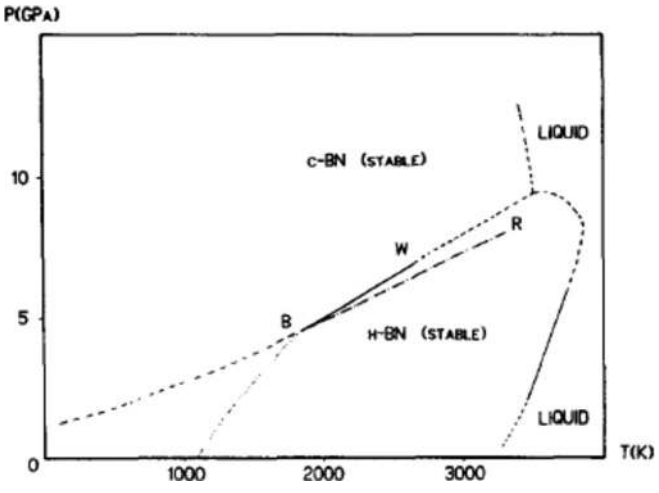

FIG. 2. Phase diagram of BN: B–W, Bundy–Wentorf equilibrium line;[71,72] B–R, equilibrium line corrected by Rapoport;[73] —, extrapolated equilibrium lines; ·····, and equilibrium line from thermodynamic calculations.[71,74] Reproduced with permission from Vel *et al.*, Mater. Sci. Eng. B **10**, 149 (1991). Copyright 1991 Elsevier.

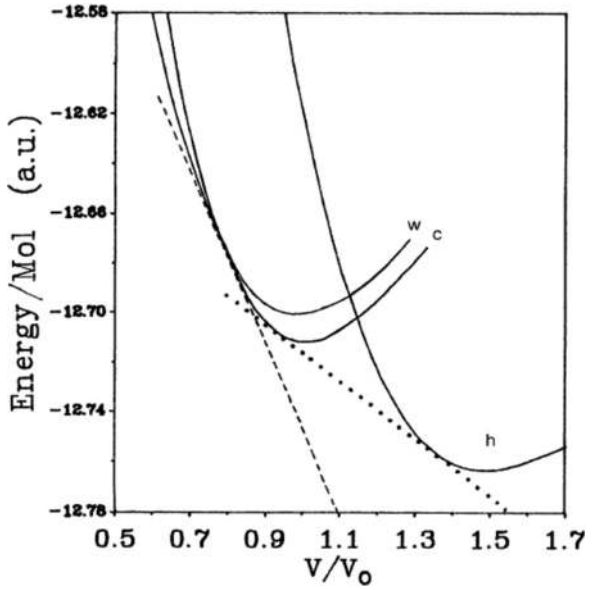

FIG. 3. Calculated total energy per BN molecule as a function of volume for three phases of BN: (c) cubic, (h) hexagonal, and (w) wurtzite. V_0 is the measured equilibrium volume of cubic BN. The dashed line shows the possible transition from *c*-BN to *w*-BN, and the dotted line shows the possible transition from *h*-BN to *c*-BN. Reproduced with permission from Y.-N. Xu and W. Y. Ching, Phys. Rev. B **44**, 7787 (1991). Copyright 1991 American Physical Society.

50–100 h at 1500 °C and 4 GPa by the temperature gradient method. In the conversion process, *h*-BN crystals were contained in CsCl powder and compressed at a pressure of 10 GPa uniaxial to the *c*-axis at 850 °C using high-pressure apparatus. Thus, *h*-BN was directly converted to *w*-BN by diffusionless transformation. A *w*-BN crystal obtained in this way is shown in Fig. 4.

Synthesis of such macro *w*-BN crystals allowed the study of the hardness and Young's modulus of *w*-BN, which were simultaneously determined to be 54 ± 2 and 860 ± 40 GPa, respectively.[56] Figure 5 shows a comparison of the hardness and Young's modulus determined for *w*-BN with different WZ III-N.

Due to the lack of access to *w*-BN crystals, experimental studies of their properties are limited to a few papers[56,60] and no reports on measurements of the bandgap or many other material parameters can

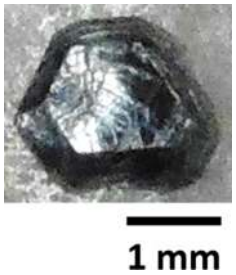

FIG. 4. Appearance of an as-synthesized *w*-BN crystal. Reproduced with permission from Deura *et al.*, Jpn. J. Appl. Phys., Part I **56**, 030301 (2017). Copyright 2017 The Japan Society of Applied Physics.

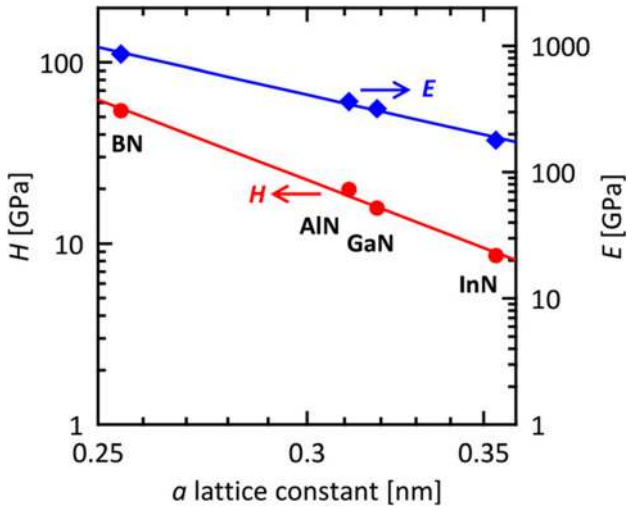

FIG. 5. Relationships between the *a* lattice constant and the hardness (*H*) and Young's modulus (*E*) of WZ-type group-III nitrides. Both the lateral and vertical axes are expressed in logarithmic scales. The points and lines indicate the experimental data and the fitting results, respectively. Reproduced with permission from Deura *et al.*, Jpn. J. Appl. Phys., Part I **56**, 030301 (2017). Copyright 2017 The Japan Society of Applied Physics.

be found in the literature. However, the electronic band structure and mechanical properties of this compound have been quite intensively studied within density functional theory (DFT).[14–28] A summary of the material parameters derived both experimentally and theoretically is given in Table I, together with the parameters of the other III-N.[75,76] In addition, proper parameters are plotted in Figs. 6–11 for the four III-N compounds to show chemical trends and evaluate the reliability of the parameters reported for *w*-BN so far and recommended in this review.

The lattice constants (*a* and *c*), bulk modulus, and its pressure derivative reported in the literature are very similar (see Table I). Therefore, average values of these parameters are recommended by this review as a first approximation. The bulk modulus (*B*) and its pressure derivative (*B′*), similar to the hardness and Young's modulus, are mechanical properties, with a clear chemical trend when plotted vs the lattice constant (Fig. 6).

Regarding the bandgap, the average values reported so far for BN are not a suitable approach as it is well known that some DFT methods significantly overestimate the bandgap. Therefore, experimental bandgap values are necessary in this case, but unfortunately they have not been reported so far. Considering the applied DFT method as well as the functional in Refs. 14, 20–22, 24, 26, and 28, the most appropriate bandgap appears to be the one reported in Ref. 28, and therefore this value is recommended here. Unfortunately, the splitting parameters related to the crystal field interaction (Δ_{cr}) and spin–orbit interaction (Δ_{so}) were not reported in Ref. 28, and therefore the Δ_{cr} from Ref. 16 is recommended in this article, as well as any value of the Δ_{so} parameter because there are no previous reports on this topic. The same applies to the A_1–A_6 parameters, which are necessary to determine the hole effective mass, and the a_1 and a_2 parameters, which are the deformation potentials for the conduction-band (CB). The deformation potentials D_1–D_6, which describe the valence band, were reported in Ref. 16 and are recommended after this work except for the D_6 parameter, which was not reported therein. The extrapolation of the missing parameters based on knowledge of the parameters of other III-N materials is not a good approximation in this case, because they are parameters related to the electronic band structure and not the mechanical properties. For III-N alloys diluted with B, it is instead recommended to use the host parameters if the proper ones for BN are unknown.

Regarding the electron effective masses ($m_e^{\perp}$ and $m_e^{||}$, which are perpendicular and parallel to the *c*-axis, respectively), the average values are recommended in Table I. The general tendency observed in semiconductors is an increase in the effective mass with increasing bandgap.[75,77] The relationship between electron effective mass and lattice constant for III-N is plotted in Fig. 7. The previously mentioned trend is present in this case, but this issue requires more careful exploration as BN is an indirect-gap semiconductor.

The elastic constants (c_{11}–c_{66}) were studied for BN in a few papers.[15,16,19,23,60] These constants, similar to the previously discussed bulk modulus and other mechanical parameters, exhibit a chemical trend when they are plotted vs the lattice constant; see Fig. 6. The average values of the parameters reported in Refs. 15, 16, 19, 23, and 60 are recommended in this review.

The piezoelectric constants (e_{33} and e_{31}) and spontaneous polarization (P_{SP}) were the subject of several papers for both BN[16,17,24,27] and the other III-N compounds. Considering the recent paper on the correct implementation of polarization constants in WZ materials and their impact on III-N (see Ref. 76), the recommended e_{33}, e_{31}, and P_{SP} parameters for BN and the other III-N are those taken from Refs. 27 and 76, respectively.

The static dielectric constant (ε_0) was reported for BN in Refs. 14 and 25. An average value of previously reported ε_0 is recommended here.

B. BAlN

The standard formula for the interpolation of a certain parameter α in ternary alloys is given by Eq. (1):

$$\alpha^{A_xB_{1-x}C} = x\alpha^{AC} + (1-x)\alpha^{BC} - b_\alpha x(1-x), \quad (1)$$

where α^{AC} and α^{BC} are the parameters of the binary AC and BC compounds, respectively, and b_α is the bowing parameter, which describes the deviation from the linear interpolation for the α parameter.

The structural and electronic properties of *w*-BAlN in the whole range of B concentration have been studied using DFT methods.[26–28] It has been observed that the lattice constant changes with the content, as shown in Fig. 9 (solid points). It is worth noting that for many alloys this relationship is described by a linear interpolation, shown as dashed lines in Fig. 9. For BAlN, some deviations from the linear dependence are clearly visible, and therefore Liu *et al.*, have interpolated these data using a second-order polynomial fitting and determined the proper coefficients in the polynomial.

The lattice constants of $B_xAl_{1-x}N$ determined by Liu *et al.*,[27] and written according to nomenclature given by Eq. (1), are listed below:

$$a^{B_xAl_{1-x}N} = x2.544 + (1-x)3.109 - 0.157x(1-x)\ (\text{Å}), \quad (2)$$

$$c^{B_xAl_{1-x}N} = x4.400 + (1-x)5.186 + 0.119x(1-x)\ (\text{Å}). \quad (3)$$

TABLE I. Material parameters for WZ BN, AlN, GaN, and InN. Parameters for AlN, GaN, and InN without references are taken from Ref. 75.

	BN				
Parameter	Recommended value	Range	AlN	GaN	InN
a (Å) at $T = 300$ K	2.54	2.54,[15] 2.534,[16] 2.525,[18] 2.557,[18] 2.525,[21] 2.556,[21] 2.532,[22] 2.558,[23] 2.500,[25] 2.52,[28] 2.53,[31] 2.553,[36] 2.549,[49] 2.550,[60] 2.55[66]	3.112	3.189	3.545
c (Å) at $T = 300$ K	4.20	4.17,[15] 4.191,[16] 4.192,[18] 4.251,[18] 4.182,[21] 4.234,[21] 4.189,[22] 4.228,[23] 4.169,[25] 4.17,[28] 4.15,[31] 4.228,[36] 4.223,[49] 4.200,[60] 4.17[66]	4.982	5.185	5.703
Bulk modulus B (GPa)	395	391,[14] 397,[15] 401,[16] 408,[18] 366,[18] 395,[20] 403,[23] 394,[25] 400[60]	220[14]	200[14]	125[14]
B pressure derivative B'	3.6	3.7,[14] 3.7,[15] 3.2,[18] 3.7,[18] 3.5,[20] 3.8,[23] 3.6,[24] 3.5[60]	3.9[14]	3.8[14]	8.1[14]
$E_g(\Gamma\rightarrow\Gamma)$ (eV) at 0 K	13.90	8.52,[14] 8.30,[20] 10.2,[26] 13.90[28]	6.18,[28] 6.25	3.510	0.78
$E_g(\Gamma\rightarrow K)$ (eV) at 0 K	6.84	5.44,[14] 7.70,[20] 6.39,[21] 6.86,[22] 6.46,[24] 6.8,[26] 6.84[28]	6.82[28]	6.6[28]	
Δ_{so} (eV)	NA	NA	0.019	0.017	0.005
Δ_{cr} (eV)	0.333	0.333[16]	−0.169	0.010	0.040
$m_e^{\perp}$	0.44	0.35,[13] 0.52[53]	0.32	0.20	0.07
$m_e^{\parallel}$	0.29	0.24,[13] 0.33[53]	0.30	0.20	0.07
A_1	NA	NA	−3.86	−7.21	−8.21
A_2	NA	NA	−0.25	−0.44	−0.68
A_3	NA	NA	3.58	6.68	7.57
A_4	NA	NA	−1.32	−3.46	−5.23
A_5	NA	NA	−1.47	−3.40	−5.11
A_6	NA	NA	−1.64	−4.90	−5.96
a_1 (eV)	NA	NA	−3.4	−4.9	−3.5
a_2 (eV)	NA	NA	−11.8	−11.3	−3.5
D_1 (eV)	−19.2	−19.2[16]	−17.1	−3.7	−3.7
D_2 (eV)	−14.0	−14.0[16]	7.9	4.5	4.5
D_3 (eV)	3.90	3.90[16]	8.8	8.2	8.2
D_4 (eV)	−3.32	−3.32[16]	−3.9	−4.1	−4.1
D_5 (eV)	−4.30	−4.30[16]	−3.4	−4.0	−4.0
D_6 (eV)	NA	NA	−3.4	−5.5	−5.5
c_{11} (GPa)	904	987,[15] 982,[16] 955,[19] 782,[23] 816[60]	396	390	223
c_{12} (GPa)	157	143,[15] 134,[16] 143,[19] 167,[23] 200[60]	137	145	115
c_{13} (GPa)	100	70,[15] 74,[16] 79,[19] 177[60]	108	106	92
c_{33} (GPa)	995	1020,[15] 1077,[16] 1019,[19] 863[60]	382,[15] 383,[16] 470[19]	392,[15] 376,[16] 470[19]	200,[15] 300[19]
c_{44} (GPa)	327	369,[15] 388,[16] 357,[19] 307,[23] 212[60]	373	398	224
c_{66} (GPa)	389	422,[15] 424,[16] 320[60]	129,[15] 128[16]	126,[15] 115[16]	74[15]
e_{31} (C/m^2)	0.3	0.27,[16] 0.3,[17] 0.28,[24] 0.3[27]	−0.676,[76] −0.63[27]	−0.551,[76] −0.35[27]	−0.604[76]
e_{33} (C/m^2)	−0.9	−0.85,[16] −0.9,[17] −1.07,[24] −0.9[27]	1.567,[76] 1.6[27]	1.020,[76] 0.5[27]	1.238[76]
P_{SP} (C/m^2)	2.12	2.12[27]	1.351[76]	1.312[76]	1.026[76]
Static dielectric constant ε_0	4.8	4.14,[14] 5.37[25]	3.86[14]	4.68,[14] 6.15[25]	7.16[14]

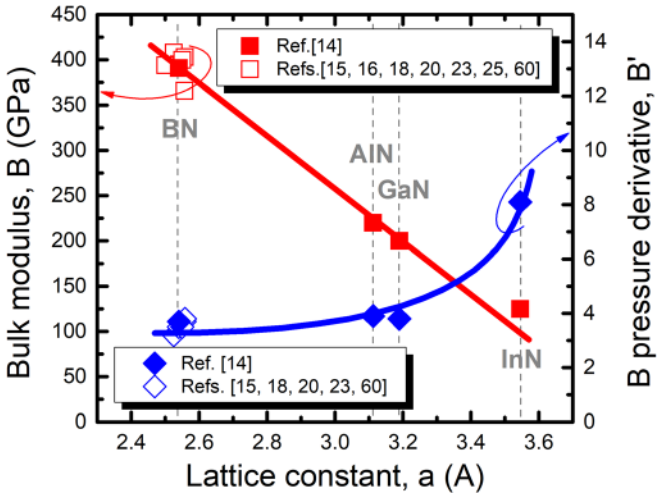

FIG. 6. Relationships between the *a* lattice constant and the bulk modulus *B* and its pressure derivative *B*′.

The obtained bowing parameters ($b_a = 0.157$ Å and $b_c = -0.119$ Å) are quite significant and cannot be neglected when the lattice constant for BAlN has to be estimated.

The bandgap of BAlN has been calculated by Shen *et al.*[28] Figure 10 shows the electronic band structure of WZ AlN and BN. The fundamental direct (AlN) and indirect (BN) transition are marked by arrows, and the orbital contribution to the states in the band structure is illustrated by a distinct color: yellow for *s* states and purple for *p* states. For BN, the *s*-like band is located 13.9 eV above the top of the valence band, whereas for AlN, the conduction-band minimum has *s*-like character. Besides the indirect character of bandgap, this is a very important difference between the electronic band structure of BN and those of the other III-N compounds.

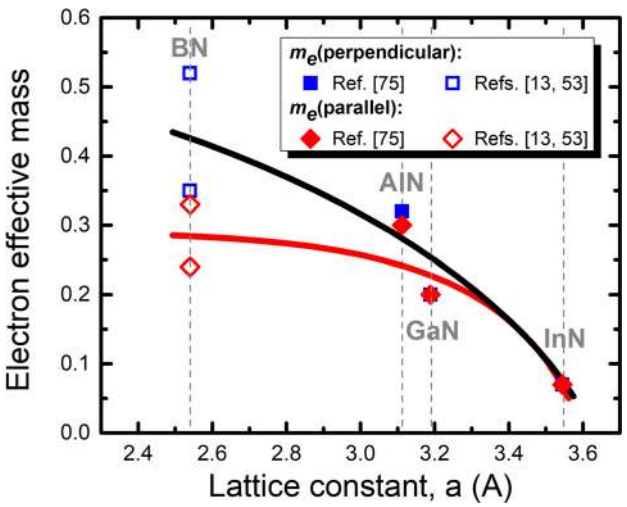

FIG. 7. Relationships between the *a* lattice constant and the effective mass perpendicular and parallel to the *c*-axis.

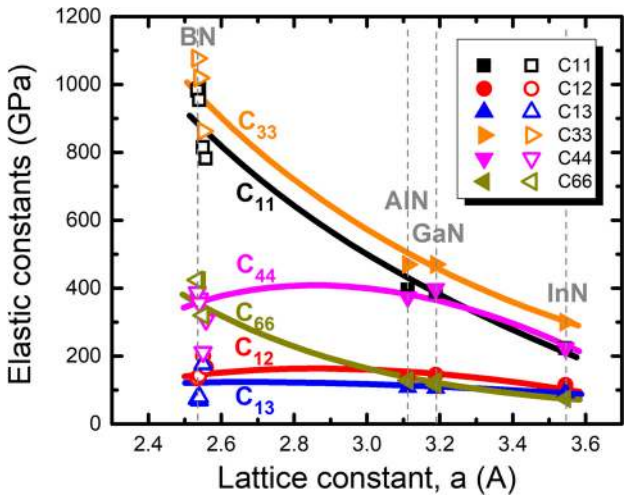

FIG. 8. Relationships between the *a* lattice constant and elastic constants.

The direct and indirect band gaps in BAlN, which are determined relative to the band edges of the same character, are shown in Fig. 10. Shan *et al.* used a proper projection scheme to identify the direct and indirect conduction-band minima, and found that the direct-to-indirect crossover in the bandgap of WZ $B_xAl_{1-x}N$ appears at $x = 0.28$, whereas in a linear interpolation, this crossing is expected at $x = 0.08$ (see Fig. 11). This difference is due to the large bandgap bowing for the direct bandgap. The bowing parameter for the direct gap varies from 8.38 eV at $x = 0.03$ to 8.67 eV at $x = 0.17$. For the indirect gap, the bowing parameter varies from 1.65 eV at $x = 0.03$ to 1.46 eV at $x = 0.17$. In the full content range, the bowing parameters for the direct and indirect gaps have been found to be $b_{dir} = 8.55$ eV and $b_{ind} = 1.49$ eV, respectively.[28] This means that both the direct and indirect band gaps in BAlN can be quite well described with a single bowing parameter.

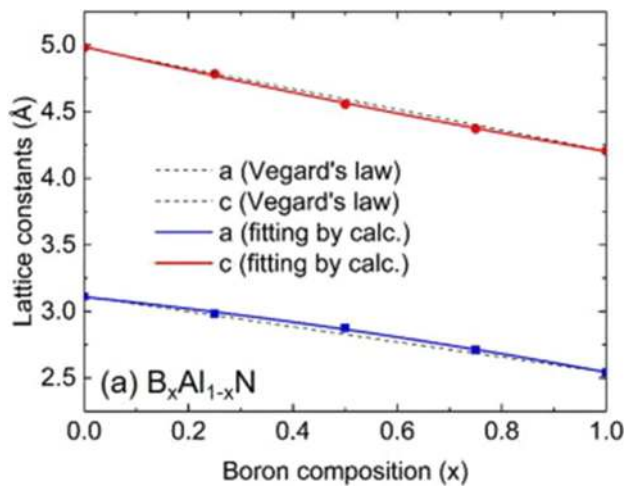

FIG. 9. Calculated lattice constants vs B composition of WZ BAlN. Reproduced with permission from Appl. Phys. Lett. **111**, 222106 (2017). Copyright 2017 AIP Publishing LLC.

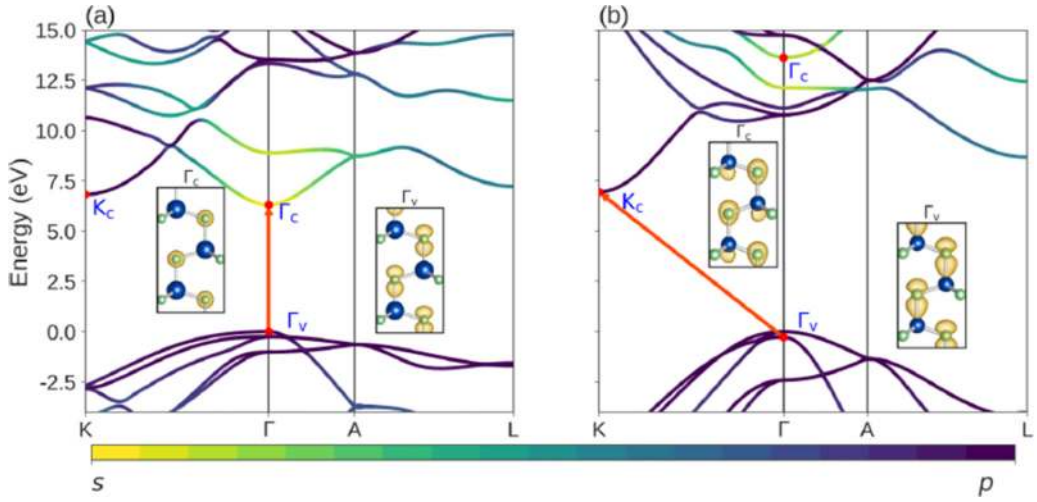

FIG. 10. Band structures of WZ bulk (a) AlN and (b) BN calculated with the Heyd–Scuseria–Ernzerhof functional. The color of each band indicates the angular momentum character of the states, according to the color bar below the plot. The valence-band maximum (VBM) at Γ was used as the zero-energy reference in each plot. The isosurfaces corresponding to the Γ_v and Γ_c wave functions are shown for each material. Reproduced with permission from Shen *et al.*, Phys. Rev. Mater. **1**, 065001 (2017). Copyright 2017 American Physical Society.

The spontaneous polarization (P_{SP}) and piezoelectric constants (e_{33} and e_{31}), which describe the polarization effects in III-N compounds, have been found to be strongly nonlinear for BAlN,[27] similar to those of the other ternary III-N compounds, i.e., AlGaN, AlInN, and GaInN.[75,78]

Figure 12 shows the spontaneous polarization for BAlN taken after Ref. 27. According to Eq. (1), this relation is described with a bowing parameter $b_{P_{SP}} = 0.629\ \mathrm{C/m^2}$; see Eq. (4)

$$P_{SP}^{B_xAl_{1-x}N} = x2.105 + (1-x)1.354 - 0.629x(1-x)\ \left(\mathrm{C/m^2}\right). \quad (4)$$

Figure 13 shows the piezoelectric constants e_{33} and e_{31} for BAlN taken from the same reference. These constants, written according to the nomenclature given by Eq. (1), are listed below:

$$e_{33}^{B_xAl_{1-x}N} = -x0.805 + (1-x)1.547 + 4.036x(1-x)\ \left(\mathrm{C/m^2}\right), \quad (5)$$

$$e_{31}^{B_xAl_{1-x}N} = x0.260 - (1-x)0.602 - 1.762x(1-x)\ \left(\mathrm{C/m^2}\right). \quad (6)$$

As the preferred crystallographic structure for AlN is WZ one and that of BN is zinc blende (ZB) or hexagonal (Hex), the stability

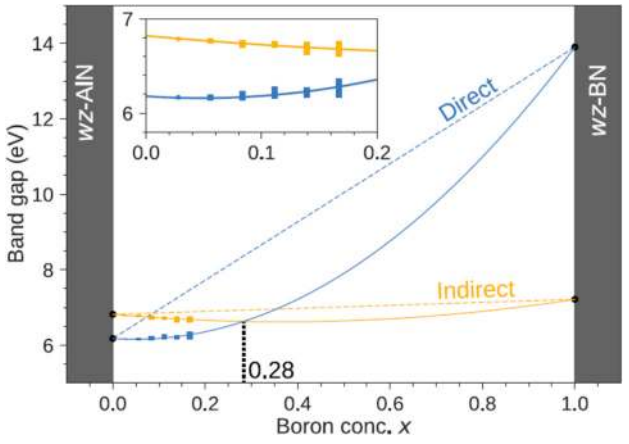

FIG. 11. Direct $\Gamma_v \rightarrow \Gamma_c$ and indirect $\Gamma_v \rightarrow K_c$ band gaps of WZ $B_xAl_{1-x}N$ alloys as a function of B concentration *x*. Linear interpolations of the direct and indirect band gaps are indicated by dashed lines. The spread of calculated values at each concentration is illustrated by the vertical bars. The solid curves indicate a quadratic fit to the calculated data [Eq. (1)]. The crossover between the direct and indirect bandgap at 28% is indicated by the vertical dotted line. The inset zooms in on the concentration range between 0 and 0.2. Reproduced with permission from Shen *et al.*, Phys. Rev. Mater. **1**, 065001 (2017). Copyright 2017 American Physical Society.

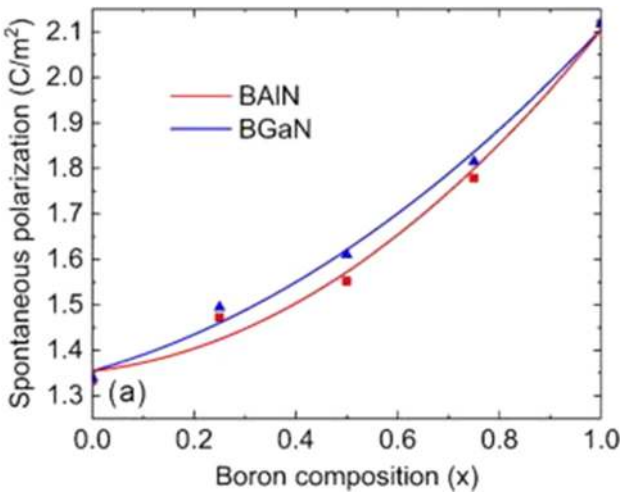

FIG. 12. (a) Spontaneous polarization vs B composition of BAlN and BGaN. Reproduced with permission from Appl. Phys. Lett. **111**, 222106 (2017). Copyright 2017 AIP Publishing LLC.

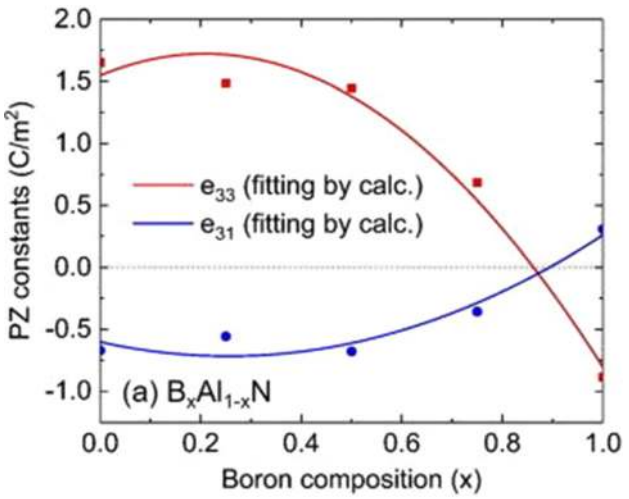

FIG. 13. Piezoelectric constants vs B composition of BAlN. Reproduced with permission from Appl. Phys. Lett. **111**, 222106 (2017). Copyright 2017 AIP Publishing LLC.

and miscibility of the BAlN alloy is not an obvious issue. This problem was studied by Hasegawa *et al.* for both BAlN and BGaN.[32,33] The authors applied empirical bond-order potential with the aid of *ab initio* calculations considering the electrostatic energies due to bond and ionic charges, to investigate the structures and miscibility of these alloys with threefold coordinated hexagonal and fourfold coordinated WZ and ZB structures. They discussed the stability and miscibility of BAlN and BGaN alloys on the basis of the excess energy obtained by using the empirical interatomic potential. Figure 14 shows the cohesive energy difference between threefold coordinated Hex and fourfold coordinated structures for $B_xAl_{1-x}N$ as a function of B concentration x. The calculated energy differences assume positive values over a wide B composition range, and therefore the Hex is stabilized only for the highest B concentrations $x > 0.9$. The ZB structure is stabilized for $0.25 < x < 0.9$, whereas the WZ structure is stabilized for $x < 0.25$. This indicates that alloying AlN with BN in this BN fraction range (i.e., BN < 25%) is promising for obtaining bulk-like *w*-BAlN.

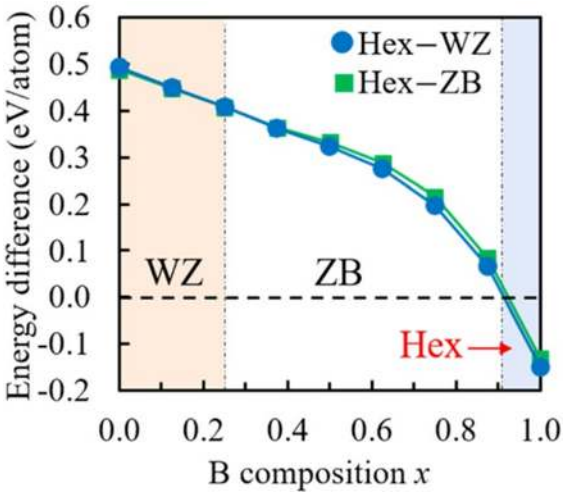

FIG. 14. Cohesive energy difference with respect to the cohesive energy of the Hex structure for the $B_xAl_{1-x}N$ alloy as a function of B composition x. The positive values indicate that the fourfold coordinated crystal structure is more stable than the Hex structure. Reproduced with permission from Hasegawa *et al.*, Jpn. J. Appl. Phys., Part I **58**, SCCB21 (2019). Copyright 2019 The Japan Society of Applied Physics.

Regarding the miscibility of BN with AlN (or GaN), Hasegawa *et al.* reported that the cohesive energy difference increases with BN fraction up to $x \sim 50\%$ and subsequently decreases. In general, a decrease in miscibility of ternary alloys with their composition increase is a typical feature of alloys. Moreover, Hasegawa *et al.* concluded that this miscibility is higher for more strongly constrained, which is present when $B_xAl_{1-x}N$ is grown on AlN.[33]

B incorporation into AlN was studied by Lymperakis using *ab initio* methods.[30] It was found that under typical metalorganic chemical vapor deposition (MOCVD) and metal-rich molecular beam epitaxy (MBE) conditions, the maximum B content at the surface is ~15%. Under MBE N-rich growth conditions, the calculations reveal a rehybridization-enhanced solubility mechanism that dominates the surface and offers a promising route to kinetically stabilizing B contents above the bulk solubility limit to as high as 25%.[30]

In general, B incorporation into AlN during the MOCVD and MBE growth process can be controlled by various parameters including temperature, which significantly influences the optical quality. To date, successful growth of BAlN layers has only been reported in a few papers,[40,42–48,50–55,57,58] and the optimal growth conditions for BAlN still do not appear to have been sufficiently well studied and determined.

First, BAlN layers were grown on sapphire by organometallic vapor-phase epitaxy at 1050 °C using triethyl-boron (TEB) as a precursor by Polyakov *et al.*[40] The authors observed that B is readily incorporated into the layers and its concentration in the solid phase can be as high as 40%, but single-phase WZ BAlN films can only be grown for compositions not exceeding 10% B. A second phase arises for higher B concentrations in the solid and is identified as pure *w*-BN. The authors concluded that the growth of this thermodynamically unfavorable *w*-BN is possible because it occurs within the boundaries provided by the WZ AlN islands that form first on the surface and set up the sites for lateral growth of *w*-BN. Thus, the film is composed of a columnar structure of AlN and BN crystallites oriented in the basal plane and existing adjacently.[40]

Successive BAlN layers were grown by low-pressure metalorganic vapor phase epitaxy (LP-MOVPE) on a (0001) 6H–SiC substrate by Shibata *et al.*[42] The authors used TEB as the precursor for the B incorporation, and reported approximately 13% B incorporation into AlN at 1180 °C.

Almost simultaneously, BAlN layers were grown by ammonia MBE on a (0001) sapphire substrate by Gupta *et al.*[43] For the B source, the authors used elemental B loaded into a pyrolytic graphite liner inside a tungsten crucible. The B cell was capable of operating at up to 2000 °C. At the maximum B cell temperature, the authors were able to incorporate up to 6% B into BAlN.

An important motivation for the experimental exploration of B-containing III-N arose from studies of the refractive index of BAlN

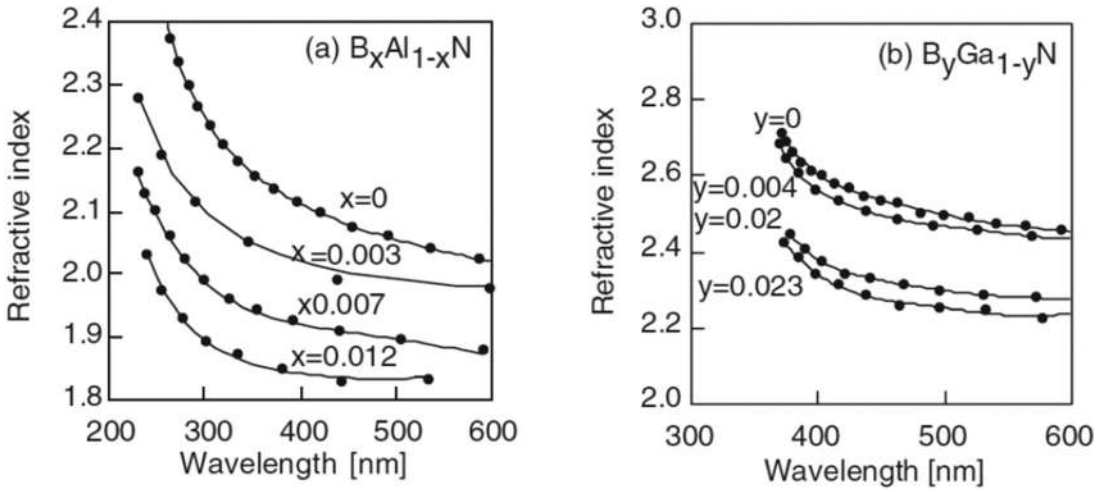

FIG. 15. Refractive indices of $B_xAl_{1-x}N$ with B content *x*, varied between 0 and 0.012. Reproduced with permission from Watanabe *et al.*, Phys. Status Solidi C **0**, 2691 (2003). Copyright 2003 John Wiley & Sons.

and BGaN by Watanabe *et al.*[44] The authors grew BAlN and BGaN layers by LP-MOVPE on (0001) 6H–SiC substrates and measured the refractive index in a broad spectral range. It was found that even a small fraction of B is able to modify the refractive index very significantly in comparison to the refractive index of the B-free host. The refractive indices determined by Watanabe *et al.*[44] for BAlN and BGaN layers are shown in Fig. 15. As seen in this figure, even a small incorporation of B into the AlN host strongly reduces the refractive index and makes the BAlN alloy very promising for Bragg reflectors.[44,48]

Further studies of the growth of BAlN have concentrated on metalorganic epitaxial methods,[46,51–53,55,58,63] including the flow modulation epitaxy (FME) mode, which increases the diffusion length of the group III atoms and reduces parasitic reactions between the metalorganic and NH_3. TEB was used as the precursor for the B incorporation, and BAlN layers were deposited on sapphire partly with AlN templates or SiC substrates.

High-quality BAlN films have been obtained on (0001) 4H–SiC via the FME approach at a growth temperature of 1000 °C.[46] However, it was observed that the B incorporation was rather low (∼1.5% B) under such conditions.

To obtain BAlN with higher B concentration, BAlN layers have been grown at 650 °C and then annealed at 1020 °C.[56] Through varying the TEB/III molar ratio from 0% to 40%, it was observed that the B concentration increased linearly up to ∼5.6%. At the FME mode, a B concentration as high as 12% was successfully achieved on both AlN/sapphire and GaN/sapphire templates. Single-solid-phase BAlN was clearly identified by high-resolution x-ray diffraction (XRD). In addition, the authors concluded that the BAlN layer consisted of columnar polycrystals and inherited the WZ structure of the substrate.[56]

High levels of B incorporation into BAlN films have also been achieved for high growth temperatures, i.e., at 1010 °C.[53,55] No evidence of phase separation was observed for these films, but a columnar structure with small columns of 10 nm was found; see Fig. 16. However, it was observed that the B content estimated from measurements using XRD and from those using Rutherford backscattering (RBS) differs significantly; see Fig. 17. The B content obtained by RBS closely follows the B/III gas-flow ratio, indicating a high efficiency of B incorporation into the film. The B content measured by XRD is noticeably less than that measured by RBS. The authors have attributed this difference to possible B segregation at the columnar boundaries and other crystalline defects, such as twinned regions.[55]

A difference between the B concentration determined by XRD and by secondary-ion mass spectroscopy (SIMS) for BAlN films was

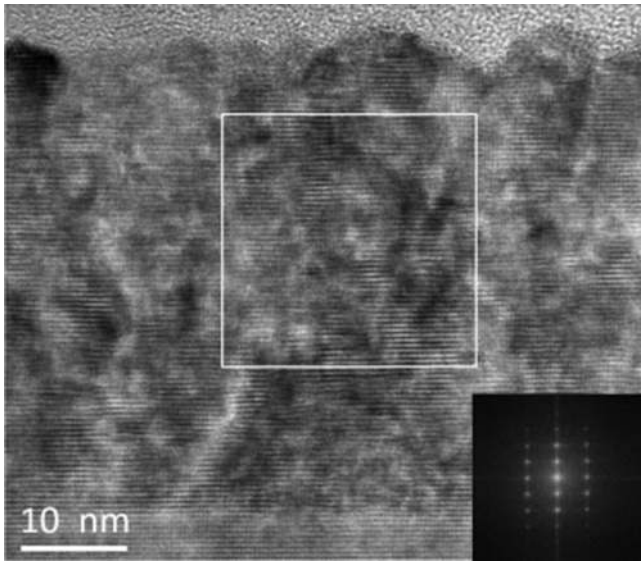

FIG. 16. Microstructure of the BAlN film grown with a B/III gas-flow ratio of 0.12. Cross-section on-axis multi-beam TEM image along the [11-20] AlN projection. The film thickness is ∼45 nm. A fast Fourier transform of the diffraction pattern of the region in the box indicates a WZ structure. Reproduced with permission from Wang *et al.*, J. Cryst. Growth **475**, 334 (2017). Copyright 2017 Elsevier.

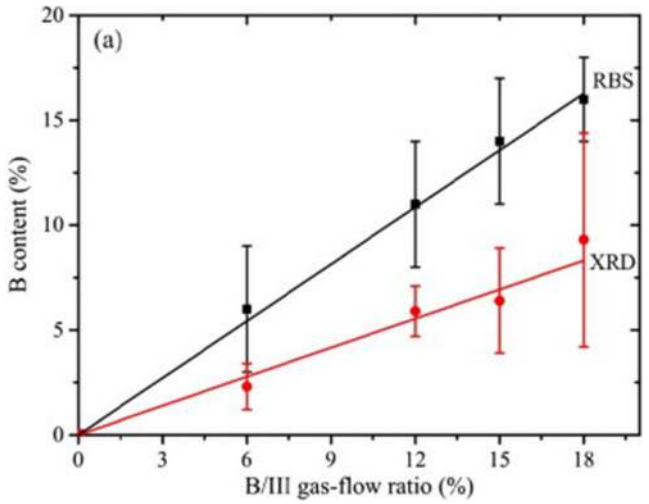

FIG. 17. B content in the film as a function of the B/III gas-flow ratio in the gas flow, determined by XRD (circles) and RBS (squares), with corresponding linear fits. Reproduced with permission from Wang *et al.*, J. Cryst. Growth **475**, 334 (2017). Copyright 2017 Elsevier.

also observed by Rettig *et al.*[58] In general, the observed differences in concentration determined by XRD and by other methods suggest that a significant proportion of the B atoms in BAlN are incorporated in inappropriate places. This might be one reasons why the optical quality of BAlN films is often very low. This is particularly expected for BAlN films grown at low temperatures. For those grown at higher temperatures, the estimated B incorporation is low but, in this case, the concentration of point defects including that of the B interstitial is expected to be lower and thereby the optical quality is expected to be better. However, this issue has not yet been explored, because it is difficult to obtain photoluminescence (PL) measurements in the UV-C spectral range. Unfortunately, most of the reports on BAlN do not include PL studies, which is very unfavorable for estimation of the optical quality of the studied material. Therefore, evaluation of the optical quality by PL appears to be necessary to further development of BAlN growth for optoelectronic applications.

It is also worth noting that most of the BAlN films were grown along the polar $+c$-direction. The growth along other crystallographic directions is still unexplored, as only one paper has reported the growth of nonpolar BAlN (11–20) and (1–100) films.[47] These films were grown at 1000 °C on SiC substrates by MOCVD within the FME approach. The B concentrations of ∼2% in the films estimated by XRD agree well with those measured by SIMS, indicating that the B atoms are incorporated predominantly into the lattice sites.

To summarize the above discussion, significant progress in the growth of BAlN layers has been obtained via MOCVD and related methods. However, there is still significant scope to study the optimal epitaxial growth conditions, the growth of QWs containing BAlN layers, and other issues associated with the B incorporation into the AlN host. Moreover, it is worth noting that the growth of BAlN by MBE is almost totally unexplored. As MBE is a powerful method of growth of III-N, it is expected that high-quality BAlN films and heterostructures containing BAlN can also be grown by this method under optimized conditions, and that lower growth temperatures favor higher B incorporation.

C. BGaN

Combining BN with GaN is more challenging than with AlN because of the larger lattice mismatch between the binary compounds ($\varepsilon_{BN/AlN} = 18\%$ vs $\varepsilon_{BN/GaN} = 20\%$). The structural and electronic properties of *w*-BGaN in the whole BN range have been studied using DFT methods.[25,27,79–81] Experimentally, this alloy was explored in the diluted regime of B incorporation only,[82–99] because of the intrinsic difficulties in mixing over the whole B range.

The lattice constants calculated by Liu *et al.*[27] for $B_xGa_{1-x}N$ are plotted in Fig. 18 (solid points) together with the parabolic fit (solid lines) and linear interpolation (dashed lines). As can be seen, deviations from the linear dependence are present for this alloy similar to BAlN. The bowing parameters for the lattice constants have been determined to be $b_a = -0.101$ Å and $b_c = 0.057$ Å. The formulas for the lattice constants, written according to the nomenclature given by Eq. (1), are listed below:

$$a^{B_xGa_{1-x}N} = x2.546 + (1-x)3.176 + 0.101x(1-x)\,(\text{Å}), \quad (7)$$

$$c^{B_xGa_{1-x}N} = x4.201 + (1-x)5.186 - 0.057x(1-x)\,(\text{Å}). \quad (8)$$

Figure 19 shows the electronic band structure of WZ GaN and BN calculated by Turiansky *et al.*[81] The fundamental direct (GaN) and indirect (BN) transitions are marked by arrows, and the orbital contribution to the states in the band structure is illustrated similar to for BAlN by distinct colors: yellow for *s* states and purple for *p* states.

As for BAlN[28] a proper projection scheme was used to identify the direct and indirect conduction-band minima.[81] Figure 20 shows the direct and indirect band gaps in $B_xGa_{1-x}N$, which are determined relative to the band edges of the same character. A direct-to-indirect crossover in the bandgap of WZ $B_xGa_{1-x}N$ appears at $x \sim 0.5$ whereas for the linear interpolation this crossing is present at $x \sim 0.3$ (see Fig. 20). A small bowing parameter was found for the indirect bandgap

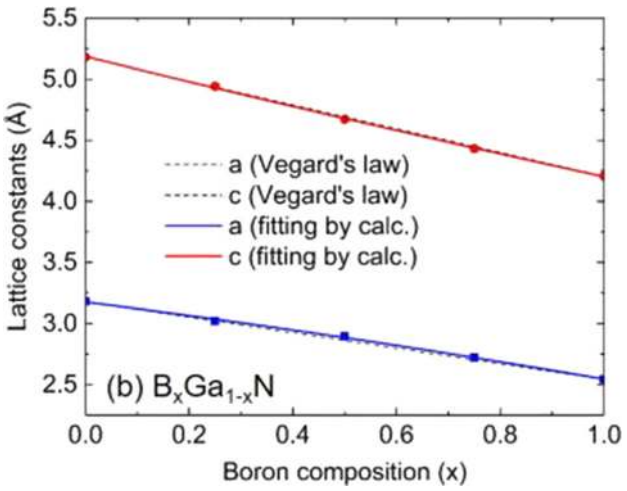

FIG. 18. Calculated lattice constants vs B composition of WZ BGaN. Reproduced with permission from Appl. Phys. Lett. **111**, 222106 (2017). Copyright 2017 AIP Publishing LLC.

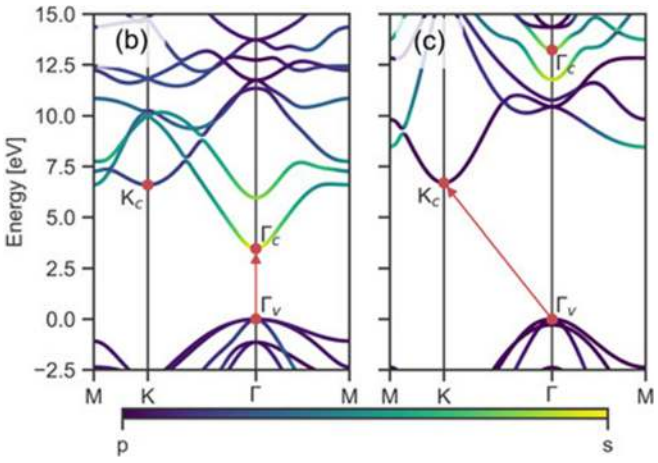

FIG. 19. Calculated band structures for (b) WZ-GaN and (c) WZ-BN. Bands are colored by the angular momentum character corresponding to *s* or *p* orbitals. The VBM of each material is used as the energy reference. Reproduced with permission from J. Appl. Phys. **126**, 095706 (2019). Copyright 2019 AIP Publishing LLC.

$b_{\text{ind}} = 0.55$ eV. Moreover, it was observed that the direct bandgap cannot be described by a quadratic fit, but for low B concentrations ($x \leq 0.2$), a bowing parameter of $b_{\text{dir}} = 8.68$ eV appears to be sufficiently accurate.[81]

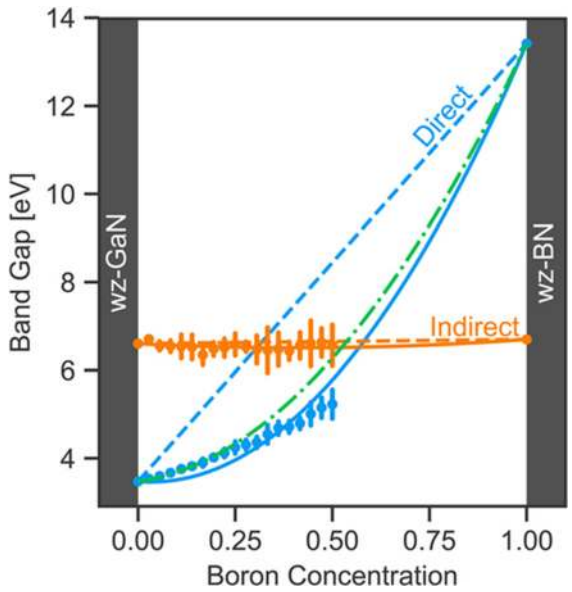

FIG. 20. Direct ($\Gamma_v \rightarrow \Gamma_c$) and indirect ($\Gamma_v \rightarrow K_c$) band gaps of WZ $B_xGa_{1-x}N$ alloys as a function of the fractional B concentration *x*. Data points represent the average of ten configurations at each B concentration, with error bars indicating the standard deviation. Linear interpolations between the gaps of the parent materials are indicated by the dashed lines. The solid lines correspond to a fit of the data to a quadratic equation [Eq. (1)]. For the direct bandgap, two fits are shown: one including all calculated direct-bandgap data (blue, solid), and the other including data up to 20% B (green, dashed-dotted). Reproduced with permission from J. Appl. Phys. **126**, 095706 (2019). Copyright 2019 AIP Publishing LLC.

The spontaneous polarization for BGaN has been calculated by Liu *et al.*[27] and is shown in Fig. 12. According to Eq. (1), this relation is described with a bowing parameter $b_{P_{SP}} = 0.438\ \text{C/m}^2$; see Eq. (9)

$$P_{SP}^{B_xGa_{1-x}N} = x2.106 + (1-x)1.354 - 0.438x(1-x)\ (\text{C/m}^2). \quad (9)$$

Figure 21 shows the piezoelectric constants e_{33} and e_{31} for BGaN taken after Ref. 27. These constants written according to the nomenclature given by Eq. (1) are listed below:

$$e_{33}^{B_xGa_{1-x}N} = -x0.833 + (1-x)0.539 + 2.189x(1-x)\ (\text{C/m}^2), \quad (10)$$

$$e_{31}^{B_xGa_{1-x}N} = x0.270 - (1-x)0.310 - 0.981x(1-x)\ (\text{C/m}^2). \quad (11)$$

As mentioned previously, the stability and miscibility of BGaN alloys were studied by Hasegawa *et al.*[32,33] Figure 22 shows the cohesive energy difference with respect to the cohesive energy of the Hex structure for $B_xGa_{1-x}N$ alloys as a function of B composition *x*. As for BAlN, the WZ structure is stabilized for $x < 0.25$ and in this range of BN fraction the growth of *w*-BGaN is expected to be promising.

To date, successful growth of epitaxial BGaN layers has been reported in several papers.[82–99] BGaN layers were first deposited by Polyakov *et al.* using MOVPE,[82] and by Vezin *et al.* using MBE.[83]

Vezin *et al.* deposited BGaN films on sapphire with proper substrate nitridation prior to the BGaN deposition. The growth was performed at different B cell temperatures and a substrate temperature of 810 °C. During these experiments, samples composed of a mixture of ZB and WZ were obtained with either WZ or ZB as the dominant phase. The minimum temperature necessary to solely obtain the WZ structure increased with the amount of B. Finally, the authors were able to achieve WZ BGaN layers with ∼2.6% B according to electron probe microanalysis and ∼4.6% according to XRD measurements.[83]

Polyakov *et al.* deposited BGaN films on a sapphire substrate at different temperatures (450, 500, 650, and 800 °C). TEB was used as a precursor for B incorporation. Following the growth, the temperature

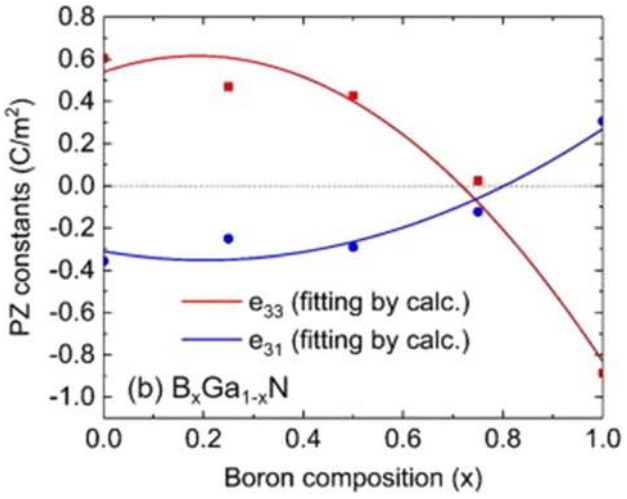

FIG. 21. Piezoelectric constants vs B composition of BGaN. Reproduced with permission from Appl. Phys. Lett. **111**, 222106 (2017). Copyright 2017 AIP Publishing LLC.

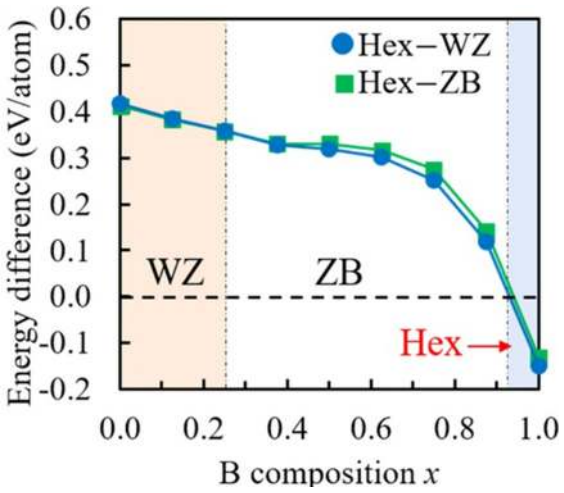

FIG. 22. Cohesive energy difference with respect to the cohesive energy of the Hex structure for $B_xGa_{1-x}N$ alloy as a function of B composition x. The positive values indicate that the fourfold coordinated crystal structure is more stable than the Hex structure. Reproduced with permission from Hasegawa *et al.*, Jpn. J. Appl. Phys., Part I **58**, SCCB21 (2019). Copyright 2019 The Japan Society of Applied Physics.

was increased to 1000 °C over approximately 10 min and the samples were kept there for 1 min before cooling down. This was done to crystallize the layers, which were amorphous at the deposition temperature. It was later observed that the B incorporation increases with decreasing growth temperature and reaches ∼7% for samples grown at 650 °C. For a BGaN layer grown at 1000 °C, the B incorporation was found to be 1%. Polyakov *et al.* also observed that the absorption edge shifts to blue for BGaN layers with B incorporation of 3.5% and 5%.

Wei *et al.*[84] deposited BGaN layers on 6H–SiC substrates at 1000 °C by low-temperature MOVPE, using diborane as a B source. It was observed that with increasing diborane flow, the solid solution of BGaN decomposed into WZ BGaN and the second B-rich phase. This phase was identified as *h*-BN with a sp^2 structure. A single-phase (WZ) BGaN alloy with 1.5% B was achieved at a gas-phase B/Ga ratio of 0.005.[84]

Systematic studies of BGaN composition as function of the TEB/III ratio at different pressures in an MOVPE reactor were performed by Ougazzaden *et al.*[85] The authors grew BGaN layers on GaN templates at a temperature of 1050 °C and observed that B incorporation into the BGaN film increases linearly with increasing TEB/III ratio; see Fig. 23. At a pressure of 600 hPa, the maximal B concentration reaches ∼2%, increasing to above 3% at lower pressure (133 hPa).

In addition, Kadys *et al.*[91] performed systematic studies of the effects of MOCVD growth conditions on the optical and structural properties of BGaN layers. The authors used TEB as a precursor for B incorporation and achieved BGaN films with a few percent of B, as shown in Fig. 24. The growth temperature was varied from 700 to 1000 °C, and the authors concluded that decreasing the growth temperature is beneficial to incorporating a larger amount of B into BGaN without drastically worsening the layer structural quality.[91]

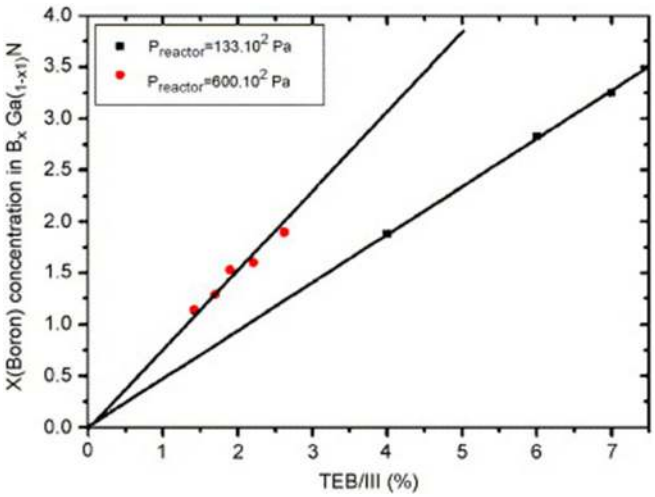

FIG. 23. BGaN boron composition (%) vs TEB/III ratio (%) for two different pressures in the reactor. Reproduced with permission from Ougazzaden *et al.*, J. Cryst. Growth **298**, 316 (2007). Copyright 2007 Elsevier.

Figure 25 shows the B content (%) in BGaN vs the TEB/III ratio (%) obtained by Kadys *et al.*[91] This dependence is similar to the one obtained by Ougazzaden *et al.*[85] (Fig. 23). Up to a TEB/III ratio of 4%, the B incorporation is low (<2%–3% B). To incorporate more B into

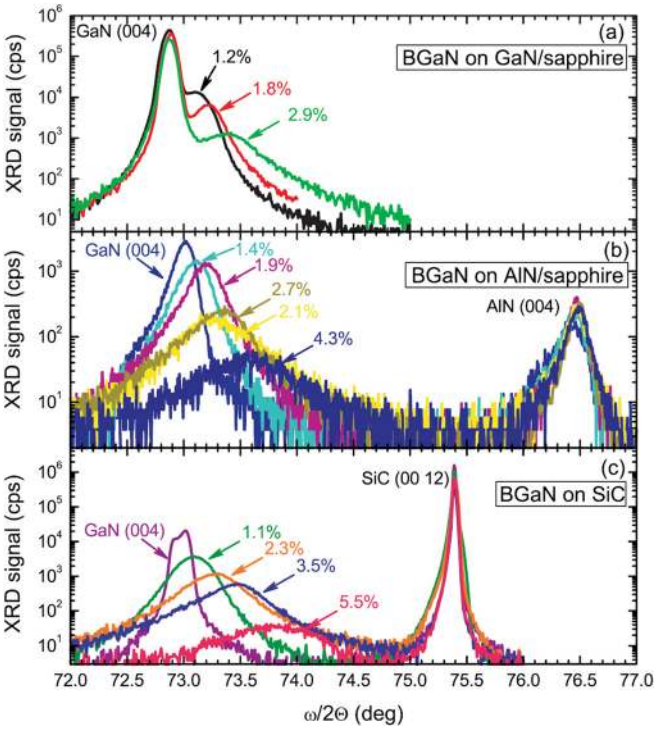

FIG. 24. XRD scans along the (004) direction for BGaN layers grown on GaN/sapphire (a), AlN/sapphire (b), and SiC (c) substrates. The estimated B content is indicated. Reproduced with permission from Kadys *et al.*, J. Phys. D: Appl. Phys. **48**, 465307 (2015). Copyright 2015 IOP Publishing.

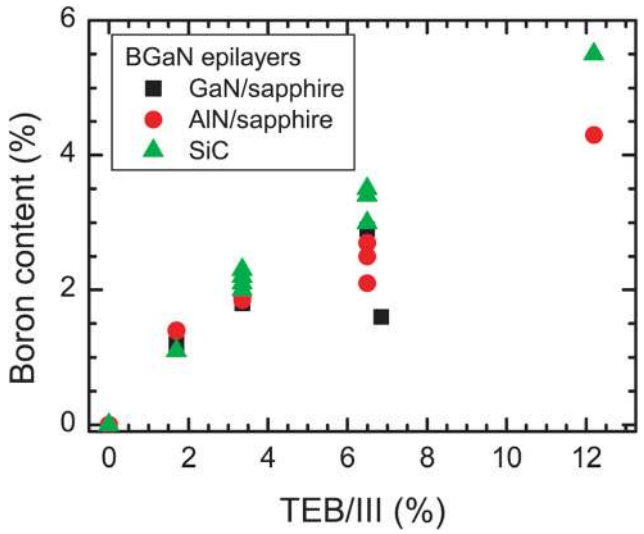

FIG. 25. BGaN boron composition vs TEB/III ratio for epilayers grown on different substrates/templates (indicated). Reproduced with permission from Kadys *et al.*, J. Phys. D: Appl. Phys. **48**, 465307 (2015). Copyright 2015 IOP Publishing.

BGaN, the TEB/III ratio must be increased and/or the growth temperature must be lowered.[91]

Similar conclusions regarding B incorporation into BGaN films grown by MOVPE were reached by Gunning *et al.*[96] The authors observed that the BGaN growth at high temperature and pressure results in rough surfaces and low B incorporation efficiency. In contrast, the growth at low temperature and pressure (750–900 °C and 20 Torr) using N carrier gas results in an improved surface morphology and higher B incorporation (up to ∼7.4%). However, careful structural studies by transmission electron microscopy and x-ray pole figures indicate a severe degradation of high-B-composition layers into a twinned cubic structure with a high density of stacking faults and poor PL at room temperature. BGaN layers with a TEB flow <1% show more intense, narrower XRD peaks, near-band edge emission at ∼362 nm, and primarily a WZ-phase structure in the x-ray pole figures. For BGaN layers with >1% TEB flow, the crystal structure becomes dominated by the cubic phase.[96]

Further studies on phase separation in BGaN films deposited by MOVPE at high temperatures (1010–1085 °C) were performed by Ebara *et al.*[99] When the growth temperature was increased, the formation and incorporation of the cubic phase was observed, voids were formed in the BGaN film, and the growth rate decreased. The authors concluded that there was a different desorption rate of adatoms in the BGaN growth regime compared to that for GaN growth. This could originate from a change in the desorption process at the surface due to different bonding states caused by the adsorption of B atoms.[99]

Considering recent studies on MOCVD growth of BGaN layers supported by careful structural investigations,[96,99] the growth of high-quality BGaN with a single WZ phase and B concentration higher than 1% appears very challenging. However, BGaN layers with B > 1% can be achieved at lower growth temperature,[82,91,96] although it is established that an excessively low growth temperature is responsible for high concentration of point defects, which deteriorates the optical quality of these layers. This could also be attributed to typical defects of GaN grown at low temperatures,[100] as well as to B incorporated into interstitial sites. The optical quality of BGaN can be quite easily evaluated by analysis of the intensity of bandgap-related emission observed in PL measurements. For all PL studies performed for BGaN layers to date, it has been observed that the bandgap-related emission decreases with increasing B concentration.[87,91,94,96,98,101] Careful analysis of this phenomenon for the samples reported in Ref. 90 was performed by Jurkevicius *et al.*[94] The authors observed that the PL intensity decreases by a few orders of magnitudes with increasing B concentration in the BGaN layers from 0 to ∼4%–5%; see Fig. 26.

Since the first growth of BGaN layers by MBE,[83] further studies on MBE growth have not been intensively carried out and only a few more papers have been published.[95,97] In Ref. 95, high-crystal-quality BGaN films with compositions of up to 3.04% were reported. These films were grown coherently on GaN-templated sapphire substrates at a temperature of 720 °C using BBr_3 gas as a B source. The high structural quality of the BGaN films was confirmed by high-resolution XRD, and the random character of this alloy was observed by atom probe tomography.[95,97] Detailed studies of alloy distribution in BGaN films were reported in Ref. 97. These results clearly show that MBE is a very promising method for growing high-quality WZ BGaN alloys.

D. BInN

The lattice mismatch between *w*-BN and InN is very high ($\varepsilon_{BN/InN} = 28\%$). Hence, the epitaxial growth of WZ BInN alloys will be very difficult or even impossible. To date, no reports on experimental studies of BInN exist in the literature. This can be attributed to the established challenges in growing highly mismatched alloys, rather than a lack of motivation regarding the potential applications of such alloys in semiconductor devices, as BInN with B = 43.1% and 35.4% should be lattice-matched (LM) to AlN and GaN, respectively, and therefore could be interesting for Bragg reflectors. Moreover, no theoretical studies on BInN by the DFT method or other theoretical methods can be found. Considering the chemical trends in the bowing

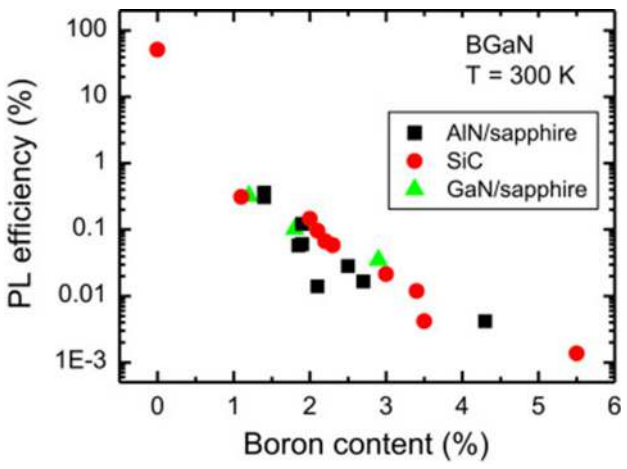

FIG. 26. PL efficiency dependence on B content in BGaN epilayers grown on different substrates. Reproduced with permission from Jurkevičius *et al.*, Phys. B **492**, 23–26 (2016). Copyright 2016 Elsevier.

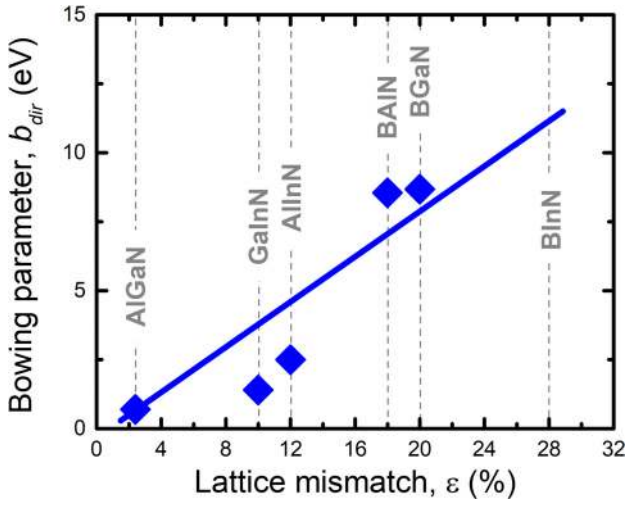

FIG. 27. Bowing parameter b_{dir} for the direct bandgap for ternary III-N compounds plotted vs the lattice mismatch ε, which is defined by the following formula: $\varepsilon = (a^{BC} - a^{AC})/a^{BC}$, where a^{AC} and a^{BC} are the lattice constants of the binary compound with a smaller and larger lattice constant, respectively.

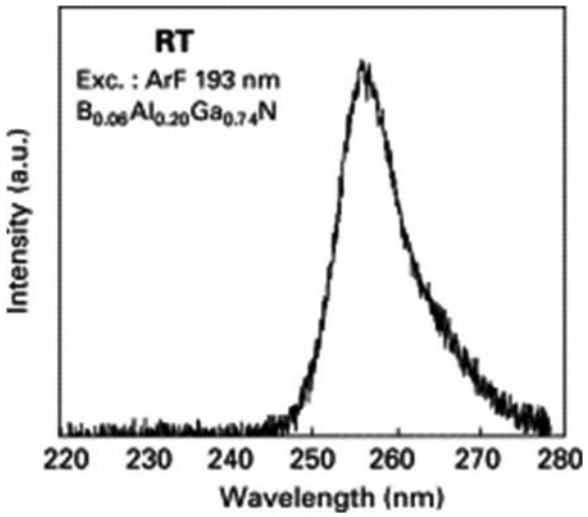

FIG. 28. PL spectrum of (BAlGaN/AlN) MQWs at room temperature. Reproduced with permission from Takano *et al.*, J. Cryst. Growth **237–239**, 972 (2002). Copyright 2002 Elsevier.

parameter describing III-N ternary alloys (i.e., an increase in bowing parameter with increasing lattice mismatch), the bowing parameter for the direct and indirect band gaps in BInN can be estimated from Fig. 27 to be ∼11 eV.

Such a large bowing parameter indicates that BAlN, BGaN, and BInN can be treated as highly mismatched alloys, i.e., alloys that cannot be described within the crystal virtual approximation as regular alloys, such as AlGaN or GaInN.

E. BAlGaN, BAlInN, and BGaInN lattice matched to AlN and GaN

III-N LM to AlN and GaN are highly desirable for optoelectronic device engineering. Without B, only AlInN with 17.8% In can be lattice-matched to GaN. For ternary III-N with B, lattice matching with AlN can be achieved for BGaN with 11.9% B and BInN with 43.1% B. According to our previous discussions, BGaN and BInN alloys with such high B concentrations are rather difficult to grow. Therefore, quaternary BAlGaN, BAlInN, and BGaInN alloys with low B concentrations are more promising for epitaxial growth with good structural and optical quality. The content relations in B-containing III-N LM to a given substrate are listed below:

$$\begin{aligned}
B_xAl_{1-x-y}Ga_yN \text{ LM to AlN at } y &= 0.135x,\\
B_xAl_{1-x-y}In_yN \text{ LM to AlN at } y &= 1.321x,\\
B_xAl_{1-x-y}In_yN \text{ LM to GaN at } y &= 1.321x + 0.178,\\
B_xGa_{1-x-y}In_yN \text{ LM to AlN at } y &= 1.823x + 0.216,\\
B_xGa_{1-x-y}In_yN \text{ LM to GaN at } y &= 1.823x.
\end{aligned}$$

The growth of quaternary BAlGaN was reported by Takano *et al.*[102] The authors deposited thick BAlGaN layers and BAlGaN/AlN multiple quantum wells (MQWs) by LP-MOVPE on a 6H–SiC substrate with TEB as a B source. The growth temperatures of the BAlGaN layer and BAlGaN/AlN MQWs were 1270 and 1170 °C, respectively. Relatively strong PL was observed for both the BAlGaN layer and BAlGaN/AlN MQWs; see Figs. 28 and 29. It is worth noting that the growth temperature was relatively high in comparison to that in reports on the growth of BAlN and BGaN alloys, which was significantly below 1050 °C (see, for example, Refs. 40, 46, 53, 55, 56, 82, 91, and 96). In this case, a high growth temperature can be favorable for good optical quality, including efficient PL. The B concentrations in these samples were determined by Auger electron spectroscopy or a combination of PL and XRD. Considering the challenge in the accuracy of composition determination for quaternary alloys, the resulting B concentrations should be treated as a rough estimation.

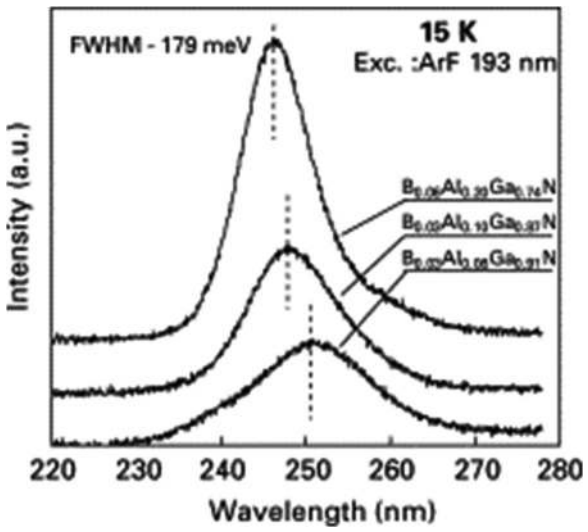

FIG. 29. PL spectra of (BAlGaN/AlN) MQWs at different compositions of BAlGaN. Reproduced with permission from Takano *et al.*, J. Cryst. Growth **237–239**, 972 (2002). Copyright 2002 Elsevier.

III. III-NITRIDES DILUTED WITH GROUP V ATOMS

Alloying III-N (AlN, GaN, and InN) with other III–V compounds (GaP, GaAs, GaSb, InP, etc.) is very difficult because of the drastically different growth conditions for the two groups of semiconductor materials, i.e., the optimal growth temperature is much higher for AlN and GaN than for III–V compounds, as shown in Fig. 30. Hence, the incorporation of group V atoms (P, As, Sb, and Bi) into a III-N host, and vice versa, is a challenge; it is well established that the incorporation of N into III–V semiconductors is difficult under both MBE and MOCVD growth conditions. For this reason, in many cases, other methods have been used for the synthesis of HMAs, such as ion implantation.[103–105] It is worth adding that III-N compounds are stable in the WZ structure, and the remaining III-V compounds are stable in the ZB structure.

III–V alloys with a few percent of N atoms (known as dilute nitrides) have been very intensively investigated in the last two decades owing to their unusual fundamental properties and applications in lasers and solar cells.[106–116] In general, it has been observed that only a few percent of N atoms (or even less than 1%) can be incorporated into a III–V host at a growth temperature close to the optimal growth conditions for the III–V host, although a decrease in growth temperature can enhance N incorporation but usually the material quality deteriorates when the alloy is grown at an excessively low temperature. Therefore, post-growth annealing is often used to improve the optical quality of dilute nitrides.[106,117]

The most important advantage of dilute nitrides is the simultaneous reduction of the lattice constant and the bandgap.[106,113] This feature is beneficial in bandgap engineering and has not been observed for any other III–V alloys. Hence, it was possible to fabricate GaAs-based lasers emitting at 1.3 and 1.55 μm,[108–110,112] and multi-junction solar cells.[111,116] These achievements clearly show that the bandgap engineering in the ZB III–V alloys is much more flexible with a few percent of N atoms. The same can be expected for WZ III-N alloys diluted with group V atoms. The incorporation of a few percent of As (or other group V atoms) strongly influences the electronic band structure and can therefore be interesting for the bandgap engineering of such wide-gap semiconductors. In addition, group V atoms can work as either surfactants or antisurfactants during the growth process. This feature opens a new field in the growth of novel nano- and micro-rods.[118] In this section, we focus on alloying III-N with III–V compounds with particular attention given to the regime of diluted concentration of group V atoms (P, As, Sb, and Bi). This regime of concentrations is promising for further development of III-N devices via bandgap engineering, which is unavailable within the standard III-N (AlN, GaN, and InN).

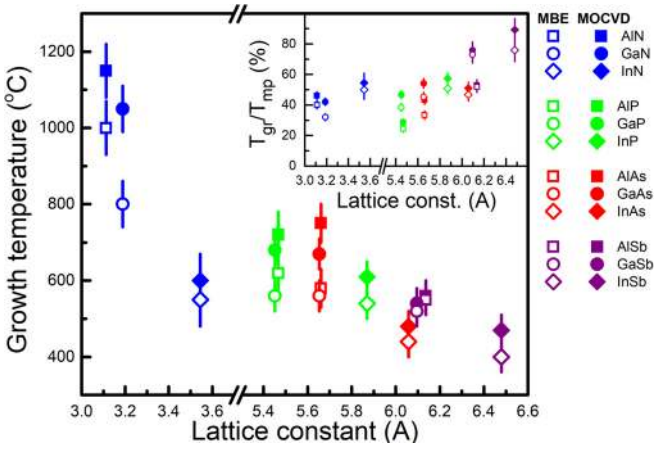

FIG. 30. Optimal MBE (open points) and MOCVD (solid points) growth temperatures of III-N (blue points), III-phosphides (green points), III-arsenides (red points), and III-antimonides (purple points). The inset shows the ratio of the optimal growth temperature (T_{gr}) and melting-point temperature (T_{mp}) for a given compound with the same nomenclature of markings.

In general, the incorporation of group V atoms into a III-N host in the diluted regime is possible at temperatures close to the optimal growth conditions for the host material while maintaining good crystalline and optical properties. Hence, the optical quality of the alloy is expected to be maintained as for dilute nitrides, but this issue still requires careful exploration. In contrast, alloying III-N with ZB III–V compounds has been achieved across the whole range of compositions by lowering the growth temperature in MBE.[119–121] For these alloys, it has been observed that the structural and optical quality of the obtained materials is poor compared to those grown at high temperatures, but it has allowed studies of the bandgap across the whole content range for GaNAs[119–123] and other HMAs, including GaNSb[124–129] and GaNBi.[130,131]

For the GaNAs, which from one side of composition is GaAs diluted with N and from the other side is GaN diluted with As, a consistent phenomenological picture of the electronic band structure can be obtained within the band anticrossing model, which was originally proposed for N diluted Ga(In)NAs alloys by Walukiewicz and coworkers.[132,133]

A. Band anticrossing model

Because of the large differences in the electronegativity of group V atoms (see Fig. 1) and the high lattice mismatch, the electronic band structure of III–(N,V) alloys cannot be described within the virtual crystal approximation. Therefore, the band anticrossing model (BAC),[132,133] is often used to describe the electronic band structure of HMAs, including III-N compounds diluted with group V atoms. Originally, this model was proposed to explain the pressure dependence of optical transitions observed in the photoreflectance spectra of GaInNAs.[132] Subsequently, it was extended to explain the electronic band structure in other HMAs, including II–VI compounds diluted with O,[134–137] ZnO diluted with group IV atoms,[138,139] and III-N compounds diluted with group V atoms.[140]

The electronic band structure modeled within the BAC model for GaNAs diluted with N is sketched in Fig. 31(a). In the regime of low N concentration, a resonant level corresponding to N atoms is located above the conduction-band (CB) minimum of the GaAs host. The interaction between N-related and CB states is modeled using the perturbation theory described by the following Hamiltonian:

$$H_{\mathrm{BAC}} = \begin{pmatrix} E_{\mathrm{CB}}(k) & C_{\mathrm{NCB}}\sqrt{x} \\ C_{\mathrm{NCB}}\sqrt{x} & E_{\mathrm{N}} \end{pmatrix}, \tag{12}$$

where x is the mole fraction of substitutional N atoms. $E_{\mathrm{CB}}(k)$ is the energy dispersion of the CB of the GaAs host and E_{N} is the energy of N-related states, all with respect to the top of the valence band of the

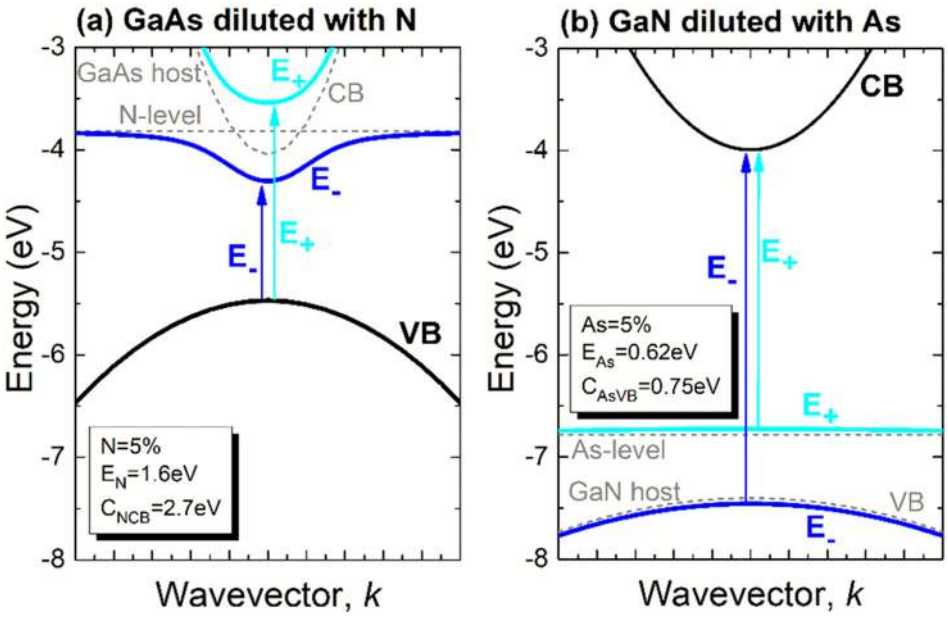

FIG. 31. Repulsive anticrossing interaction of (a) localized N-states with the extended GaAs conduction-band (CB) states and (b) localized As-states with the extended GaN valence-band (VB) states. Bands are plotted vs the vacuum level.

host. C_{NCB} is a constant that describes the interaction between N-related and CB states. $C_{NCB} = 2.7\,\text{eV}$ and $E_N = 1.65\,\text{eV}$ can be assumed for GaAs-rich GaNAs from Refs. 132 and 133.

Due to the band anticrossing interaction between N-related and CB states, two highly non-parabolic subbands, $E_-(k)$ and $E_+(k)$, are formed. The dispersion of these subbands is given by Eq. (13):

$$E_\pm(k) = \frac{1}{2}\left[E_N + E_{CB}(k) \pm \sqrt{\left[E_N - E_{CB}(k)\right]^2 + 4C_{NCB}^2 x}\right]. \quad (13)$$

The electronic band structure of GaNAs diluted with As is sketched in Fig. 31(b). In this case, a resonant level corresponding to As atoms is located above the valence band (VB) of the GaN host. The interaction between As-related and VB states is modeled using a Hamiltonian analogous to the previous one

$$H_{\text{simplified}}^{\text{N-rich}} = \begin{pmatrix} E_{VB}(k) & C_{AsVB}\sqrt{x} \\ C_{AsVB}\sqrt{x} & E_{As} \end{pmatrix}, \quad (14)$$

where x is the mole fraction of substitutional As atoms, $E_{VB}(k)$ is the energy dispersion of the VB of the GaN host, E_{As} is the energy of As-related states, and C_{AsVB} is a constant describing the interaction between the As-related and VB states. According to previous work,[140] the coupling parameter $C_{AsVB} = 0.75\,\text{eV}$ and the As energy level located 0.62 eV above the VB in GaN can be adopted for GaN-rich GaNAs. In this case, highly non-parabolic subbands are formed in the VB as given by Eq. (15):

$$E_\pm(k) = \frac{1}{2}\left[E_{As} + E_{VB}(k) \pm \sqrt{\left[E_{As} - E_{VB}(k)\right]^2 + 4C_{AsVB}^2 x}\right]. \quad (15)$$

It is worth noting that the Hamiltonian in Eq. (14) is simplified, as in reality the VB is composed of three subbands. Therefore, the full Hamiltonian for the band anticrossing interaction in the VB should be composed of three subbands typical of WZ GaN and three As-related states associated with the p_x, p_y, and p_z symmetry. A Hamiltonian with three valence subbands and one As-related level (all states with spin up and spin down) was reported for GaNAs in Ref. 140 and subsequently applied to study of the electronic band structure in Refs. 141 and 142. To date, the full-valence BAC Hamiltonian with three host subbands and three resonant levels (all with spin up and spin down) has been used to describe the VB in dilute bismides, i.e., ZB III–V alloys with a few percent of Bi atoms with the band anticrossing interaction between the Bi-related and VB states.[143,144] As the parameters of the full-valence BAC model are not well established, the use of a simplified Hamiltonian as above is fully justified in many cases.

According to previous discussion, the BAC model is applied in the regime of low concentration of an isovalent dopant. However it is worth noting that this model has been also extended for full content range for some highly mismatched alloys including GaNAs and GaNSb.[129,145] In this review, we focus on bandgap engineering in WZ III-N compounds and therefore we limit to III-N compounds diluted with a few percent of group V atoms.

B. Phosphorus-diluted III-nitrides

P is the most similar group V atom to N in terms of size, ionicity, and electronegativity; see Fig. 1. In addition, the optimal growth temperature of GaP and AlP is the highest among ZB III–V compounds. Hence, the incorporation of P atoms into a III-N host is potentially the most promising from a thermodynamics perspective. To date, GaNP alloys have been grown via both MBE[146–150] and MOCVD.[151–159] However, the first GaNP layers were grown by the vapor-phase reaction during the initial development of III-N,[160–162] when understanding of HMAs was not yet sufficient.

Gonda *et al.*[146–148,150] deposited GaNP layers on (0001) sapphire substrates via gas-source MBE. Thermally cracked phosphine (PH_3) was used as a P source. Prior to the growth of the GaNP layer, a GaN buffer layer was deposited on the sapphire at a temperature of 750 °C. Next, the GaNP layer was grown by adding the PH_3 flow. The flow rate of PH_3 ranged from 0.1 to 1.0 SCCM and the PH_3 cracking

temperature was 750 °C. Under these growth conditions, it was possible to incorporate up to 1.5% P into the GaNP layers, but a phase separation was observed at the highest P concentration (1.5%).

The phase separation was also observed by Seong *et al.*[149] for $GaN_{1-x}P_x$ layers grown via gas-source MBE on (0001) GaN/sapphire at lower temperatures in the range 500–760 °C. Careful structural studies indicated that the samples grown at $T_g \leqslant 600$ °C undergo a phase separation, resulting in a mixture of GaN-rich and GaP-rich GaNP with a ZB structure. The samples grown at $T_g \geqslant 730$ °C were found to be binary ZB GaN(P) single-crystalline materials. This indicates that the GaNP alloy is very sensitive to the growth conditions and thus deposition of homogeneous GaNP layers is challenging.

A large incorporation of P atoms into GaNP films has been achieved in MOCVD at growth temperatures significantly lower than the optimal growth temperature of GaN layers (850–950 °C vs ~1050 °C).[151–153,155] Kikawa *et al.*[151] deposited GaNP layers on a (0001) sapphire substrate in a system with a pulsed ArF laser (192 nm line) to illuminate precursors before deposition. Tertiarybutylphosphine (TBP) was used as a P precursor. GaNP layers were deposited at 850–950 °C. At lower temperatures (<900 °C), the GaNP growth was island-like, resulting in a roughening of the surface morphology. The surface morphology was improved at temperatures above 900 °C. To improve the crystal quality, GaNP layers were annealed after growth at high temperatures (1000–1100 °C). Under these conditions, GaNP layers with P concentrations of up to 9% were achieved.[151] Moreover, the authors reported the growth of GaNP QWs with PL at ~400 nm at 77 K, and the fabrication of GaNP QW LEDs emitting at 425 nm at room temperature (RT); see Fig. 32.[152]

Chen *et al.*[153,155,158] reported the growth of GaNP layers with P concentrations of up to 15%. These layers were grown by means of light-radiation, low-pressure MOCVD on (0001) sapphire substrates with PH_3 as the P source. GaNP layers were deposited at a temperature of 925 °C on a GaN buffer layer deposited at a high temperature (980–1000 °C). Further studies of these layers suggest a phase separation.[157,158]

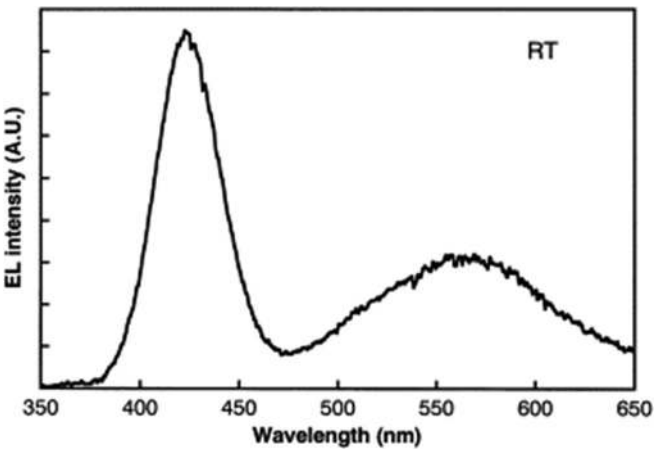

FIG. 32. Electroluminescence (EL) spectrum of GaNP QW LEDs. Reproduced with permission from Yoshida *et al.*, J. Cryst. Growth **237–239**, 1037 (2002). Copyright 2002 Elsevier.

Li *et al.*[156] deposited GaNP layers in MOCVD with a PH_3 precursor at the same growth temperature as used to grow the high-temperature GaN buffer layer, i.e., 1050 °C. The authors observed that the P incorporation was below 0.1% at this temperature. This indicates that the incorporation of P atoms at the optimal growth temperature for the III-N host is very low.

A decrease in P incorporation with increasing growth temperature was observed by Fehse *et al.*[159] for GaNP layers deposited on GaN/Si(111) substrates in a horizontal MOVPE reactor. The authors used PH_3 as the P source. The PH_3 flow and growth temperature were varied from 2.2–223 μmol/min and 800–1100 °C, respectively. Energy-dispersive x-ray measurements revealed a strong decrease in incorporated P with increasing growth temperature, from 4.4% at 900 °C to 3.1% at 1000 °C and 1.8% at 1100 °C, for samples grown with the lower phosphine flux. The samples were single-crystalline WZ-type epitaxial GaPN (0001) films, but x-ray and transmission electron diffraction measurements showed a reduction in both the *c*- and *a*-lattice parameters without a change in the WZ-type crystal structure. This indicates that P is incorporated as P^{3+} or P^{5+} likely substituting the Ga lattice sites of the GaN-crystal, i.e., the formation of $Ga_{1-x}P_xN$ and not $GaN_{1-x}P_x$ as might be expected. Substitution of Ga with P atoms was also reported by Tsuda *et al.*[154] for GaNP films grown by MOCVD with a PH_3 precursor at a temperature of 900 °C.

Theoretical studies of the solubility of P in GaN were performed by Wu *et al.*[163] The calculated *T*–*x* phase diagram for GaNP is shown in Fig. 33. According to these calculations, the incorporation of a few percent of P atoms into the GaN host does not pose a problem, but according to the previously discussed results, the growth of high-quality homogeneous GaNP films is a challenge. For GaNP films with a higher P content, phase separation effects and a variety of different phases have been observed.[159]

Only a few articles exist on DFT calculations of the electronic band structure and mechanical properties of III-N containing P.[164,165] No experimental studies on the growth of AlNP or InNP alloys diluted with P have been published to date.

C. Arsenic-diluted III-nitrides

Of the III-N diluted with As, only GaNAs alloys have been grown and studied experimentally.[166–179] Theoretical studies of the electronic band structure within DFT methods have been reported for

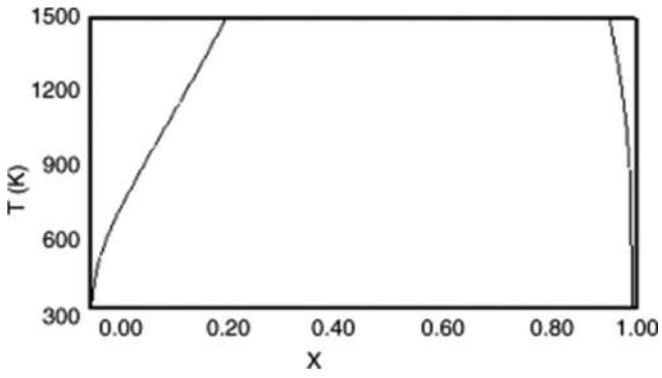

FIG. 33. Calculated *T*–*x* phase diagram for $GaN_{1-x}P_x$. Reproduced with permission from Wu *et al.*, Appl. Surf. Sci. **250**, 182 (2005). Copyright 2005 Elsevier.

GaNAs[142,180] and AlNAs.[181] Several experimental studies have been devoted to GaNAs alloys with high As concentrations, which are achieved at a very low growth temperature ($T < 300\,^{\circ}C$).[119–123,182–187] However, these alloys are out of the scope of this review, as the most promising alloys for bandgap engineering of III-N compounds appear to be those obtained at temperatures close to the optimal growth temperature of the III-N host.

Iwata *et al.*[166] grew GaNAs layers on (0001) sapphire substrates via gas-source MBE. Thermally cracked AsH_3 was used as the As source. Prior to growth of the GaNAs layer, a GaN buffer layer was deposited on the sapphire and subsequently a GaNAs layer was grown at 750 °C by adding AsH_3 flow. The flow rate of AsH_3 ranged from 0.1–1.0 SCCM. A large red shift in the PL peak was observed for GaNAs layers with As $\leq$ 0.24%. The maximum As concentration in GaNAs was 0.94%, and phase separation was observed under growth conditions of high AsH_3 flow rate.

Zhao *et al.*[167] deposited GaNAs layers on GaN/sapphire templates via gas-source MBE with AsH_3 as the As source, and found that As mainly acts as a surfactant that dramatically improves the surface morphology of GaN when the growth temperature is over 700 °C. GaNAs with 1% As was achieved when the growth temperature was as low as 500 °C. In addition, the authors measured optical absorption and concluded that GaNAs is a direct-bandgap material with a much lower bandgap, indicating a large bandgap bowing. For a GaNAs layer with 1% As, the bandgap was estimated to be ~2.5 eV at room temperature.[167]

Further growth of GaNAs by MBE[168–173] at high temperatures (~800 °C) leads to GaNAs layers with a strong PL at approximately 2.7 eV. The authors grew GaNAs layers on sapphire using As_2 (or As_4) molecules as an As source and varied the As fluxes across a very broad range. The As incorporation in GaNAs layers was found to be very low at ~0.2%. The PL spectra obtained for these layers are shown in Fig. 34.

In the context of the BAC model applied to GaNAs, the strong emission at ~2.7 eV and the absorption edge at ~2.5 eV observed by Zhao *et al.* were the first evidence of As-related impurity-like band formation in GaNAs. The impurity character of this band was confirmed by Zdanowicz *et al.*[173] via temperature-dependent studies of the absorption edge for GaNAs films grown by MBE. The authors observed that the incorporation of a small quantity of As atoms (As $\leqslant$ 0.6%) into the GaN host leads to a significant reduction in the bandgap due to the formation of an impurity-like band above the VB of the GaN host. The position of this band does not change with temperature on an absolute scale, as shown in Fig. 35, and therefore a reduced temperature dependence of the bandgap is observed for As-diluted GaNAs compared to the pure GaN host. The absorption coefficient α_0 in the investigated GaNAs alloys was found to be one order of magnitude weaker than that in GaN. Moreover, it confirms the impurity-like character of the E_+ band. According to the BAC model, the E_- band inherits the host character (that of GaN in this case), whereas the E_+ band has an impurity-like character; see Fig. 31(b) and Ref. 173.

Very low As incorporation into GaNAs films was observed in MOCVD, in which GaNAs layers were deposited at temperatures optimal (or close to optimal) for GaN deposition.[174–179] Tertiarybutylarsine ($C_4H_9AsH_2$, TBA) was used as an As source and sapphire as a substrate. All authors observed a significant increase in

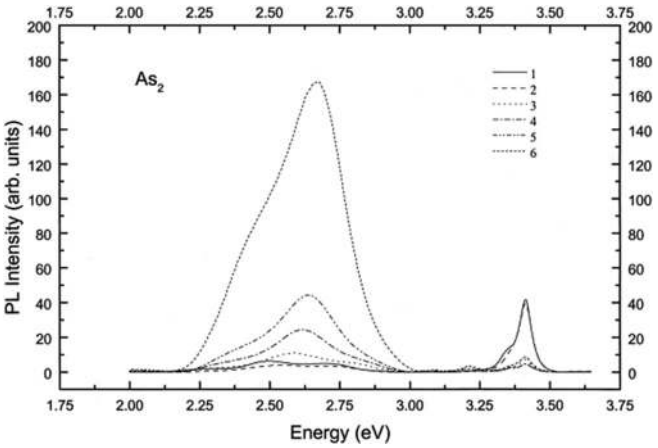

FIG. 34. Influence of As flux on the room-temperature PL of GaNAs films. 1 corresponds to background As, 2 to 1×10^{-7}, 3 to 5×10^{-7}, 4 to 1×10^{-6}, 5 to 3×10^{-6}, and 6 to 1×10^{-5} mbar. Reproduced with permission from Foxon *et al.*, J. Cryst. Growth **219**, 327 (2000). Copyright 2000 Elsevier.

As incorporation with decreasing growth temperature. Figure 36 shows the As concentration in GaNAs layers grown at different temperatures reported by Na.[179] Approaching the 1000 °C temperature required for the growth of high-quality GaN, almost no As incorporation is observed. To incorporate fractions of a percentage of As, the growth temperature has to be decreased below 900 °C. In this case, a maximal As concentration of ~0.9% was achieved for GaNAs layers grown at ~600 °C.

Kimura *et al.*[176] observed the same trend in temperature dependence of As concentration in GaNAs layers, but were able to achieve a significantly higher As concentration by properly varying the molar flow rates of precursors and the V/III ratio; see Fig. 37. GaNAs alloys with As content up to 6.4% were achieved by decreasing the growth temperature, decreasing the overall V/III ratio, and increasing the TBAs to the NH_3 ratio in the gas phase.

For GaNAs layers with larger As concentration (3.5% and 6.7%), Kimura *et al.*[176] observed the absorption edge to be significantly shifted compared to the GaN host; see Fig. 38. Detailed studies of the optical gap for GaNAs layers grown by MOVPE were reported in Ref. 177 and are summarized in Fig. 39.

D. Antimony-diluted III-nitrides

Sb is very different from N in terms of size, iconicity, and electronegativity. Therefore, the growth of III-N compounds diluted with Sb at temperatures typical for the III-N host is not simple. However, it is well known that Sb can work as a surfactant in MBE[188] and MOCVD[189–194] growth of III-N compounds, and therefore this issue has also been a subject of DFT studies.[195]

Surfactants are typically characterized by low vapor phase and low solubility in the epitaxial layer (epilayer). They affect surface properties, such as the surface energy and reconstruction. In addition, they change the surface kinetic processes of the growing surface. Thus, a small amount of surfactant impurities can significantly modify the growth characteristics and result in an epilayer structure without a

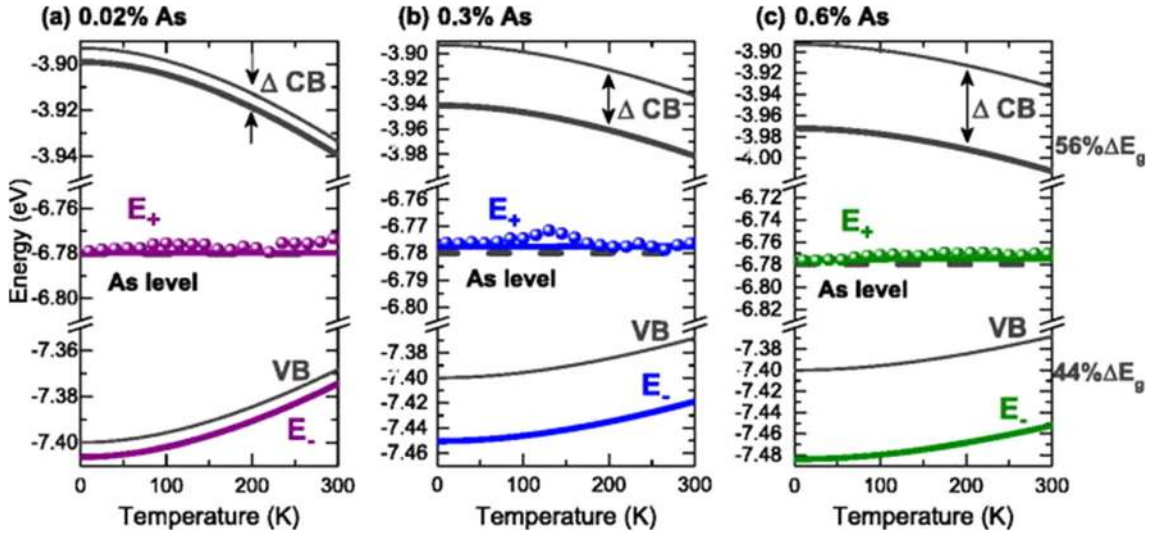

FIG. 35. Temperature dependence of particular band edge positions in relation to the vacuum level for samples containing 0.02% As, 0.3% As, and 0.6% As. Thin black lines represent the CB and VB edges in GaN. Thick black lines show the CB edge in the GaNAs alloy. Dashed lines indicate the As impurity level. Colored solid lines represent the E_+ and E_- subbands, whereas points show the E_+ levels determined experimentally. The composition-induced conduction-band shift is titled ΔCB. Reproduced with permission from Appl. Phys. Lett. **115**, 092106 (2019). Copyright 2019 AIP Publishing LLC.

high level of incorporation into the epilayer. Therefore, the motivation for using surfactants in MBE and MOCVD is to improve the structural and optical quality of epitaxial layers, i.e., surface roughness, intensity of PL, etc.

It has been shown that Sb significantly improves the optical quality of N-diluted GaInNAs QWs.[113,196] In addition, in this material system Sb can work as a substituent, which significantly modifies the electronic band structure.[113,197,198] This modification appears mainly in the VB.[113,197,198] Thus, the role of Sb in dilute nitrides can be twofold. This is possible because the incorporation of Sb into dilute nitrides is not limited by the growth temperature. In Fig. 30, it can be seen that the optimal growth temperatures for III–As and III–Sb are comparable to that for GaN. Therefore, the situation with Sb in III-N compounds is different from that in dilute nitrides.

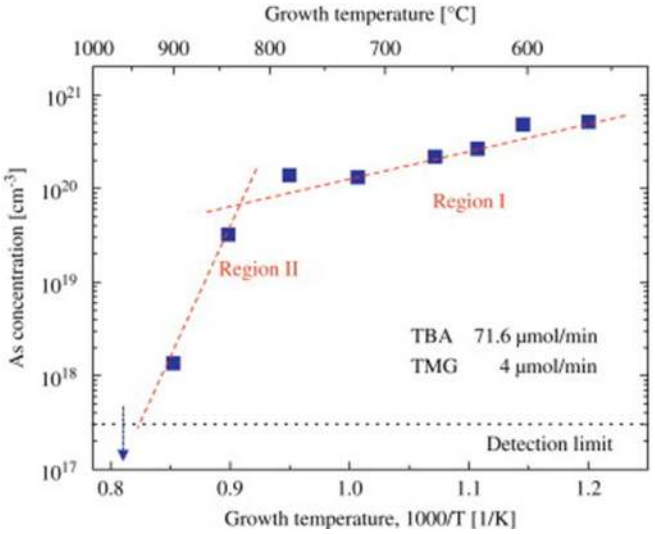

FIG. 36. As concentration characterized by SIMS for GaNAs layers grown at various temperatures (565–970 °C). As the detection limit of SIMS was 3×10^{17} cm^{-3}, and the As concentration in GaNAs grown at 970 °C could not be detected, this indicates that its concentration was below 3×10^{17} cm^{-3}. Reproduced with permission from H. Na, J. Cryst. Growth **312**, 2019 (2010). Copyright 2010 Elsevier.

In the regime of optimal growth temperatures for GaN (~800 °C for MBE and 1050 °C for MOCVD), Sb works as a surfactant and its incorporation into GaN is negligible. Pei *et al.*[188] reported significant improvement in the structural quality of GaN layers grown by MBE with the presence of Sb. The FWHM of the (0004) XRD peak narrowed from 140 to 80 arc sec due to Sb acting as an effective surfactant during growth. Zhang *et al.*[189,190] used triethylantimony (TESb) as a surfactant during the lateral epitaxial overgrowth (ELO) of GaN by MOVPE. The temperature was varied over the range of 1000–1100 °C. Adding Sb resulted in changes in the GaN surface morphology, a remarkable effect on facet formation, and increases in the growth rates of GaN during the ELO process. The role of TESb as a surfactant was also studied for GaNAs layers grown by MOVPE at 700 °C.[191] In this case, a decrease in growth rate and As content in the epilayer was observed with increasing TESb flow rate. Although Sb was not detected inside the epilayers, appreciable surface concentrations of Sb were measured, indicating a surface segregation of Sb during the growth. The Sb surfactant effect was also studied for GaInN layers and QWs.[192–195] A significant improvement in PL was reported for GaInN QWs emitting in the green spectral range,[194,195] but no improvement in the surface morphology was reported for the GaInN layers.[192] Because the intensities of the precursor (atom) streams and their

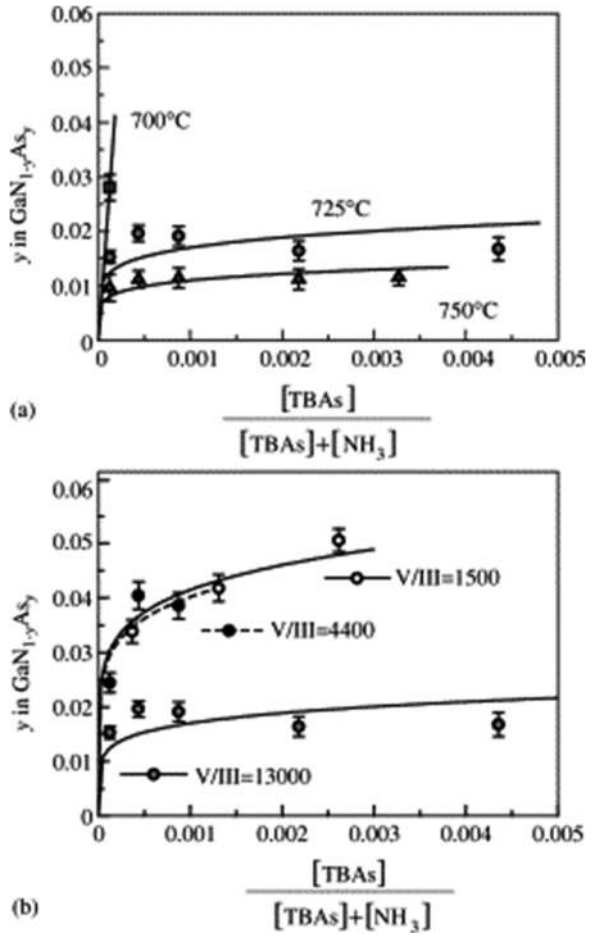

FIG. 37. As incorporation into the GaNAs layers increased through both (a) a decrease in growth temperature and (b) a decrease in the V/III ratio. Lines are guides for the reader. Reproduced with permission from Kimura *et al.*, J. Cryst. Growth **265**, 71 (2004). Copyright 2004 Elsevier.

interrelationships can be varied over wide ranges, the Sb surfactant effect has been investigated selectively in many cases to date. Therefore, further studies of the Sb-related surfactant effect will be very interesting for III-N compounds, including AlGaN and GaInN alloys.

It is possible to alloy GaN with GaSb over the whole concentration range[124–129,145] in the regime of low growth temperatures ($T < 300\,^{\circ}C$ for MBE), but the GaNSb films obtained under such conditions are polycrystalline or amorphous.[124,126,127,129] These alloys offer many interesting features and applications, which have been reviewed by Yu *et al.*[145] and are not discussed in this article. However, it is worth noting that GaNSb can be grown by MBE in a very broad range of temperatures.[124–129,199–203]

To improve the functionality of III-N compounds in semiconductor devices, good-quality crystalline GaNSb is needed. Such alloys can be achieved in the diluted Sb regime at moderate temperatures ($>500\,^{\circ}C$).[129,202,203] They can inherit the good structural and optical quality of the III-N host and include significant

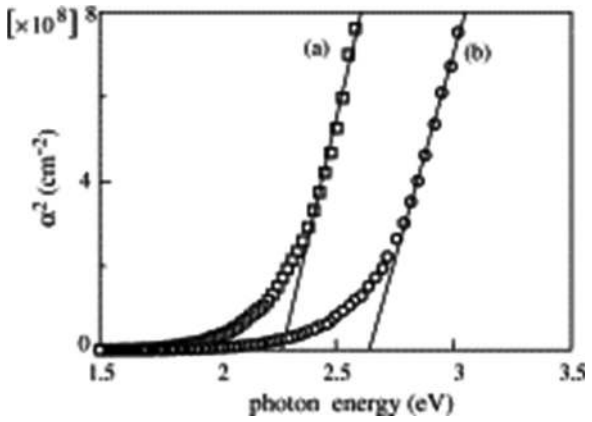

FIG. 38. Typical data obtained from optical absorption measurements on (a) a $GaN_{0.933}As_{0.067}$ sample, which was the sample with highest As content in the present study and (b) a $GaN_{0.965}As_{0.035}$ sample. The optical bandgap was obtained from the *x*-axis intercept calculated from a fit of the linear relationship to a plot of the square of the absorption coefficient, α, as a function of photon energy. Reproduced with permission from Kimura *et al.*, J. Cryst. Growth **265**, 71 (2004). Copyright 2004 Elsevier.

modifications in the electronic band structure that are associated with Sb incorporation.

It is also worth noting that Sb-diluted GaNSb alloys can be also achieved at low temperatures. They exhibit strong bandgap reduction due to Sb incorporation, as shown in Fig. 40, but no PL has been reported for such alloys. In general, a lack of PL can be attributed to poor optical and structural quality of layers grown at low temperatures, i.e., high concentrations of point defects and other imperfections. It is interesting to note that GaNSb films grown at low

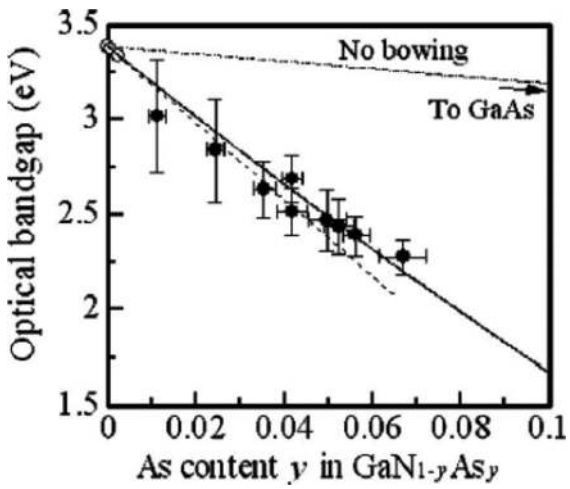

FIG. 39. As-content dependence of the optical bandgap within the GaNAs alloy. The open circles and dashed lines represent the data of Iwata *et al.*,[166] which yielded a bowing parameter value of 19.58 eV. The solid line and closed circles are the results of the experimental study, which yields an improved bowing parameter value of 16.9 ± 1.2 eV. Reproduced with permission from Appl. Phys. Lett. **84**, 1489 (2004). Copyright 2004 AIP Publishing LLC.

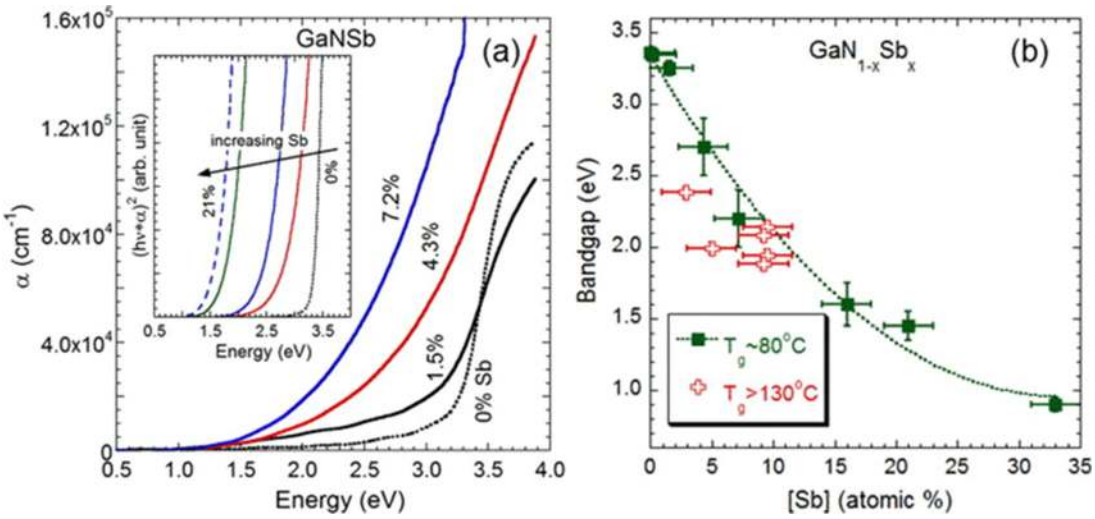

FIG. 40. Absorption coefficient α as a function of photon energy for films with different Sb content (in at. %). The inset shows the square of the product of α and energy, $(h\nu\cdot\alpha)^2$ for samples with different Sb contents. (b) Absorption edge energies for $GaN_{1-x}Sb_x$ alloys with different Sb contents obtained by linear extrapolation of the curves in (a). Reproduced with permission from Appl. Phys. Lett. **102**, 102104 (2013). Copyright 2013 AIP Publishing LLC.

temperatures exhibit a relatively sharp absorption edge, despite being amorphous.[125,145]

According to the BAC model, Sb-related states are located above the VB of the GaN host and interact strongly with the VB states, leading to the formation of the E_+ band. In the regime of low Sb concentration (Sb $\ll$ 1%), this band has an impurity-like character and is therefore weakly manifested in absorption. However, with increasing Sb concentration a strong absorption edge, associated with optical transitions between the E_+ band and CB, is clearly observed for the GaNSb layers as shown in Fig. 40.

As GaNSb is a direct-gap semiconductor, bandgap-related emission is expected for this alloy if it has sufficient optical quality. To date, a PL band that could be attributed to bandgap-related emission has been observed for GaNSb layers grown at relatively high temperatures (>500 °C).[127,199,202] For an example, see Fig. 41 from Ref. 199. The strong emission band observed in cathodoluminescence (CL) and PL at 2.2 eV is associated with the formation of a Sb-related impurity-like band in GaNSb. A similar emission band was observed for GaNAs alloys grown at higher temperatures; see Fig. 34 and Refs. 167–170. In this case, the band is associated with the formation of an As-related impurity-like band in GaNAs. The difference in the spectral position of this band (2.2 eV in GaNSb vs 2.7 eV in GaNAs) results mainly from the different energy positions of the Sb and As levels in the GaN host. The spectral position of this emission band also depends on the concentration of the isovalent dopant. A significant shift of this emission was observed by Chowdhury *et al.*[202] for GaNSb nanowires with various Sb concentrations.

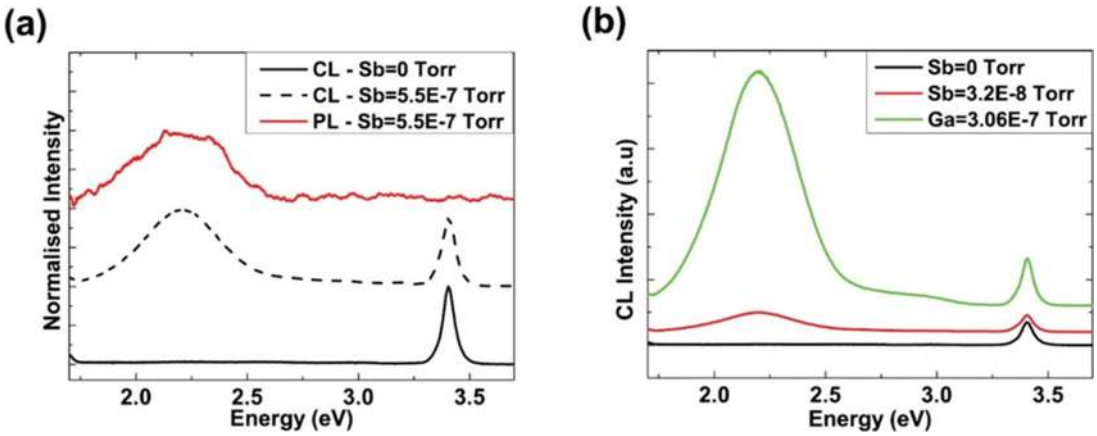

FIG. 41. (a) Typical room-temperature cathodoluminescence (CL) and PL spectra for samples with Ga flux = 2.3×10^{-7} Torr, with and without Sb, and (b) room-temperature CL spectra for samples with various Ga fluxes and fixed Sb flux = 3×10^{-8} Torr. Reproduced with permission from Shaw *et al.*, J. Phys. D **47**, 465102 (2014). Copyright 2014 IOP Publishing.

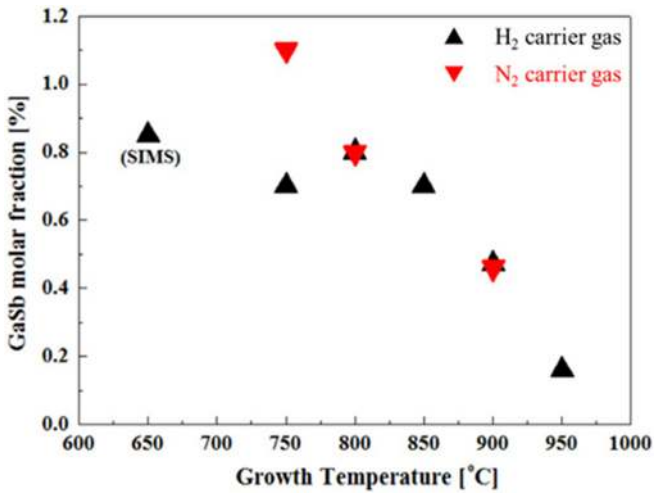

FIG. 42. GaSb molar fractions estimated from *c*-axis lattice constants of GaNSb layers grown with H_2 and N_2, as a function of growth temperature. Reproduced with permission from Komori *et al.*, Jpn. J. Appl. Phys., Part I **55**, 05FD01 (2016). Copyright 2016 The Japan Society of Applied Physics.

GaNSb layers diluted with Sb have been grown by MOCVD.[204–206] Moon *et al.*[204] deposited GaNSb layers on a (0001) sapphire substrate at various growth temperatures ranging from 770 to 970 °C. TMSb was used as an Sb precursor. A decrease in Sb incorporation into the GaNSb film from 0.05% to 0.005% was observed with an increase in growth temperature from 770 to 970 °C. An absorption band at ∼2 eV was detected for these films. A decrease in Sb incorporation with increasing growth temperature was observed by Komori *et al.*[206] for GaNSb layers deposited by MOCVD; see Fig. 42.

Sunkara *et al.*[205] grew GaNSb films by MOCVD with TMSb as a precursor at temperatures ranging from 565 to 640 °C. In this growth temperature range, which is significantly lower than those used by Moon[204] and Komori,[206] the authors obtained much higher Sb incorporation and observed a sharp absorption edge; see Fig. 43. This edge is significantly shifted compared to the GaN absorption edge, and is consistent with the absorption studies of GaNSb with ultra-low Sb concentration (0.005–0.05% Sb) performed by Moon *et al.*[204] These results are strong evidence for the formation of an Sb-related impurity-band in GaNSb, and support the interpretation that the strong emission at 2.0 eV is the bandgap-related emission in GaNSb.

This interpretation is consistent with the BAC model as well as with DFT calculations of the electronic band structure performed for Sb-diluted GaNSb.[202,207–209] Shi *et al.*[209] analyzed the Sb-related bandgap reduction in GaNSb by calculating the density of states (DOS) of the material. The authors found that the Sb atoms only contribute to the VB of GaSbN and introduce impurity states inside the bandgap of the GaN host at a low Sb concentration; see Fig. 44. They also found that the VB DOS of GaSbN below the zero point of the horizontal axis in Fig. 44 is very similar to that of pure GaN, indicating that the main effect of Sb is to introduce impurity states inside the bandgap of the GaN host. This shows that the sharp reduction in the bandgap and strong bandgap bowing of GaSbN are due to these impurity states. The authors also showed that Sb has very little influence on the CB.

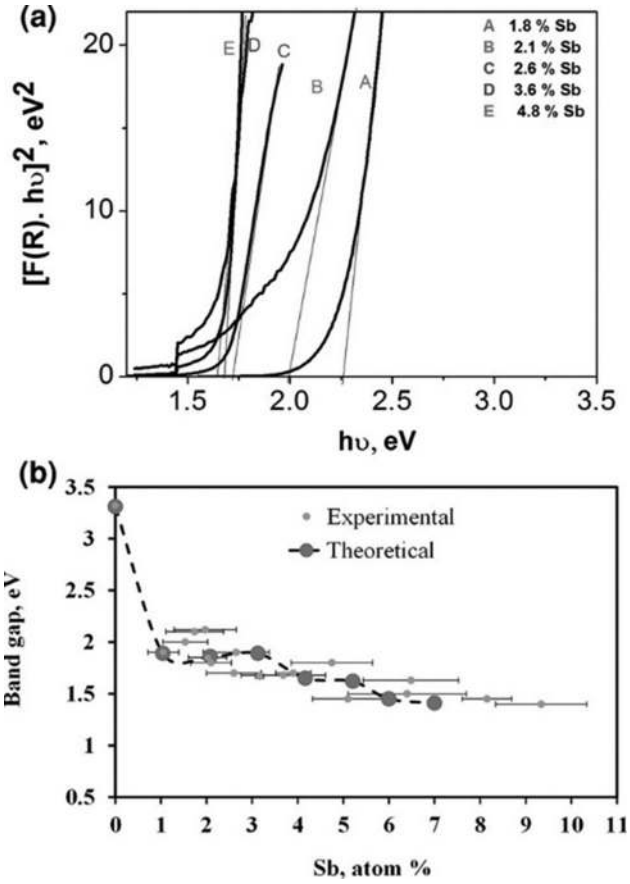

FIG. 43. (a) UV–vis absorption spectra of samples. (b) Experimental and theoretical energy bandgap of $Ga(Sb_x)N_{1-x}$ as a function of Sb concentration. Reproduced with permission from Sunkara *et al.*, Adv. Mater. **26**, 2878 (2014). Copyright 2014 Wiley.

E. Bismuth-diluted III-nitrides

III–Bi (AlBi, GaBi, and InBi) are compounds that have not yet been intensively explored experimentally, with AlBi and GaBi not even having been synthesized yet. Therefore, these compounds are not plotted in Fig. 30. However, their electronic band structure has been predicted by DFT study. It has been reported that AlBi is a narrow-gap semiconductor,[210] whereas GaBi and InBi are semimetals.[211–213]

In contrast, cubic III–V alloys with a few percent of Bi atoms (diluted bismides) have been very intensively explored in recent years,[144,214–218] as a small amount of Bi is an excellent bandgap-engineering component in these alloys.[144,214,215,217] The same is expected for III-N compounds diluted with Bi, but the difference between Bi and N in terms of size, ionicity, and/or electronegativity is larger than that between Sb and N. Therefore, GaNBi is a highly mismatched alloy and its growth poses a challenge.

To date, high Bi incorporation into GaNBi has been achieved by MBE in a low-temperature growth regime (∼100 °C)[130,131,219,220] similar to the high As incorporation into GaNAs and Sb into GaNSb, which were previously discussed.

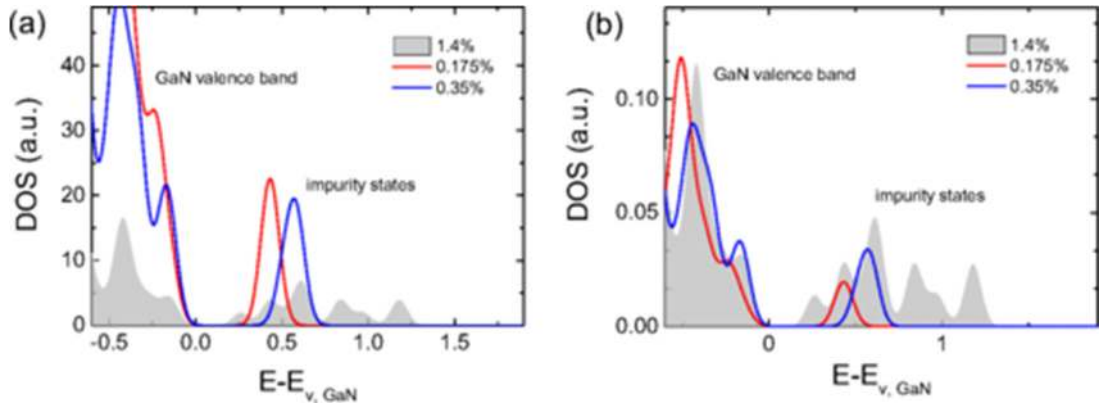

FIG. 44. DOS of $GaSb_xN_{1-x}$ at the VB side of the Fermi level. (a) Total DOS normalized to the same number of Sb atoms at different x. The band edge of GaN, $E_{v,\ GaN}$, is used as a reference to align the DOS at different Sb concentrations. (b) Total DOS per atom. For clarity, (a) and (b) do not include the calculated data at $x = 0.7\%$, 2.7%, or 5.6% as they are similar to the presented curves of $x = 0.35\%$ and 1.4%. Reproduced with permission from Shi *et al.*, Phys. Rev. Mater. **1**, 034602 (2017). Copyright 2017 American Physical Society.

In Ref. 130, the authors deposited GaNBi layers on (0001) sapphire and decreased the growth temperature from 700 to 100 °C to achieve Bi incorporation into GaN. They observed no Bi incorporation above 700 °C and a monotonous increase in Bi concentration with decreasing temperature, as shown in Fig. 45. At the same time a significant deterioration of sample crystallinity was observed with decreasing temperature. Despite this, a distinct absorption edge was observed in measurements; see Fig. 46. A monotonous increase in Bi concentration with increasing Bi equivalent beam pressure was observed for GaNBi films grown at very low temperatures (80–90 °C).[131,219] In this case, it was also observed that the sample crystallinity deteriorates with increasing Bi concentration. Thus, the low structural quality of GaNBi films can be attributed to both the low growth temperature and the high lattice mismatch, which is more strongly manifested at higher Bi concentrations.

Bi is also known as a surfactant, and this aspect has been studied in the growth of GaN layers by MBE[221–223] and MOCVD.[224] GaN layers were deposited on (0001) sapphire by MBE at 800 °C for a wide range of Bi fluxes.[221,222] The authors concluded that the incorporation of Bi is negligible in these conditions. In addition, the reported data show no significant improvement in the quality of the GaN film. Raman studies confirmed that the additional Bi flux favors the

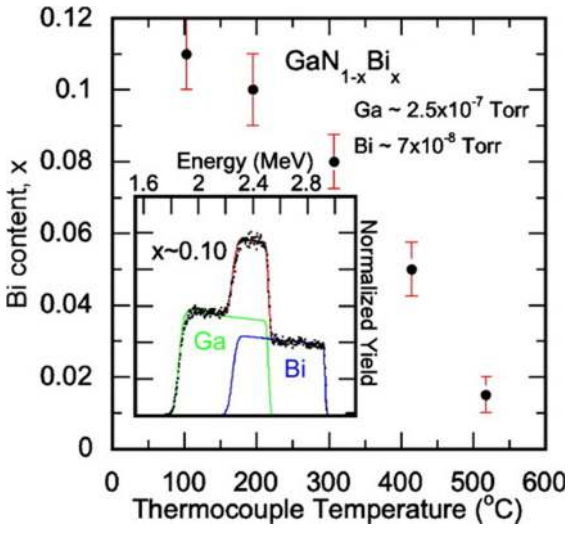

FIG. 45. Bi composition in $GaN_{1-x}Bi_x$ measured by RBS as a function of LT-MBE thermocouple temperature. The III–V ratio was approximately 1:1 and the films were homogeneous in the growth direction within the resolution limit of RBS. The inset contains a representative RBS spectrum for a film with $x \sim 0.10$. The blue, green, and red lines correspond to the Bi, Ga, and total simulated contributions to the spectrum, respectively. Reproduced with permission from Appl. Phys. Lett. **97**, 141919 (2010). Copyright 2010 AIP Publishing LLC.

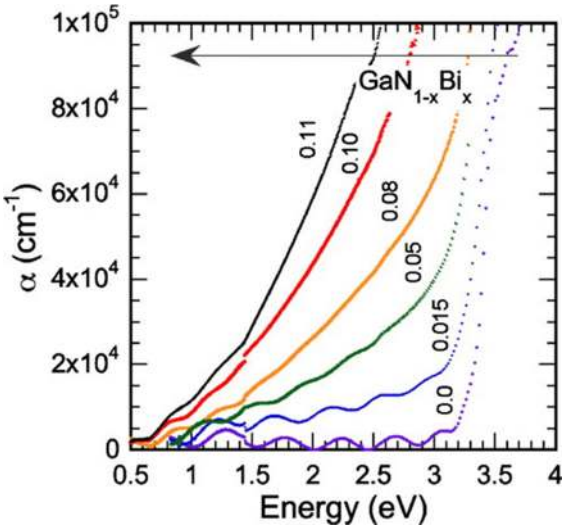

FIG. 46. Absorption spectra for $GaN_{1-x}Bi_x$ films grown at different growth temperatures. The composition of each film is given in the figure. Reproduced with permission from Appl. Phys. Lett. **97**, 141919 (2010). Copyright 2010 AIP Publishing LLC.

formation of submicrometer cubic domains, which results in layers with reduced crystalline quality and lower PL.[223]

Zhang *et al.*[224] deposited GaN layers on a (0001) sapphire substrate by MOVPE with TMBi as a surfactant at 1050 °C, which is the optimal growth temperature for GaN in MOVPE. The addition of TMBi during the growth resulted in a decrease in surface roughness as measured by atomic force microscopy. The symmetrical and asymmetrical x-ray rocking curves were narrowed slightly at low Bi gas-phase concentrations. No significant amount of Bi was incorporated over a broad range of gas-phase concentrations.

Based on the research carried out for GaNP, GaNAs, and GaNSb, a decrease in the substrate temperature in MOVPE growth can be expected to lead to the incorporation of Bi in the GaN layer. To date, only Sadi *et al.*[225] have reported a deposition of GaNBi layers by MOVPE under such conditions. The authors grew GaNBi layers on a (0001) sapphire substrate at 480 °C. TMBi was used as a precursor for Bi incorporation. A significant improvement in film roughness was observed with increasing TMBi flow rate, but the incorporation of Bi into GaNBi films was not determined.

Bi incorporation into GaN and AlGaN has also been a subject of theoretical studies. Bernardini *et al.*[226] found that the Bi solubility in GaN and AlGaN is very low and that Bi does not incorporate in GaN as an isoelectronic substitutional impurity. Under *n*-type and moderate *p*-type conditions, Bi behaves like a donor or an isoelectronic impurity substituting Ga at the cation site, whereas under extreme *p*-type conditions a multiple-donor Bi_N defect is formed that hinders efficient *p*-type doping.[226]

The electronic band structure and mechanical properties of GaNBi were studied by DFT methods. Strong bandgap bowing and significant mechanical bowing parameters (for the lattice constant, elastic constants, etc.) were observed in these studies,[227–229] as expected due to GaNBi being a highly mismatched alloy. To date, no articles have been published on the growth or theoretical study of Bi-diluted AlNBi or InNBi alloys.

F. Electronic band structure of P, As, Sb, and Bi diluted III-nitrides

Currently, DFT methods are the state-of-the-art approach to determine the many properties of semiconductor alloys. The electronic band structure of III-N compounds containing group V atoms was studied by DFT methods in several papers.[142,164,165,180,181,202,207–209,227] However, the phenomenological BAC model appears to be very rational approach in the first approximation to predict the bandgap and simulate the absorption spectrum, material gain, and other features of this material system. To date, the BAC model has been successfully applied to GaNAs[140,145,173] and GaNSb.[127,128,145]

As shown at the beginning of this section, two parameters are needed for the BAC model: the energy position of the isovalent dopant in the III-N host (E_V, V: P, As, Sb, and Bi) and the constant describing the repulsive BAC interaction between the isovalent dopant and the VB states of the III-N host ($C_{V\,VB}$, V: P, As, Sb, and Bi). These parameters are determined experimentally by fitting experimental data. The best approach to determine E_V and $C_{V\,VB}$ is to measure the energies of the E_- and E_+ transitions as a function of hydrostatic pressure.[132] Another approach is to determine the energy of these transitions for alloys with different isovalent dopant concentrations.[133] To date, much attention has been paid to the study of BAC parameters in dilute nitrides[106] and dilute bismides.[214] Some conclusions from this study may be used in the analysis of BAC parameters for group V diluted III-N compounds.

A summary of PL studies on group V diluted III-N is shown in Fig. 47(a). An extra PL band has been identified upon the incorporation of an isovalent group V dopant for GaNP,[152] GaNAs,[167–170] GaNSb,[127,199,202] and GaNBi.[221,222] This PL band can be interpreted as an emission between the CB and the impurity band, which is formed above the VB due to the incorporation of the isovalent dopant; see thick gray bars in Fig. 47(a). At the first approximation, the energy position of the impurity band corresponds to the E_V value needed for the BAC model. This is because this emission is observed for samples with ultralow concentration of isovalent dopants (i.e., samples obtained at high temperatures), and the change in CB position, associated with the incorporation of the isovalent dopant, is much smaller than that of the isovalent impurity band [$\Delta CB \ll \Delta VB$, as schematically shown in Fig. 47(a)]. From this analysis, E_V for the GaN host are determined and listed in Fig. 47(b), in which the positions of the CB and VB in AlN, GaN, and InN are plotted vs the vacuum level according to Ref. 230.

To date, group V diluted AlN and InN compounds have not been studied in PL because such samples have not yet been

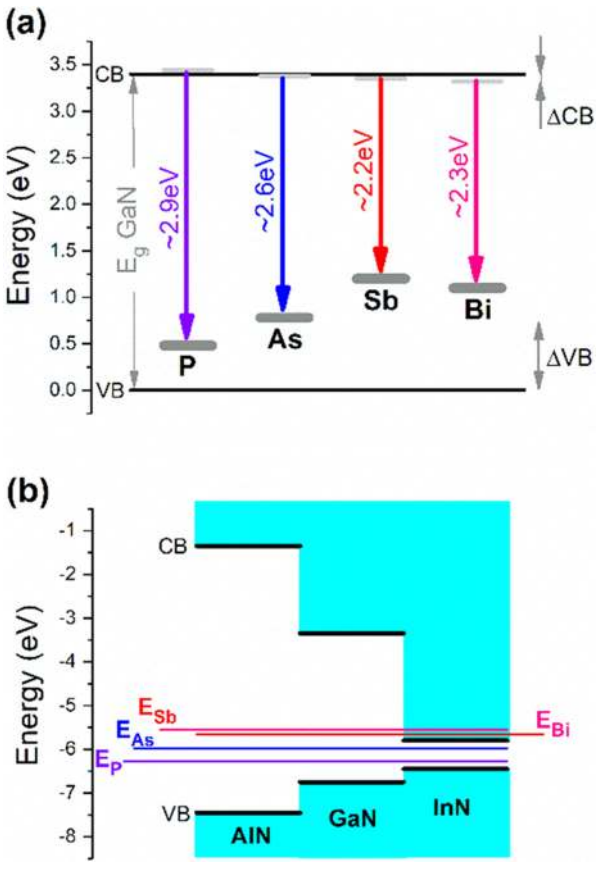

FIG. 47. (a) Emission bands in GaN with ultralow concentrations of P, As, Sb, and Bi. (b) Position of the E_V level (V: P, As, Sb, and Bi) in GaN and its extrapolation to AlN and InN.

synthesized, with a few exceptions; see InNAs in Ref. 124. Therefore, the E_V values from a PL study are unknown for these hosts. To find the E_V for AlN and InN, the P, As, Sb, and Bi levels can be extrapolated from GaN to AlN and InN, as shown in Fig. 47(b). This is a first approximation, in which the E_V in AlN and InN differ from that E_V in GaN by the VB offset. Finally, E_V must be determined experimentally for AlN and InN as its value can vary with the host, but the expected difference in E_V determined experimentally should be relatively small.

It is expected that the repulsive BAC interaction between the isovalent dopant and the VB states decreases when the difference between atom electronegativities decreases. This trend has been observed for dilute bismides,[214] and therefore the repulsive BAC interaction in dilute bismides is plotted in Fig. 48(a) together with those for GaNAs and GaNSb. The observed trend in both systems is very similar; see the green bars. Therefore, it can be assumed that the repulsive BAC interaction in GaNP, GaNBi, and other III(N, V) alloys should fulfill this trend in a first approximation. It is also worth noting that the repulsive BAC interaction in dilute nitrides is significantly larger ($E_N = 3.05$ eV for GaNP and $E_N = 2.7$ eV for GaNAs[132,133]). However, a comparison with dilute nitrides is not recommended in this case because of the interaction between *s*-like states in dilute nitrides. Here, the BAC repulsive reaction occurs in the VB between *p*-like states, and therefore it is better to compare this system with dilute bismides, in which the repulsive BAC interaction also takes place in the VB.

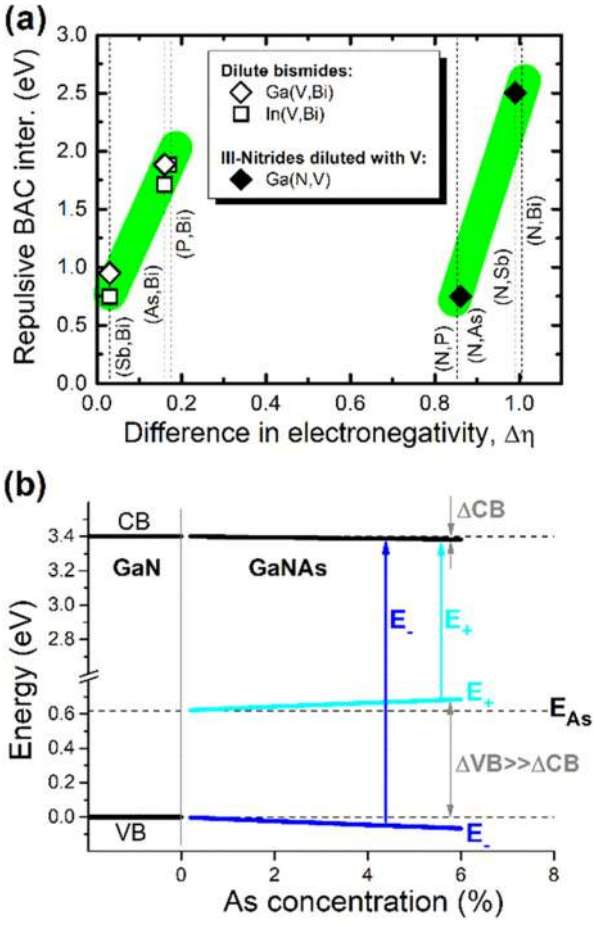

FIG. 48. (a) Repulsive BAC interaction in dilute bismides (open points) and V dilute III-N compounds (solid points). (b) As-related changes in the GaNAs electronic band structure obtained within the BAC model for different As concentrations.

Figure 48(b) shows the As-related changes in the electronic band structure of GaNAs. First, it is clearly seen that the main change in the energy gap is abrupt and results from the impurity-band formation. The bandgap of GaNAs corresponds to the E_+ transition in Fig. 48(b). With an increase in As concentration, a further change in the electronic band structure occurs in both the CB and VB. For the CB, this change can be calculated within the virtual crystal approximation, i.e., the CB position can be interpolated between GaN and GaAs. For the VB, this change is described by the BAC model. In both cases, these changes are much smaller than the E_{As} energy. This shows that the main bandgap engineering in this material system is due to impurity-band formation above the VB of the III-N host. Therefore, the isovalent impurity-related changes in the CB can be neglected in a first approximation.

Very similar changes in the electronic band structure take place for GaNP, GaNSb, and GaNBi. In the case of an AlN host, the situation is very similar, but for an InN host, it can change significantly because of its narrow bandgap. InN diluted with group V atoms appears to be a very interesting topic of exploration because of (i) the comparable growth temperature to other III–V compounds (see Fig. 30), and (ii) the interesting spectral range for mid-infrared emitters and detectors.

IV. APPLICATIONS IN DEVICES

Because the main motivation for studying semiconductors is their applications, this section reviews the current applications of (B, III)N and III–(N, V) semiconductors and discusses further prospects for the use of these materials.

A. BAlN/SiC templates for UV emitters

Inefficient light extraction from the active region of Al-rich AlGaN QWs grown on *c*-plane AlGaN templates or AlN substrates is one of the causes of low efficiency in LEDs operating in the UV-C region. This problem is associated with the polarization of spontaneous emission, which changes from TE to TM with increasing Al concentration.[10] For unstrained AlGaN, the TE/TM crossing appears at ∼6% Al but can be shifted to higher Al contents due to the built-in compressive strain, as shown in Fig. 49. To achieve light emission in the UV-C range, AlGaN QWs with higher Al concentration are needed and therefore the polarization of spontaneous emission poses a serious problem for light extraction, as shown in the sketch in Fig. 49.

As shown in Fig. 1, BAlN with ∼5% B is lattice-matched to 6H–SiC and thereby can be grown on SiC as a template. Because there is no lattice mismatch between $B_{0.05}Al_{0.95}N$ and 6H–SiC, it is expected that high-quality templates with significantly lower dislocation densities can be developed. Due to the high thermal conductivity of SiC and BN, it is also expected that such templates can solve basic problems with heat dissipation in UV-LEDs. However, the most important advantage of such templates is their smaller lattice constant, which allows introduction of a higher compressive strain to AlGaN QWs with high Al concentration and can change the polarization of emission from TM to the desired TE, as shown in Fig. 49. This strain

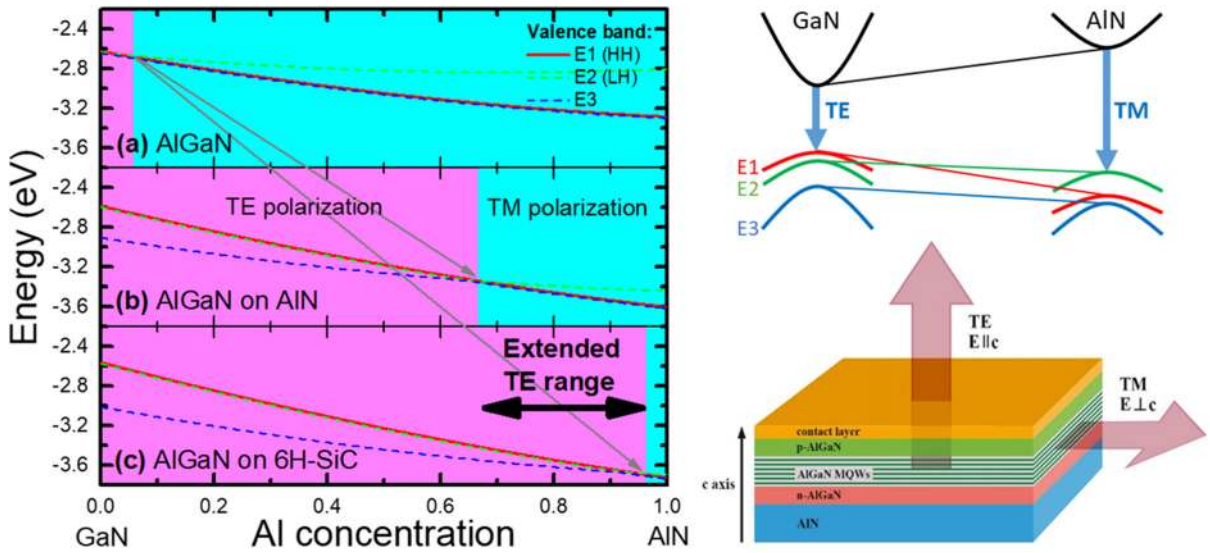

FIG. 49. Position of the VB (E1, E2, and E3 bands) in (a) GaN, (b) GaN strained on AlN, and (c) GaN strained on a BAlN/6H–SiC template.

engineering could be a key breakthrough for LEDs operating in the UV-C range. It is worth noting that the lattice constant engineering in this range (i.e., below the lattice constant of AlN) is possible only with BN, and the lattice matching with 6H–SiC provides a unique opportunity for the growth of thick BAlN templates with low dislocation densities.

B. AlGaN/GaN transistors

In AlGaN/GaN high-electron-mobility transistors (HEMTs), bulk GaN comprises the buffer but also serves as the electron carrier channel, which is located close to the interface. The unintentional impurities in GaN and the high threading dislocation density favor the current leakage phenomenon and limit the output power at high-frequency operation. To eliminate the current leakage, two strategies are realized: (i) doping the GaN buffer by Fe, C, or other dopants, which can improve the buffer resistivity and/or (ii) using wide bandgap materials such as AlGaN. BGaN can implement both of these strategies and is therefore a very interesting option for further optimization of AlGaN/GaN HEMTs. This problem has been studied experimentally[231] and theoretically.[232–235]

Ravindran *et al.*[231] have presented designs for GaN-based HEMTs that introduce BGaN back barrier layers. The authors found that the use of an ultrathin BGaN back barrier (BB) with a B content of 1% and a thickness of 1 nm significantly enhances the DC and RF performances of the transistors. An example of pulsed $I_{DS}(V_{GS}, V_{DS})$ characteristics for two transistors with and without a BGaN BB is shown in Fig. 50. In this case, the trapping phenomenon is reduced for the sample with the BB, which exhibits excellent behavior at high frequencies. At $V_{DS0} = 4$ V, the drop in current is 25.8% and 6.2% due to the gate and drain lag effects, respectively. BGaN BB layers in the studied HEMTs limit leakage in the GaN buffer due to two effects: a polarization-induced band discontinuity and a resistive barrier originating from the excellent insulation properties of BGaN. Hence, the AlGaN/GaN HEMTs grown with a BGaN BB showed significant improvement in static performances, transport properties, and trapping effects involving a limited current collapse in the dynamic regime.

C. BGaN-based neutron detectors

Semiconductor-based neutron detection devices require a material with a neutron capture element, a material with low γ-radiation detection sensitivity, and high-quality *pn* diode properties. For this purpose, ^{10}B atoms, which have large neutron-capture cross sections, could potentially be used in conjunction with GaN as a wide-gap semiconductor, which can distinguish neutrons from γ-rays because the γ-ray detection sensitivity of GaN is low.

This idea was utilized for the first time by Atsumi *et al.*[236] The authors fabricated proper BGaN Schottky diodes by optimizing the BGaN growth conditions. In this detector, the (n, α) reactions occur when neutrons are captured by the B atoms in BGaN. These reactions generate α-rays that can be converted to a signal in the base semiconductor, and the GaN distinguishes neutrons from γ-rays. The BGaN Schottky diode has sufficient α-ray detection capability, and successful neutron detection was realized using just this semiconductor material. Figure 51 shows a profile of the neutron detection signal provided by BGaN with two bias voltages. These results indicate that BGaN can be used to produce semiconductor neutron detectors.

D. Distributed Bragg reflectors (DBRs)

Monolithic distributed Bragg reflectors (DBRs) are essential components in the development of deep-UV photonics devices such as vertical-cavity surface-emitting lasers (VCSELs). To date, no VCSELs operating in the deep UV range have been demonstrated, partly due to the difficulty in developing highly reflective DBRs with a broad bandwidth. These difficulties are mainly related to the low contrast between the refractive indices of AlGaN and AlInN, as well as the lack of transparency of AlInN in the required UV range. The strong dependence of

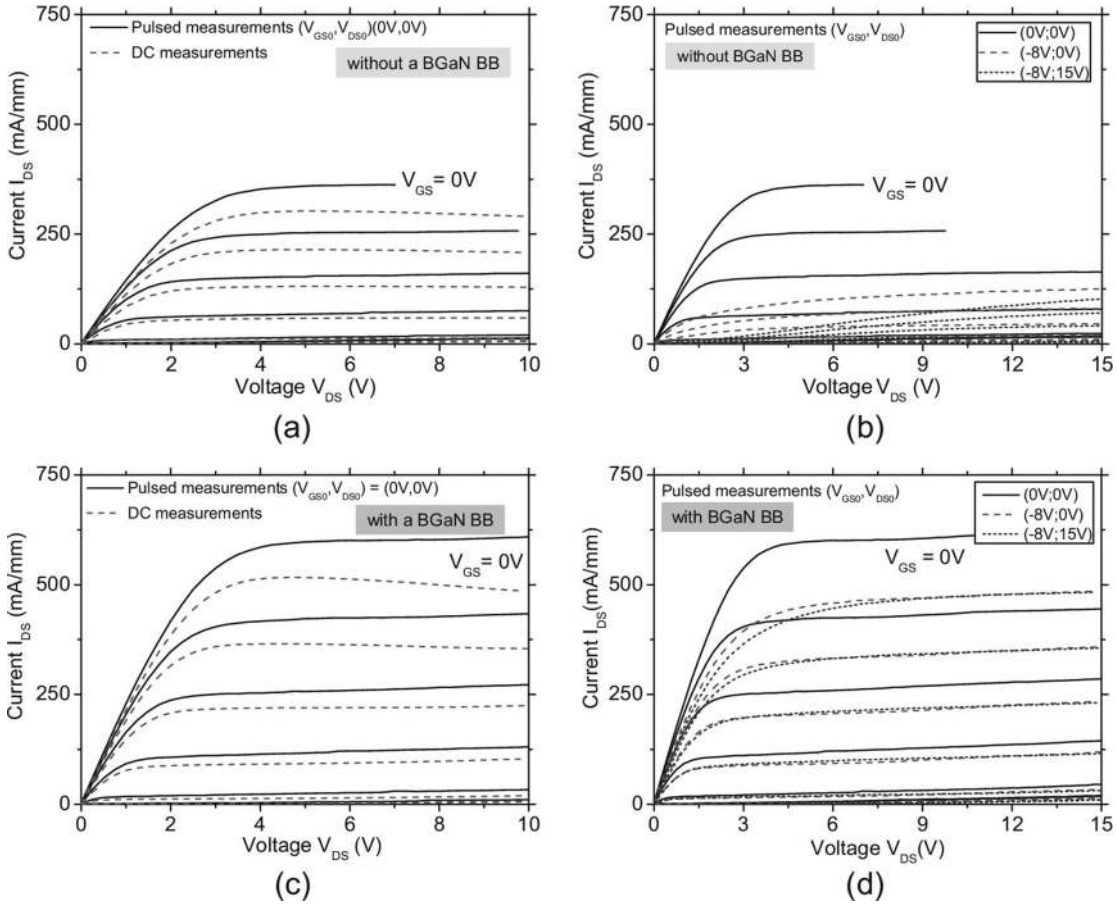

FIG. 50. $I_{DS}(V_{DS})$ DC measurement and pulsed regimes on a device without [(a) and (c)] and with [(b) and (d)] an ultrathin BGaN BB. (a) and (b) DC measurement and pulsed regime with a quiescent point at (V_{GS}, V_{DS}): (0 V, 0 V) and (c) and (d) DC measurement and pulsed regime with a quiescent point at (V_{GS}, V_{DS}): (0 V, 0 V), (−8 V, 0 V), and (−8 V, 15 V). Reproduced with permission from Appl. Phys. Lett. **100**, 243503 (2012). Copyright 2012 AIP Publishing LLC.

refractive index on increasing B content[44,48] and the BAlN transparency enable the development of BAlN-based DBRs for applications in the deep UV range.

Highly reflective deep-UV DBRs based on the BAlN material system have been grown by Abid *et al.*[48] The growth was performed at 1000 °C in a low-pressure MOVPE system using a TEB precursor as a B source on a 0.9 μm thick AlN layer on sapphire templates. Figure 52 shows the experimental and calculated reflectivity spectra of 18- and 24-period $B_{0.47}Al_{0.53}N$/AlN DBR structures. The 18-pair BAlN/AlN DBRs showed experimental peak reflectivity of 82% at 311 nm and a stop-bandwidth of 20 nm. The 24-pair DBRs reaching the deep UV wavelength of 282 nm exhibit a peak reflectivity of 60% and a bandwidth of 16 nm. The measured reflectivity is lower than the predicted reflectivity (97% and 99%, respectively), which was calculated using the transfer matrix method based on the refractive index values determined experimentally for the same material. The observed discrepancy between the measured and theoretically expected peak reflectivity is explained by the still poor-quality BGaN/AlN interfaces that were analyzed by transmission electron microscopy; see Fig. 52.

E. Light-emitting diodes

The development of III-N LEDs emitting in the UV and red spectral range is a challenge. Including B and group V elements to the bandgap engineering in III-N compounds extends the options and can solve some problems associated with strains, band offsets, or *p*-type doping. Regarding UV LEDs, the earlier discussed BAlN is an alloy that can be very useful because of the BAlN/SiC templates for LEDs operating in the UV-C range and UV BAl(Ga)N/AlN Bragg reflectors.

B incorporation in III-N compounds can be also interesting for LEDs operating in the green–red region. GaInN/GaN QWs are the active region of LEDs emitting blue and green light. Extending this emission to longer wavelengths requires higher In content, but for QWs grown on GaN substrates (or templates) this content cannot be too high because of the critical thickness limited by the compressive strain. Through the incorporation of B into GaInN QWs, it is possible to shift the emission to red because the B in the BGaInN/GaN QWs significantly reduces the compressive strain (i.e., it increases the critical thickness of BGaInN and allows higher In incorporation), and its influence on the BGaInN bandgap is negligible at a low B

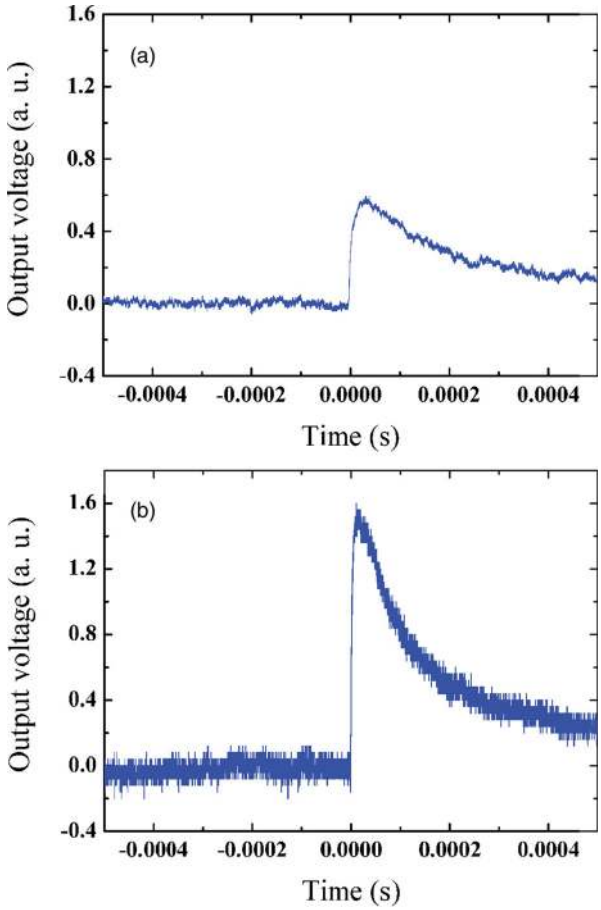

FIG. 51. Profile of the neutron detection signal provided by BGaN with bias voltages of (a) 3 V and (b) 5 V. Reproduced with permission from APL Mater. **2**, 032106 (2014). Copyright 2014 AIP Publishing LLC.

concentration due to high bandgap bowing. Therefore, from the perspective of the electronic band structure, BGaInN/GaN QWs are an excellent active region for red emitters, but the challenge is to grow BGaInN/GaN QWs with low point defect concentrations and high quantum efficiencies.

P, As, and Sb are the other elements capable of shifting the emission from III-N LEDs to longer wavelengths. A successful realization of LEDs with GaInNP QWs was reported by Yoshida *et al.*[237] several years ago. The authors grew an LED structure on a sapphire substrate by MOCVD. GaInNP QWs were deposited at 900 °C. The P and In concentrations in the GaInNP were determined by SIMS to be 5×10^{21} cm^{-3} and 3×10^{20} cm^{-3}, respectively. To improve the crystal quality, the structure was post-growth annealed at 1050 °C for 5 min. The electroluminescence (EL) from the GaInNP LED at various currents is shown in Fig. 53. This EL is observed at ∼420 nm. This spectral position is mainly attributed to the P incorporation because these atoms significantly change the bandgap in GaInNP, especially in the diluted regime; i.e., note that the formation of an impurity-like band appears at an energy significantly smaller than the bandgap of the host; see the E_+ band in Fig. 31(b). A further increase in the P concentration may be less beneficial for changing the emission wavelength, but an increase in the In concentration can be very beneficial in shifting the emission toward longer wavelengths. This result is the first evidence that the impurity-like band can be utilized in light emitters.

A strong PL band between the CB and the E_+ band was also reported by Chowdhury *et al.*[202] for GaNSb layers deposited by MOCVD. The authors used this emission band to fabricate a LED operating at 550 nm; see Fig. 54. The LED structure was grown on an n-type (111) Si substrate by MBE. GaNSb nanowires were deposited in the range 650–705 °C and the Sb concentration was estimated to be in the range of 0%–0.66%.

F. Water splitting

The direct conversion of sunlight into hydrogen by photoelectrochemical (PEC) water splitting is one of the most promising

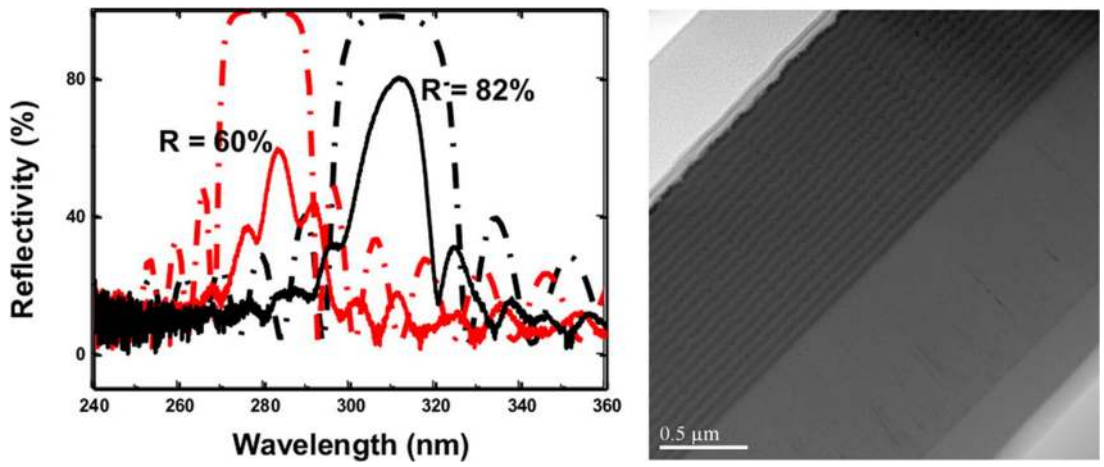

FIG. 52. (left panel) Experimental (dotted lines) and simulated (solid lines) reflectivity spectrum of 18/24-pair BAlN/AlN DBR. The spectra are centered at 311 and 282 nm, respectively. (right panel) Cross section of an 18-pair BAlN/AlN stack grown on an AlN template. Reproduced with permission from Appl. Phys. Lett. **100**, 051101 (2012). Copyright 2012 AIP Publishing LLC.

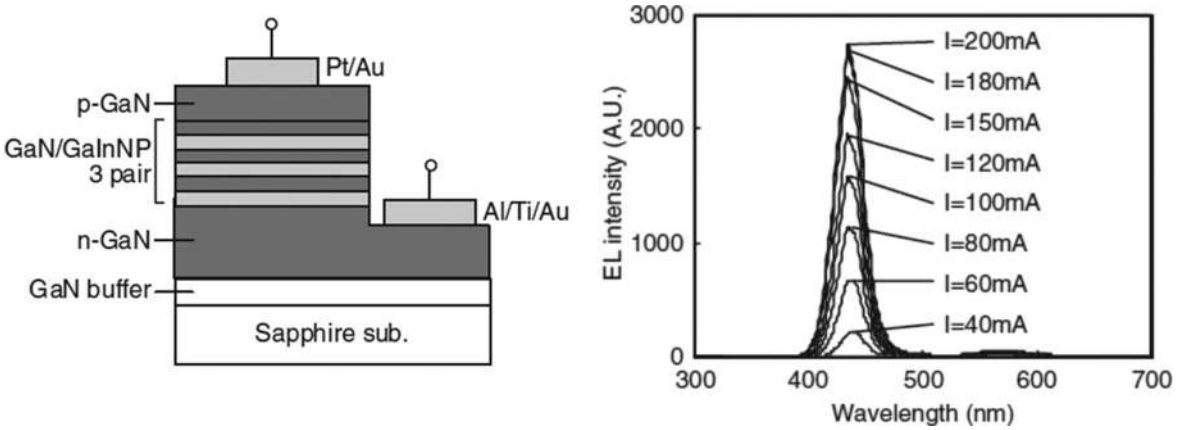

FIG. 53. (left panel) Schematic drawing of the GaInNP MQW structure. (right panel) EL spectra of GaInNP MQW LED. Reproduced with permission from Yoshida *et al.*, Phys. Status Solidi C **0**, 2236 (2003). Copyright 2003 John Wiley & Sons.

approaches to utilizing solar energy to produce clean fuels.[238,239] The key issue in this technology is the photoelectrode material, which must meet the relevant requirements. An ideal photoelectrode must meet three basic criteria: band edges straddling the H and O redox potentials located at ∼4.5 and ∼5.7 eV below the vacuum level, respectively,[239] a bandgap small enough to absorb a significant fraction of the solar spectrum, and corrosion stability. To date, it has been difficult to find a material that satisfies all these requirements. Recently, significant

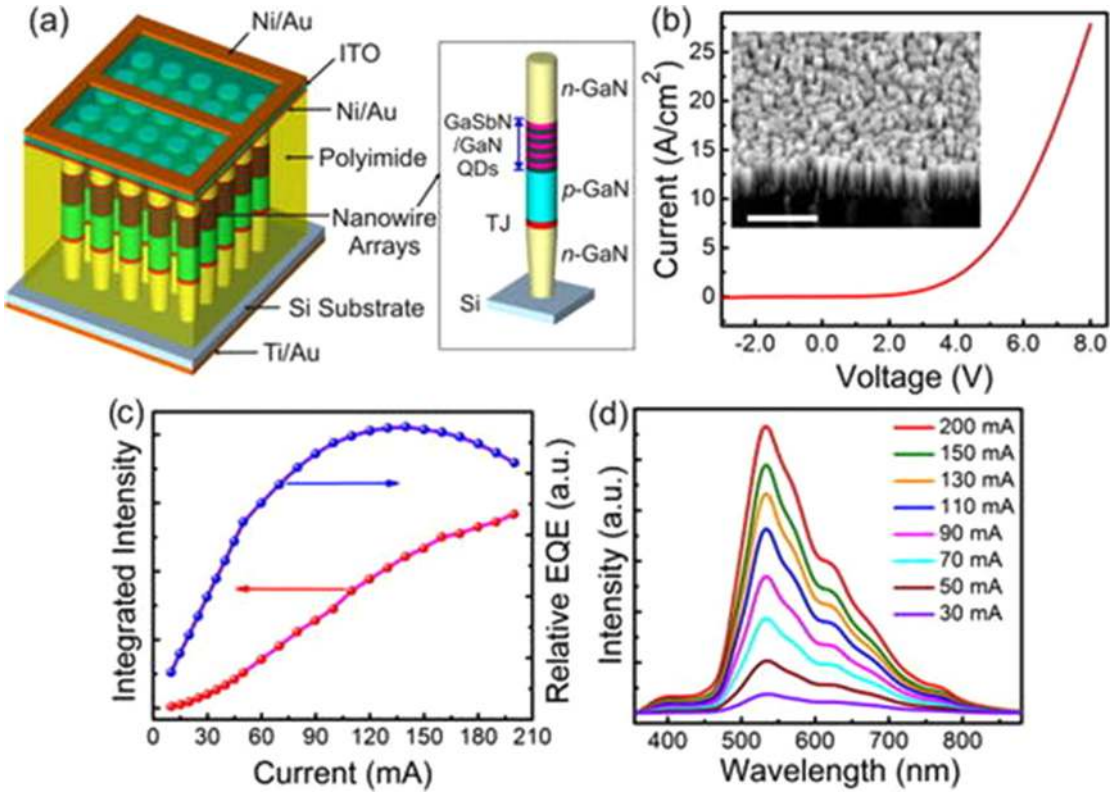

FIG. 54. (a) Schematic representation of the GaSbN/GaN dot-in-wire tunnel junction (TJ) LED structure. Schematic view of different layers incorporated in the nanowire arrays of GaSbN LEDs is also presented in the inset. (b) Room-temperature I–V characteristics of GaSbN LEDs. The inset shows the 45° tilted SEM image of as-grown GaSbN dot-in-nanowire arrays. Scale bar: 1 μm. (c) L–I characteristics and relative EQE of the GaSbN LEDs as a function of injection current. (d) EL spectra of the GaSbN LEDs under the pulsed biasing condition (10% duty cycle) at room-temperature. Reproduced with permission from Appl. Phys. Lett. **111**, 061101 (2017). Copyright 2017 AIP Publishing LLC.

attention has been drawn toward using GaN for water splitting,[240] as GaN is a corrosion-resistant semiconductor with the CB and VB energy straddling the redox potential and hence could be a good candidate for a photoelectrode for PEC water dissociation. However, the GaN bandgap is not small enough to absorb the solar spectrum. Therefore, proper bandgap engineering is needed for better utilization of GaN in water splitting. As the water oxidation potential is located ∼2 eV above the VB in GaN, the required bandgap reduction must be realized by an upward shift of the VB rather than a downward shift of the CB energy. This can be achieved by incorporation of As or Sb into the GaN host.[145] In this context, GaNSb has been quite intensively explored.[145,205]

Successful water splitting with a GaNSb electrode was achieved by Sunkara *et al.*[205] The authors showed that polycrystalline GaNSb films grown by MOCVD with small grain sizes (11 nm) are photoactive. They concluded that the photocurrent magnitude is limited by the shorter carrier-diffusion lengths due to the small grain sizes, limited film thickness for light absorption, and accumulation of charge carriers at the semiconductor–water interface. Figure 55 shows the photocurrent density vs light intensity for the water-splitting process with a GaNSb electrode at 0.9 V vs Ag/AgCl. In addition, the band edge positions of GaN, GaSb, and GaNSb vs the vacuum level are plotted in panel (a) together with the H (H_2O/H_2) and O (O_2/H_2O) redox potentials. The observed increase in the current density with light intensity and the transient decay associated with the current density [panel (b)] indicate that the low light absorption in the thin films and the interfacial charge accumulation are important factors limiting the photocurrents for the polycrystalline samples. The obtained current density at a high light intensity (ca. 700 μA cm^{-2} at 5 sun and 0.9 V vs Ag/AgCl) indicates that this material holds promise for solar water splitting.

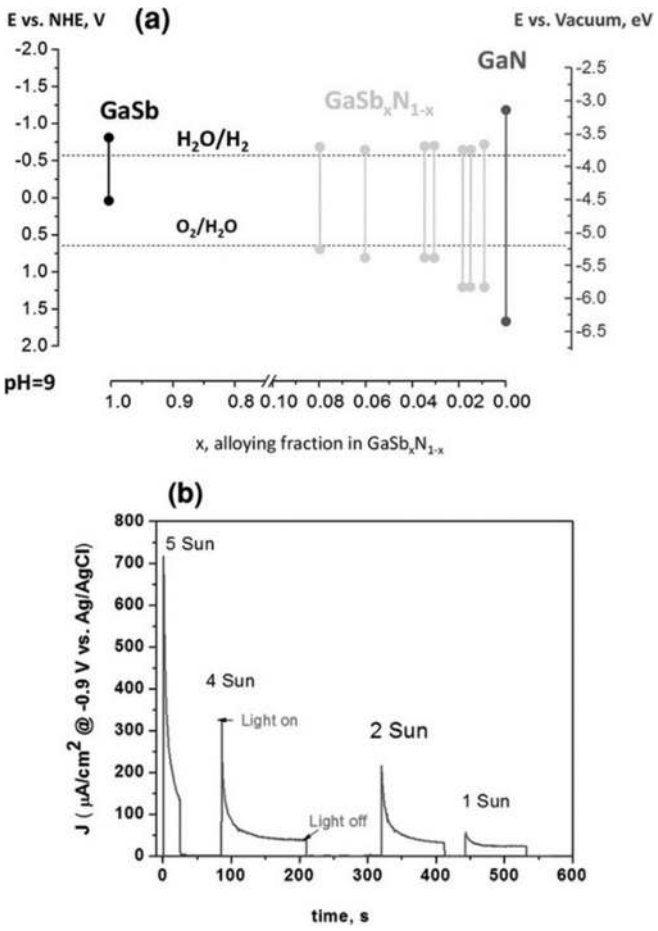

FIG. 55. (a) Energy diagram showing the band edge positions of $GaSb_xN_{1-x}$. The band edge positions of GaN and GaSb are also added for reference. (b) Photocurrent density vs light intensity for a $GaSb_xN_{1-x}$ sample at 0.9 V vs Ag/AgCl. Reproduced with permission from Sunkara *et al.*, Adv. Mater. **26**, 2878 (2014). Copyright 2014 John Wiley & Sons.

G. As-induced growth of microrods

As micro- and nanorods offer many interesting features that are not present in flat nanostructures, it is highly desirable to develop methods of growing such objects. A new mechanism of microrod growth was reported by Ciechanowicz *et al.*[118] The authors showed that the growth of GaN microrods can be induced by As in Ga-rich conditions due to the antisurfactant properties of As atoms under these growth conditions (i.e., high Ga flux and a high growth temperature of 800 °C, which is optimal for GaN in MBE). Under N-rich conditions, flat GaNAs layers with a low As concentration were obtained; see Fig. 56. The low incorporation of As into GaNAs film is due to the high growth temperature, and agrees with the previous discussion on MBE growth of GaNAs. In the case of As-induced GaN microrods, the incorporation of As inside the microrod core is negligible, but As is present at the surfaces of the microrods. This indicates that the growth of GaN microrods is a self-catalyst vapor–liquid–solid process with native Ga droplets. The formation of Ga droplets is induced by As and its presence during the epitaxial process promotes the growth of dodecagonal microrods with 12 walls: six *m*-planes and six *a*-planes.

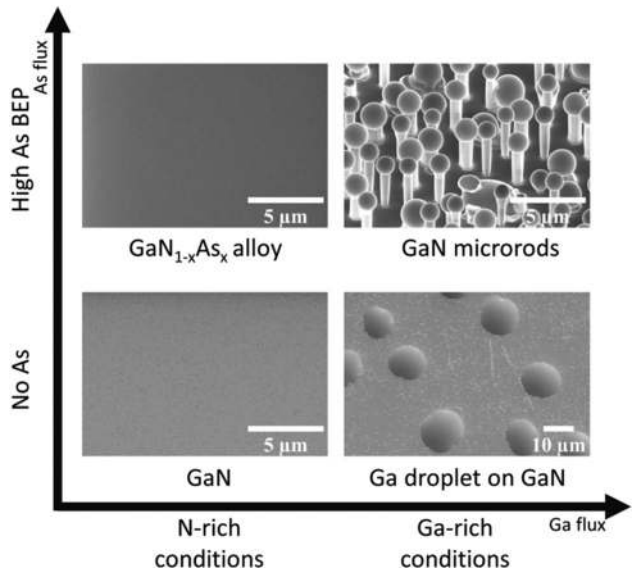

FIG. 56. Graph showing the optimum growth window for obtaining As-induced dodecagonal microrods.

It is worth noting that hexagonal GaN microrods with *m*-plane walls are usually formed as a result of faster growth rate for these walls. The growth of GaN microrods with six *m*-plane and six *a*-plane walls is possible because As changes the growth rates for GaN compared to As-free conditions. The obtained GaN microrods with GaNAs surfaces[118] are promising for water splitting and other applications in which an extended surface area is required, i.e., gas sensors, etc.

The results reported in Ref. 118 show that the introduction of As in the growth of III-N compounds under proper conditions opens new possibilities in the growth of microstructures. As the growth of semiconductor layers under metal-rich conditions is possible in other III-N compounds (AlN and InN), it will be very interesting to explore antisurfactant-induced growth of microrods for these materials as well. Moreover, it will be interesting to explore the roles of other group V atoms (P, Sb, and Bi) during epitaxy under metal-rich conditions. To date, the growth of III-N compounds under metal-rich conditions with the presence of P, Sb, or Bi has not been intensively explored.

V. SUMMARY AND FURTHER PERSPECTIVES

III-N compounds comprise a mature material system that has led to the development of many semiconductor devices (white LEDs, blue lasers, and high-power transistors) that are now widely used, but further development of bandgap engineering in III-N compounds cannot be limited to three compounds (AlN, GaN, and InN). It is obvious that this engineering will be increasingly expanded to include *w*-BN and other III–V compounds. An overview of this activity since the beginning of the development of III-N compounds has been presented in this work. Substantial activity in this subject comes from the research groups at the University of California at Santa Barbara, Lawrence Berkeley National Laboratory, Georgia Institute of Technology, NTT Basic Research Laboratories, University of Nottingham, University of Wisconsin, King Abdullah University of Science and Technology, Osaka University, and the University of California at San Diego. Moreover, a significant contribution to this subject originates from work performed at the Université des Sciences et de la Technologie d'Oran at Algeria, Otto-von-Guericke-Universität Magdeburg, Sandia National Laboratories, University of Michigan, Vilnius University, University of Louisville, Kohgakuin University, Carnegie Mellon University, Ulm University, Nanjing University, Shizuoka University, Seoul National University, University of Tokushima, and additional contribution has come from PORT at Wrocław. Our interest in this topic is due to the unusual bandgap engineering, which is typical for HMAs including dilute nitrides[106] and dilute bismides.[218] III-N compounds with a few percent of B or group V atoms belong to the family of HMAs.

Alloying III-N compounds with *w*-BN and other III–V compounds over the whole composition range is very difficult because of the widely contrasting growth temperatures of individual compounds, high lattice mismatches between them, and phase separation. However, in the diluted regime of isovalent dopants (B or group V atoms), this alloying is possible and can be beneficial in many cases. Therefore, the interest in bandgap engineering in III-N compounds with B and group V atoms should systematically increase. A summary of further perspectives on this subject with short comments is given below.

A. Strain engineering in III-N via B incorporation

Incorporation of a few percent of B in AlN and GaN is an important perspective in strain engineering. The small lattice constant of *w*-BN makes it possible to achieve quaternary alloys (BAlGaN, BAlInN, and BGaInN) that are lattice-matched to AlN and/or GaN, which can be utilized in Bragg reflectors. As the low concentration of B exerts almost no change on the bandgap due to the large bandgap bowing parameter, its low incorporation into GaInN/GaN QWs can be beneficial for shifting the emission wavelength to red due to the compressive strain reduction (it reduces the strain-related blueshift of the bandgap and allows higher In incorporation). In addition, developing $B_{0.05}Al_{0.95}N$/6H–SiC templates appears to be a promising perspective in developing deep UV emitters.

B. VB engineering in III-N compounds via group V incorporation

The formation of an impurity-like band in GaN upon the incorporation of a few percent of group V atoms is potentially interesting itself, as such a band can be utilized in multicolor emission in LEDs, intermediated absorption in solar cells, and broadened absorption of the solar spectrum in water-splitting devices. However, the isovalent doping of III-N compounds by group V can also be utilized to enhance *p*-type doping in AlGaN, in which the high activation energy of Mg dopants poses a significant problem. Moreover, incorporation of P or As into GaInN/GaN QWs can be very beneficial to shifting emission to longer wavelengths.

C. Ferromagnetism in GaN diluted with Mn and group V atoms

GaMnN is a quite intensively explored material due to its potential ferromagnetism at room temperature. Unfortunately, the *p*-type doping required for the exchange mechanism in this material is very challenging. An enhancement of *p*-type doping due to VB engineering via incorporation of group V atoms could be quite promising for GaMnN. In this case, a GaMnNAs:Mg or GaMnNSb:Mg alloy could be very interesting, but such alloys have not yet been synthesized. Analyzing the growth conditions for individual ternary alloys (GaMnN and GaNAs or GaNSb), the growth of quaternary alloys looks very promising.

D. Alloying InN with III–V compounds for mid-infrared applications

Because the growth temperature of InN is quite similar to those of III–V compounds, alloying these materials in a broad concentration regime is more achievable than alloying GaN or AlN with III–V compounds. However, this topic has not yet been explored. In relation to this, a well-developed (Ga, In, As, and Sb) technology exists for the mid-infrared spectral region, the development of III-N compounds has been concentrated in the visible and UV spectral region, and the growth of high-quality InN is difficult itself. However, InN-based technology can be an alternative approach to infrared and mid-infrared emitters. In this case, a narrow bandgap is expected because of the large bandgap bowing parameter for InN alloys diluted with group V atoms. This is due to the large differences in the electronegativity of the group V atoms.

E. Group V induced anti-surfactant growth of III-N microrods under metal-rich conditions

The growth of GaN under Ga-rich conditions with the presence of As leads to the growth of GaN microrods. This is possible because of the antisurfactant properties of As under these growth conditions. This demonstrates an example of growth engineering in III-N compounds via group V atoms. Further studies of this phenomenon for other materials (AlN and InN) grown under metal-rich conditions, and other group V atoms, is potentially very interesting as it is still an unexplored area.

ACKNOWLEDGMENTS

This work was performed with the Grant No. TEAM TECH/2016–3/16 from the Foundation for Polish Science (the European Regional Development Fund, POIR.04.04.00-00-3E14/16).

DATA AVAILABILITY

Data sharing is not applicable to this article as no new data were created or analyzed in this study.

REFERENCES

[1]I. Akasaki, "Nobel lecture: Fascinated journeys into blue light," Rev. Mod. Phys. **87**, 1119 (2015).
[2]H. Amano, "Nobel lecture: Growth of GaN on sapphire via low-temperature deposited buffer layer and realization of p-type GaN by Mg doping followed by low-energy electron beam irradiation," Rev. Mod. Phys. **87**, 1133 (2015).
[3]S. Nakamura, "Nobel Lecture: Background story of the invention of efficient blue InGaN light emitting diodes," Rev. Mod. Phys. **87**, 1139 (2015).
[4]H. Morkoc, *Handbook of Nitride Semiconductors and Devices, GaN Based Optical and Electronic Devices* (WILEY-VCH, Weinheim, 2009), Vol. 3.
[5]M. Beeler, E. Trichas, and E. Monroy, "III-nitride semiconductors for intersubband optoelectronics: A review," Semicond. Sci. Technol. **28**, 074022 (2013).
[6]M. H. Wong, S. Keller, N. S. Dasgupta, D. J. Denninghoff, S. Kolluri, D. F. Brown, J. Lu, N. A. Fichtenbaum, E. Ahmadi, U. Singisetti, A. Chini, S. Rajan, S. P. DenBaars, J. S. Speck, and U. K. Mishra, "N-polar GaN epitaxy and high electron mobility transistors," Semicond. Sci. Technol. **28**, 074009 (2013).
[7]S. Zhao, H. P. T. Nguyen, M. G. Kibria, and Z. Mi, "III-Nitride nanowire optoelectronics," Prog. Quantum Electron. **44**, 14–68 (2015).
[8]G. Li, W. Wang, W. Yang, Y. Lin, H. Wang, Z. Lin, and S. Zhou, "GaN-based light-emitting diodes on various substrates: A critical review," Rep. Prog. Phys. **79**, 056501 (2016).
[9]U. Chatterjee, J.-H. Park, D.-Y. Um, and C.-R. Lee, "III-nitride nanowires for solar light harvesting: A review," Renewable Sustainable Energy Rev. **79**, 1002–1015 (2017).
[10]D. Li, K. Jiang, X. Sun, and C. Guo, "AlGaN photonics: Recent advances in materials and ultraviolet devices," Adv. Opt. Photonics **10**, 43 (2018).
[11]*III-Nitride Ultraviolet Emitters—Technology and Applications*, Springer Series in Materials Science Vol. 227, edited by M. Kneissl and J. Rass (Springer, 2016).
[12]H. Amano, R. Collazo, C. de Santi, S. Einfeldt, M. Funato, J. Glaab, S. Hagedorn, A. Hirano, H. Hirayama, R. Ishii, Y. Kashima, Y. Kawakami, R. Kirste, M. Kneissl, R. Martin, F. Mehnke, M. Meneghini, A. Ougazzaden, P. Parbrook, S. Rajan, P. Reddy, F. Römer, J. Ruschel, B. Sarkar, F. Scholz, L. Schowalter, P. Shields, Z. Sitar, L. Sulmoni, T. Wang, T. Wernicke, M. Weyers, B. Witzigmann, Y.-R. Wu, T. Wunderer, and Y. Zhang, "The 2020 UV emitter roadmap," J. Phys. D: Appl. Phys. **53**, 503001 (2020).
[13]Y.-N. Xu and W. Y. Ching, "Calculation of ground-state and optical properties of boron nitrides in the hexagonal, cubic, and wurtzite structures," Phys. Rev. B **44**, 7787 (1991).
[14]N. E. Christensen and I. Gorczyca, "Optical and structural properties of III-V nitrides under pressures," Phys. Rev. B **50**, 4397 (1994).
[15]K. Kim, W. R. L. Lambrecht, and B. Segall, "Elastic constants and related properties of tetrahedrally bonded BN, AlN, GaN, and InN," Phys. Rev. B **53**, 16310 (1996).
[16]K. Shimada, T. Sota, and K. Suzuki, "First-principles study on electronic and elastic properties of BN, AlN, and GaN," J. Appl. Phys. **84**, 4951 (1998).
[17]K. Shimada, T. Sota, K. Suzuki, and H. Okumura, "First-principles study on piezoelectric constants in strained BN, AlN, GaN," Jpn. J. Appl. Phys., Part I **37**, 1421 (1998).
[18]A. Janotti, S.-H. Wei, and D. J. Singh, "First-principles study of the stability of BN and C," Phys. Rev. B **64**, 174107 (2001).
[19]S. Q. Wang and H. Q. Ye, "First-principles study on elastic properties and phase stability of III–V compounds," Phys. Status Solidi B **240**, 45–54 (2003).
[20]Y. Al-Douri, "Structural phase transition of boron nitride compound," Solid State Commun. **132**, 465–470 (2004).
[21]R. Ahmed, Fazal-e-Aleem, S. J. Hashemifar, and H. Akbarzadeh, "First principles study of structural and electronic properties of different phases of boron nitride," Phys. B **400**, 297–306 (2007).
[22]S.-P. Gao, "Cubic, wurtzite, and 4H-BN band structures calculated using GW methods and maximally localized Wannier functions interpolation," Comput. Mater. Sci. **61**, 266–269 (2012).
[23]M. Ustundag, M. Aslan, and B. G. Yalcin, "The first-principles study on physical properties and phase stability of Boron-V (BN, BP, BAs, BSb and BBi) compounds," Comput. Mater. Sci. **81**, 471–477 (2014).
[24]C. E. Dreyer, J. L. Lyons, A. Janotti, and C. G. Van de Walle, "Band alignments and polarization properties of BN polymorphs," Appl. Phys. Express **7**, 031001 (2014).
[25]A. Said, M. Debbichi, and M. Said, "Theoretical study of electronic and optical properties of BN, GaN and $B_xGa_{1-x}N$ in zinc blende and wurtzite structures," Optik **127**, 9212–9221 (2016).
[26]M. Zhang and X. Li, "Structural and electronic properties of wurtzite $B_xAl_{1-x}N$ from first-principles calculations," Phys. Status Solidi B **254**, 1600749 (2017).
[27]K. K. Liu, H. D. Sun, F. AlQatari, W. Z. Guo, X. W. Liu, J. T. Li, C. G. T. Castanedo, and X. H. Li, "Wurtzite BAlN and BGaN alloys for heterointerface polarization engineering," Appl. Phys. Lett. **111**, 222106 (2017).
[28]J. X. Shen, D. Wickramaratne, and C. G. Van de Walle, "Band bowing and the direct-to-indirect crossover in random BAlN alloys," Phys. Rev. Mater. **1**, 065001 (2017).
[29]L. Weston, D. Wickramaratne, and C. G. Van de Walle, "Hole polarons and p-type doping in boron nitride polymorphs," Phys. Rev. B **96**, 100102(R) (2017).
[30]L. Lymperakis, "Ab-initio study of boron incorporation and compositional limits at GaN and AlN (0001) surfaces," AIP Adv. **8**, 065301 (2018).
[31]T. Akiyama, K. Nakamura, and T. Ito, "Effects of lattice constraint on structures and electronic properties of BAlN and BGaN alloys: A first-principles study," Appl. Phys. Express **11**, 025501 (2018).
[32]Y. Hasegawa, T. Akiyama, A. M. Pradipto, K. Nakamura, and T. Ito, "Empirical interatomic potential approach to the stability of graphitic structure in BAlN and BGaN alloys," J. Cryst. Growth **504**, 13 (2018).
[33]Y. Hasegawa, T. Akiyama, A. M. Pradipto, K. Nakamura, and T. Ito, "Theoretical investigations on the structural stability and miscibility in BAlN and BGaN alloys: Bond-order interatomic potential calculations," Jpn. J. Appl. Phys., Part I **58**, SCCB21 (2019).
[34]H. M. H. Ahmed, H. Benaissa, A. Zaoui, and M. Ferhat, "Exploring new insights in BAlN from evolutionary algorithms ab initio computations," Phys. Lett. A **383**, 1385 (2019).
[35]S. Sridara, R. Kumara, and K. C. H. Kumar, "Thermodynamic modelling of Al-B-N system," Calphad **65**, 291–298 (2019).
[36]T. Soma, A. Sawaoka, and S. Saito, "Characterization of wurtzite type boron nitride synthesized by shock compression," Mater. Res. Bull. **9**, 755–762 (1974).
[37]M. Sokolowski, "Deposition of wurtzite type boron nitride layers by reactive pulse plasma crystallization," J. Cryst. Growth **46**, 136 (1979).
[38]B. P. Singh, "Characterization of wurtzitic boron nitride compacts," J. Mater. Sci. **22**, 495–498 (1987).
[39]A. Inaba and A. Yoshiasa, "Low-temperature heat capacity of wurtzite-type boron nitride," Jpn. J. Appl. Phys., Part I **36**, 5644 (1997).

[40]A. Y. Polyakov, M. Shin, W. Qian, M. Skowronski, D. W. Greve, and R. G. Wilson, "Growth of AlBN solid solutions by organometallic vapor-phase epitaxy," J. Appl. Phys. **81**, 1715 (1997).
[41]T.-c. Zhang, S. Yu, D.-m. Li, W.-l. Guo, C.-x. Gao, and G.-t. Zou, "Wurtzite boron nitride crystal growth in the region of cubic boron nitride crystal synthesizing," Chin. Phys. Lett. **15**, 70 (1998).
[42]M. Shibata, M. Kurimoto, J. Yamamoto, T. Honda, and H. Kawanishi, "GaN/BAlN heterostructure grown on a (0001)6H–SiC substrate by metalorganic vapor phase epitaxy," J. Cryst. Growth **189–190**, 445–447 (1998).
[43]V. K. Gupta, C. C. Wamsley, M. W. Koch, and G. W. Wicks, "Molecular beam epitaxy growth of boron-containing nitrides," J. Vac. Sci. Technol., B **17**, 1246 (1999).
[44]S. Watanabe, T. Takano, K. Jinen, J. Yamamoto, and H. Kawanishi, "Refractive indices of $B_xAl_{1-x}N$ (x = 0–0.012) and $B_yGa_{1-y}N$ (y = 0–0.023) epitaxial layers in ultraviolet region," Phys. Status Solidi C **0**, 2691–2694 (2003).
[45]A. Nakajima, Y. Furukawa, H. Yokoya, and H. Yonezu, "Growth of $B_xAl_{1-x}N$ layers using decaborane on SiC substrates," J. Cryst. Growth **278**, 437 (2005).
[46]T. Akasaka and T. Makimoto, "Flow-rate modulation epitaxy of wurtzite AlBN," Appl. Phys. Lett. **88**, 041902 (2006).
[47]T. Akasaka, Y. Kobayashi, and T. Makimoto, "Nonpolar AlBN and films grown on SiC substrates," Appl. Phys. Lett. **91**, 041914 (2007).
[48]M. Abid, T. Moudakir, G. Orsal, S. Gautier, A. En Naciri, Z. Djebbour, J.-H. Ryou, G. Patriarche, L. Largeau, H. J. Kim, Z. Lochner, K. Pantzas, D. Alamarguy, F. Jomard, R. D. Dupuis, J.-P. Salvestrini, P. L. Voss, and A. Ougazzaden, "Distributed Bragg reflectors based on diluted boron-based BAlN alloys for deep ultraviolet optoelectronic applications," Appl. Phys. Lett. **100**, 051101 (2012).
[49]A. Nagakubo, H. Ogi, H. Sumiya, K. Kusakabe, and M. Hirao, "Elastic constants of cubic and wurtzite boron nitrides," Appl. Phys. Lett. **102**, 241909 (2013).
[50]T. L. Williamson, N. R. Weisse-Bernstein, and M. A. Hoffbauer, "Growth of ternary wurtzite BAlN and BGaN by ENABLE-MBE," Phys. Status Solidi C **11**, 462 (2014).
[51]X. Li, S. Sundaram, Y. E. Gmili, T. Moudakir, F. Genty, S. Bouchoule, G. Patriarche, R. D. Dupuis, P. L. Voss, J. P. Salvestrini, and A. Ougazzaden, "BAlN thin layers for deep UV applications," Phys. Status Solidi A **212**, 745 (2015).
[52]X. Li, S. Sundaram, Y. E. Gmili, F. Genty, S. Bouchoule, G. Patriache, P. Disseix, F. Réveret, J. Leymarie, J.-P. Salvestrini, R. D. Dupuis, P. L. Voss, and A. Ougazzaden, "MOVPE grown periodic AlN/BAlN heterostructure with high boron content," J. Cryst. Growth **414**, 119–122 (2015).
[53]X. Li, S. Wang, H. Liu, F. A. Ponce, T. Detchprohm, and R. D. Dupuis, "100-nm thick single-phase wurtzite BAlN films with boron contents over 10%," Phys. Status Solidi B **254**, 1600699 (2017).
[54]H. Sun, Y. J. Park, K.-H. Li, C. G. Torres Castanedo, A. Alowayed, T. Detchprohm, R. D. Dupuis, and X. Li, "Band alignment of $B_{0.14}Al_{0.86}N/Al_{0.7}Ga_{0.3}N$ heterojunction," Appl. Phys. Lett. **111**, 122106 (2017).
[55]S. Wang, X. Li, A. M. Fischer, T. Detchprohm, R. D. Dupuis, and F. A. Ponce, "Crystal structure and composition of BAlN thin films: Effect of boron concentration in the gas flow," J. Cryst. Growth **475**, 334–340 (2017).
[56]M. Deura, K. Kutsukake, Y. Ohno, I. Yonenaga, and T. Taniguchi, "Nanoindentation measurements of a highly oriented wurtzite-type boron nitride bulk crystal," Jpn. J. Appl. Phys., Part I **56**, 030301 (2017).
[57]B. Vishal, R. Singh, A. Chaturvedi, A. Sharma, M. B. Sreedhara, R. Sahu, U. Bhat, U. Ramamurty, and R. Datta, "Chemically stabilized epitaxial wurtzite-BN thin film," Superlattices Microstruct. **115**, 197–203 (2018).
[58]O. Rettig, J. P. Scholz, N. Steiger, S. Bauer, T. Hubacek, M. Zikova, Y. L. Li, H. Y. Qi, J. Biskupek, U. Kaiser, K. Thonke, and F. Scholz, "Investigation of boron containing AlN and AlGaN layers grown by MOVPE," Phys. Status Solidi B **255**, 1700510 (2018).
[59]S. Wang, K. March, F. A. Ponce, and P. Rez, "Identification of point defects using high-resolution electron energy loss spectroscopy," Phys. Rev. B **99**, 115312 (2019).
[60]C. P. Yadav and D. K. Pandey, "Pressure dependent ultrasonic characterization of nano-structured w-BN," Ultrasonics **96**, 181–184 (2019).
[61]Y. Liu, G. Zhan, Q. Wang, D. He, J. Zhang, A. Liang, T. E. Moellendick, L. Zhao, and X. Li, "Hardness of polycrystalline wurtzite boron nitride (wBN) compacts," Sci. Rep. **9**, 10215 (2019).
[62]A. Segura, R. Cuscó, T. Taniguchi, K. Watanabe, G. Cassabois, B. Gil, and L. Artús, "Nonreversible transition from the hexagonal to wurtzite phase of boron nitride under high pressure: Optical properties of the wurtzite phase," J. Phys. Chem. C **123**, 20167–20173 (2019).
[63]P. Vuong, A. Mballo, S. Sundaram, G. Patriarche, Y. Halfaya, S. Karrakchou, A. Srivastava, K. Krishnan, N. Y. Sama, T. Ayari, S. Gautier, P. L. Voss, J. P. Salvestrini, and A. Ougazzaden, "Single crystalline boron rich B(Al)N alloys grown by MOVPE editors-pick," Appl. Phys. Lett. **116**, 042101 (2020).
[64]Y. L. Godeca, D. Martinez-Garciab, V. L. Solozhenkoc, M. Mezouard, G. Syfossea, and J. M. Besson, "Compression and thermal expansion of rhombohedral boron nitride at high pressures and temperatures," J. Phys. Chem. Solids **61**, 1935 (2000).
[65]T. Oku, K. Hiraga, T. Matsuda, T. Hirai, and M. Hirabayashi, "Twin structures of rhombohedral and cubic boron nitride prepared by chemical vapor deposition method," Diamond Relat. Mater. **12**, 1138–1145 (2003).
[66]C. B. Samantaray and R. N. Singh, "Review of synthesis and properties of cubic boron nitride (c-BN) thin films," Int. Mater. Rev. **50**(6), 313–344 (2005).
[67]R. R. Wills, "Wurtzitic boron nitride–A review," Int. J. High Technol. Ceram. **1**, 139–153 (1985).
[68]S. P. S. Arya and A. Damico, "Preparation, properties and applications of boron-nitride thin-films," Thin Solid Films **157**, 267–282 (1988).
[69]W. J. Zhang, Y. M. Chong, I. Bello, and S. T. Lee, "Nucleation, growth and characterization of cubic boron nitride (cBN) films," J. Phys. D: Appl. Phys. **40**, 6159–6174 (2007).
[70]J. Wang, F. Ma, and M. Sun, "Graphene, hexagonal boron nitride, and their heterostructures: Properties and applications," RSC Adv. **7**, 16801 (2017).
[71]V. L. Solozhenko, Dokl. Akad. Nauk SSSR **301**, 147 (1988).
[72]E. Tani, T. Soma, A. Sawaoka, and S. Saito, Jpn. J. Appl. Phys. **14**, 1605 (1975).
[73]E. Rapoport, Ann. Chim. Fr. **10**, 607 (1985); L. Vel, G. Demazeau, and J. Etourneau, "Cubic boron nitride: Synthesis, physicochemical properties and applications," Mater. Sci. Eng. B **10**, 149–164 (1991).
[74]V. L. Solozhenko and V. Ya. Leonidov, Zh. Fiz. Khim. **62**, 3145 (1988) [Russ. J. Phys. Chem. **62**, 1646 (1988) (in English)].
[75]I. Vurgaftman and J. R. Meyer, "Band parameters for nitrogen-containing semiconductors," J. Appl. Phys. **94**, 3675 (2003).
[76]C. E. Dreyer, A. Janotti, C. G. Van de Walle, and D. Vanderbilt, "Correct implementation of polarization constants in wurtzite materials and impact on III-nitrides," Phys. Rev. X **6**, 021038 (2016).
[77]I. Vurgaftman, J. R. Meyer, and L. R. Ram-Mohan, "Band parameters for III–V compound semiconductors and their alloys," J. Appl. Phys. **89**, 5815 (2001).
[78]F. Bernardini and V. Fiorentini, "Nonlinear macroscopic polarization in III-V nitride alloys," Phys. Rev. B **64**, 085207 (2001).
[79]V. V. Ilyasov, T. P. Zhadanova, and I. Y. Nikiforov, "Electronic energy structure and x-ray spectra of GaN and $B_xGa_{1-x}N$ crystals," Phys. Solid State **48**, 654–662 (2006).
[80]M. B. Kanoun and S. Goumri-Said, "Theoretical study of structural parameters and energy gap composition dependence of $Ga_{1-x}B_xN$ alloys," Semicond. Sci. Technol. **23**, 125036 (2008).
[81]M. E. Turiansky, J.-X. Shen, D. Wickramaratne, and C. G. Van de Walle, "First-principles study of bandgap bowing in BGaN alloys," J. Appl. Phys. **126**, 095706 (2019).
[82]A. Y. Polyakov, M. Shin, M. Skowronski, D. W. Greve, R. G. Wilson, A. V. Govorkov, and R. M. Desrosiers, "Growth of GaBN ternary solutions by organometallic vapor phase epitaxy," J. Electron. Mater. **26**, 237–242 (1997).
[83]V. Vezin, S. Yatagai, H. Shiraki, and S. Uda, "Growth of $Ga_{1-x}B_xN$ by molecular beam epitaxy," Jpn. J. Appl. Phys. **36**, L1483 (1997).
[84]C. H. Wei, Z. Y. Xie, J. H. Edgar, K. C. Zeng, J. Y. Lin, H. X. Jiang, J. Chaudhuri, C. Ignatiev, and D. N. Braski, "MOCVD growth of GaBN on 6H-SiC (0001) substrates," J. Electron. Mater. **29**, 452–456 (2000).

[85]A. Ougazzaden, S. Gautier, C. Sartel, N. Maloufi, J. Martin, and F. Jomard, "BGaN materials on GaN/sapphire substrate by MOVPE using N_2 carrier gas," J. Cryst. Growth **298**, 316–319 (2007).

[86]T. Akasaka, Y. Kobayashi, and T. Makimoto, "BGaN micro-islands as novel buffers for growth of high-quality GaN on sapphire," J. Cryst. Growth **298**, 320–324 (2007).

[87]A. Ougazzaden, S. Gautier, T. Moudakir, Z. Djebbour, Z. Lochner, S. Choi, H. J. Kim, J.-H. Ryou, R. D. Dupuis, and A. A. Sirenko, "Bandgap bowing in BGaN thin films," Appl. Phys. Lett. **93**, 083118 (2008).

[88]G. Orsal, N. Maloufi, S. Gautier, M. Alnot, A. A. Sirenko, M. Bouchaour, and A. Ougazzaden, "Effect of boron incorporation on growth behavior of BGaN/GaN by MOVPE," J. Cryst. Growth **310**, 5058–5062 (2008).

[89]M. Abid, T. Moudakir, Z. Djebbour, G. Orsal, S. Gautier, A. En Naciri, A. Migan-Dubois, and A. Ougazzaden, "Blue–violet boron-based distributed bragg reflectors for VCSEL application," J. Cryst. Growth **315**, 283–287 (2011).

[90]S. Gautier, G. Patriarche, T. Moudakir, M. Abid, G. Orsal, K. Pantzas, D. Troadec, A. Soltani, L. Largeau, O. Mauguin, and A. Ougazzaden, "Deep structural analysis of novel BGaN material layers grown by MOVPE," J. Cryst. Growth **315**, 288–291 (2011).

[91]A. Kadys, J. Mickevičius, T. Malinauskas, J. Jurkevičius, M. Kolenda, S. Stanionytė, D. Dobrovolskas, and G. Tamulaitis, "Optical and structural properties of BGaN layers grown on different substrates," J. Phys. D: Appl. Phys. **48**, 465307 (2015).

[92]T. Malinauskas, A. Kadys, S. Stanionyte, K. Badokas, J. Mickevicius, J. Jurkevicius, D. Dobrovolskas, and G. Tamulaitis, "Growth of BGaN epitaxial layers using close-coupled showerhead MOCVD," Phys. Status Solidi B **252**, 1138–1141 (2015).

[93]K. Ueyama, H. Mimura, Y. Inoue, T. Aoki, and T. Nakano, "Effect of substrate offcut angle on BGaN epitaxial growth," Jpn. J. Appl. Phys., Part I **55**, 05FD05 (2016).

[94]J. Jurkevičius, J. Mickevičius, A. Kadys, M. Kolenda, and G. Tamulaitis, "Photoluminescence efficiency of BGaN epitaxial layers with high boron content," Phys. B **492**, 23–26 (2016).

[95]R. C. Cramer, B. Bonef, J. English, C. E. Dreyer, C. G. Van de Walle, and J. S. Speck, "Growth of coherent BGaN films using BBr_3 gas as a boron source in plasma assisted molecular beam epitaxy editors-pick," J. Vac. Sci. Technol., A **35**, 041509 (2017).

[96]B. P. Gunning, M. W. Moseley, D. D. Koleske, A. A. Allerman, and S. R. Lee, "Phase degradation in $B_xGa_{1-x}N$ films grown at low temperature by metalorganic vapor phase epitaxy," J. Cryst. Growth **464**, 190–196 (2017).

[97]B. Bonef, R. Cramer, and J. S. Speck, "Nanometer scale composition study of MBE grown BGaN performed by atom probe tomography featured," J. Appl. Phys. **121**, 225701 (2017).

[98]J. Mickevičius, M. Andrulevicius, O. Ligor, A. Kadys, R. Tomašiūnas, G. Tamulaitis, and E.-M. Pavelescu, "Type-II band alignment of low-boron-content BGaN/GaN heterostructures," J. Phys. D: Appl. Phys. **52**, 325105 (2019).

[99]K. Ebara, K. Mochizuki, Y. Inoue, T. Aoki, K. Kojima, S. F. Chichibu, and T. Nakano, "Impact of growth temperature on the structural properties of BGaN films grown by metal-organic vapor phase epitaxy using trimethylboron," Jpn. J. Appl. Phys., Part I **58**, SC1042 (2019).

[100]M. A. Reshchikov and H. Morkoç, "Luminescence properties of defects in GaN," J. Appl. Phys. **97**, 061301 (2005).

[101]E. Zdanowicz, D. Iida, L. Pawlaczyk, J. Serafinczuk, R. Szukiewicz, R. Kudrawiec, D. Hommel, and K. Ohkawa, "Boron influence on bandgap and photoluminescence in BGaN grown on AlN," J. Appl. Phys. **127**, 165703 (2020).

[102]T. Takano, M. Kurimoto, J. Yamamoto, and H. Kawanishi, "Epitaxial growth of high quality BAlGaN quaternary lattice matched to AlN on 6H–SiC substrate by LP-MOVPE for deep-UV emission," J. Cryst. Growth **237–239**, 972–977 (2002).

[103]K. M. Yu, W. Walukiewicz, J. Wu, J. W. Beeman, J. W. Ager III, E. E. Haller, W. Shan, H. P. Xin, C. W. Tu, and M. C. Ridgway, "Formation of diluted III–V nitride thin films by N ion implantation," J. Appl. Phys. **90**, 2227 (2001).

[104]K. M. Yu, M. A. Scarpulla, R. Farshchi, O. D. Dubon, and W. Walukiewicz, "Synthesis of highly mismatched alloys using ion implantation and pulsed laser melting," Nucl. Instrum. Methods Phys. Res. B **261**, 1150–1154 (2007).

[105]K. Gao, S. Prucnal, W. Skorupa, M. Helm, and S. Zhou, "Formation and photoluminescence of $GaAs_{1-x}N_x$ dilute nitride achieved by N-implantation and flash lamp annealing," Appl. Phys. Lett. **105**, 012107 (2014).

[106]*Dilute Nitride Semiconductors*, edited by M. Henini (Elsevier Ltd., 2005).

[107]D. J. Friedman, J. F. Geisz, S. R. Kurtz, and J. M. Olson, "1-eV solar cells with GaInNAs active layer," J. Cryst. Growth **195**, 409–415 (1998).

[108]M. Fischer, M. Reinhardt, and A. Forchel, "GaInAsN/GaAs laser diodes operating at 1.52 μm," Electron. Lett. **36**, 1208–1209 (2000).

[109]N. Tansu, N. J. Kirsch, and L. J. Mawst, "Low-threshold-current-density 1300-nm dilute-nitride quantum well lasers," Appl. Phys. Lett. **81**, 2523 (2002).

[110]J. S. Harris, Jr., "GaInNAs long-wavelength lasers: Progress and challenges," Semicond. Sci. Technol. **17**, 880–891 (2002).

[111]D. B. Jackrel, S. R. Bank, H. B. Yuen, M. A. Wistey, J. S. Harris, A. J. Ptak, S. W. Johnston, D. J. Friedman, and S. R. Kurtz, "Dilute nitride GaInNAs and GaInNAsSb solar cells by molecular beam epitaxy," J. Appl. Phys. **101**, 114916 (2007).

[112]S. R. Bank, H. Bae, L. L. Goddard, H. B. Yuen, M. A. Wistey, R. Kudrawiec, and J. S. Harris, "Recent progress on 1.55-μm dilute-nitride lasers," IEEE J. Quantum Electron. **43**, 773 (2007).

[113]J. S. Harris, Jr., R. Kudrawiec, H. B. Yuen, S. R. Bank, H. P. Bae, M. A. Wistey, D. Jackrel, E. R. Pickett, T. Sarmiento, L. L. Goddard, V. Lordi, and T. Gugov, "Development of GaInNAsSb alloys: Growth, band structure, optical properties and applications," Phys. Status Solidi B **244**, 2707–2729 (2007).

[114]V.-M. Korpijärvi, M. Guina, J. Puustinen, P. Tuomisto, J. Rautiainen, A. Härkönen, A. Tukiainen, O. Okhotnikov, and M. Pessa, "MBE grown GaInNAs-based multi-Watt disk lasers," J. Cryst. Growth **311**, 1868–1871 (2009).

[115]S. Chen, M. Jansson, J. E. Stehr, Y. Huang, F. Ishikawa, W. M. Chen, and I. A. Buyanova, "Dilute nitride nanowire lasers based on a GaAs/GaNAs core/shell structure," Nano Lett. **17**, 1775–1781 (2017).

[116]A. Aho, R. Isoaho, A. Tukiainen, G. Gori, R. Campesato, and M. Guina, "Dilute nitride triple junction solar cells for space applications: Progress towards highest AM0 efficiency," Prog. Photovoltaics **26**, 740–744 (2018).

[117]S. G. Spruytte, C. W. Coldren, J. S. Harris, W. Wampler, P. Krispin, K. Ploog, and M. C. Larson, "Incorporation of nitrogen in nitride arsenides: Origin of improved luminescence efficiency after anneal," J. Appl. Phys. **89**, 4401 (2001).

[118]P. Ciechanowicz, S. Gorantla, E. Zdanowicz, J.-G. Rousset, D. Hlushchenko, K. Adamczyk, D. Majchrzak, R. Kudrawiec, and D. Hommel, "As-induced growth of dodecagonal GaN microrods with stable *a*-planes walls," Adv. Opt. Mater. (to be published).

[119]S. V. Novikov, C. R. Staddon, A. V. Akimov, R. P. Campion, N. Zainal, A. J. Kent, C. T. Foxon, C. H. Chen, K. M. Yu, and W. Walukiewicz, "Molecular beam epitaxy of crystalline and amorphous GaN layers with high As content," J. Cryst. Growth **311**, 3417–3422 (2009).

[120]S. V. Novikov, C. R. Staddon, C. T. Foxon, K. M. Yu, R. Broesler, M. Hawkridge, Z. Liliental-Weber, W. Walukiewicz, J. Denlinger, and I. Demchenko, "Molecular beam epitaxy of GaNAs alloys with high As content for potential photoanode applications in hydrogen production," J. Vac. Sci. Technol., B **28**, C3B12 (2010).

[121]K. M. Yu, S. V. Novikov, R. Broesler, I. N. Demchenko, J. D. Denlinger, Z. Liliental-Weber, F. Luckert, R. W. Martin, W. Walukiewicz, and C. T. Foxon, "Highly mismatched crystalline and amorphous $GaN_{1-x}As_x$ alloys in the whole composition range," J. Appl. Phys. **106**, 103709 (2009).

[122]K. M. Yu, S. V. Novikov, R. Broesler, Z. Liliental-Weber, A. X. Levander, V. M. Kao, O. D. Dubon, J. Wu, W. Walukiewicz, and C. T. Foxon, "Low gap amorphous $GaN_{1-x}As_x$ alloys grown on glass substrate," Appl. Phys. Lett. **97**, 101906 (2010).

[123]S. V. Novikov, C. R. Staddon, C. T. Foxon, K. M. Yu, R. Broesler, M. Hawkridge, Z. Liliental-Weber, J. Denlinger, I. Demchenko, F. Luckert, P. R. Edwards, R. W. Martin, and W. Walukiewicz, "Growth by molecular beam epitaxy of amorphous and crystalline GaNAs alloys with band gaps from 3.4 to 0.8 eV for solar energy conversion devices," J. Cryst. Growth **323**, 60–63 (2011).

[124]S. V. Novikov, K. M. Yu, A. Levander, D. Detert, W. L. Sarney, Z. Liliental-Weber, M. Shaw, R. W. Martin, S. P. Svensson, W. Walukiewicz, and C. T. Foxon, "Molecular beam epitaxy of highly mismatched N-rich $GaN_{1-x}Sb_x$ and $InN_{1-x}As_x$ alloys," J. Vac. Sci. Technol., B **31**, 03C102 (2013).

[125]K. M. Yu, W. L. Sarney, S. V. Novikov, D. Detert, R. Zhao, J. D. Denlinger, S. P. Svensson, O. D. Dubon, W. Walukiewicz, and C. T. Foxon, "Highly mismatched N-rich $GaN_{1-x}Sb_x$ films grown by low temperature molecular beam epitaxy," Appl. Phys. Lett. **102**, 102104 (2013).

[126]W. L. Sarney, S. P. Svensson, S. V. Novikov, K. M. Yu, W. Walukiewicz, and C. T. Foxon, "$GaN_{1-x}Sb_x$ highly mismatched alloys grown by low temperature molecular beam epitaxy under Ga-rich conditions," J. Cryst. Growth **383**, 95–99 (2013).

[127]K. M. Yu, S. V. Novikov, M. Ting, W. L. Sarney, S. P. Svensson, M. Shaw, R. W. Martin, W. Walukiewicz, and C. T. Foxon, "Growth and characterization of highly mismatched $GaN_{1-x}Sb_x$ alloys," J. Appl. Phys. **116**, 123704 (2014).

[128]N. Segercrantz, K. M. Yu, M. Ting, W. L. Sarney, S. P. Svensson, S. V. Novikov, C. T. Foxon, and W. Walukiewicz, "Electronic band structure of highly mismatched $GaN_{1-x}Sb_x$ alloys in a broad composition range," Appl. Phys. Lett. **107**, 142104 (2015).

[129]W. L. Sarney, S. P. Svensson, M. Ting, N. Segercrantz, W. Walukiewicz, K. M. Yu, R. W. Martin, S. V. Novikov, and C. T. Foxon, "Intermixing studies in $GaN_{1-x}Sb_x$ highly mismatched alloys," Appl. Opt. **56**, B64–B69 (2017).

[130]A. X. Levander, K. M. Yu, S. V. Novikov, A. Tseng, C. T. Foxon, O. D. Dubon, J. Wu, and W. Walukiewicz, "$GaN_{1-x}Bi_x$: Extremely mismatched semiconductor alloys," Appl. Phys. Lett. **97**, 141919 (2010).

[131]S. V. Novikov, K. M. Yu, A. X. Levander, Z. Liliental-Weber, R. dos Reis, A. J. Kent, A. Tseng, O. D. Dubon, J. Wu, J. Denlinger, W. Walukiewicz, F. Luckert, P. R. Edwards, R. W. Martin, and C. T. Foxon, "Molecular beam epitaxy of $GaN_{1-x}Bi_x$ alloys with high bismuth content," Phys. Status Solidi A **209**, 419–423 (2012).

[132]W. Shan, W. Walukiewicz, J. W. Ager, E. E. Haller, J. F. Geisz, D. J. Friedman, J. M. Olson, and S. R. Kurtz, "Band anticrossing in GaInNAs alloys," Phys. Rev. Lett. **82**, 1221 (1999).

[133]J. Wu, W. Shan, and W. Walukiewicz, "Band anticrossing in highly mismatched III–V semiconductor alloys," Semicond. Sci. Technol. **17**, 860 (2002).

[134]K. M. Yu, W. Walukiewicz, J. Wu, J. W. Beeman, J. W. Ager III, and E. E. Haller, "Band anticrossing in group II-O_xVI_{1-x} highly mismatched alloys: $Cd_{1-x}Mn_yO_xTe_{1-x}$ quaternaries synthesized by O ion implantation," Appl. Phys. Lett. **80**, 1571 (2002).

[135]K. M. Yu, W. Walukiewicz, J. Wu, W. Shan, J. W. Beeman, M. A. Scarpulla, O. D. Dubon, and P. Becla, "Diluted II–VI oxide semiconductors with multiple band gaps," Phys. Rev. Lett. **91**, 246403 (2003).

[136]M. Welna, R. Kudrawiec, Y. Nabetani, and W. Walukiewicz, "Band anticrossing in ZnOSe highly mismatched alloy," Appl. Phys. Express **7**, 071202 (2014).

[137]M. Wełna, R. Kudrawiec, Y. Nabetani, T. Tanaka, M. Jaquez, O. D. Dubon, K. M. Yu, and W. Walukiewicz, "Effects of a semiconductor matrix on the band anticrossing in dilute group II-VI oxides," Semicond. Sci. Technol. **30**, 085018 (2015).

[138]M. Ting, R. dos Reis, M. Jaquez, O. D. Dubon, S. S. Mao, K. M. Yu, and W. Walukiewicz, "Electronic band structure of ZnO-rich highly mismatched $ZnO_{1-x}Te_x$ alloys," Appl. Phys. Lett. **106**, 092101 (2015).

[139]M. Welna, M. Baranowski, W. M. Linhart, R. Kudrawiec, K. M. Yu, M. Mayer, and W. Walukiewicz, "Multicolor emission from intermediate band semiconductor $ZnO_{1-x}Se_x$," Sci. Rep. **7**, 44214 (2017).

[140]J. Wu, W. Walukiewicz, K. M. Yu, J. D. Denlinger, W. Shan, J. W. Ager III, A. Kimura, H. F. Tang, and T. F. Kuech, "Valence band hybridization in N-rich $GaN_{1-x}As_x$ alloys," Phys. Rev. B **70**, 115214 (2004).

[141]C.-K. Tan, D. Borovac, W. Sun, and N. Tansu, "InGaN/Dilute-As GaNAs interface quantum well for red emitters," Sci. Rep. **6**, 19271 (2016).

[142]J. C. Goodrich, D. Borovac, C.-K. Tan, and N. Tansu, "Band anti-crossing model in dilute-As GaNAs alloys," Sci. Rep. **9**, 5128 (2019).

[143]K. Alberi, J. Wu, W. Walukiewicz, K. M. Yu, O. D. Dubon, S. P. Watkins, C. X. Wang, X. Liu, Y.-J. Cho, and J. Furdyna, "Valence-band anticrossing in mismatched III-V semiconductor alloys," Phys. Rev. B **75**, 045203 (2007).

[144]M. Gladysiewicz, R. Kudrawiec, and M. S. Wartak, "8-band and 14-band kp modeling of electronic band structure and material gain in Ga(In)AsBi quantum wells grown on GaAs and InP substrates," J. Appl. Phys. **118**, 055702 (2015).

[145]K. M. Yu, W. L. Sarney, S. V. Novikov, N. Segercrantz, M. Ting, M. Shaw, S. P. Svensson, R. W. Martin, W. Walukiewicz, and C. T. Foxon, "Highly mismatched $GaN_{1-x}Sb_x$ alloys: Synthesis, structure and electronic properties," Semicond. Sci. Technol. **31**, 083001 (2016).

[146]K. Iwata, H. Asahi, K. Asami, and S. Gonda, "Gas source molecular beam epitaxial growth of $GaN_{1-x}P_x$($x \lesssim 0.015$) using ion-removed electron cyclotron resonance radical cell," Jpn. J. Appl. Phys., Part II **35**, L1634 (1996).

[147]K. Iwata, H. Asahi, K. Asami, and S. Gonda, "Gas source MBE growth of GaN rich side of $GaN_{1-x}P_x$, using ion-removed ECR radical cell," J. Cryst. Growth **175–176**, 150–155 (1997).

[148]R. Kuroiwa, H. Asahi, K. Asami, S.-J. Kim, K. Iwata, and S. Gonda, "Optical properties of GaN-rich side of GaNP and GaNAs alloys grown by gas-source molecular beam epitaxy," Appl. Phys. Lett. **73**, 2630 (1998).

[149]T.-Y. Seong, I.-T. Bae, C.-J. Choi, D. Y. Noh, Y. Zhao, and C. W. Tu, "Microstructures of $GaN_{1-x}P_x$ layers grown on (0001) GaN substrates by gas source molecular beam epitaxy," J. Appl. Phys. **85**, 3192 (1999).

[150]H. Asahi, H. Tampo, H. Hiroki, K. Asami, and S. Gonda, "Gas source MBE growth of GaN-related novel semiconductors," Mater. Sci. Eng. B **75**, 199–203 (2000).

[151]J. Kikawa, S. Yoshida, and Y. Itoh, "Hexagonal $GaN_{1-x}P_x$ growth by laser-assisted metalorganic chemical vapor deposition," J. Cryst. Growth **229**, 48–52 (2001).

[152]S. Yoshida, J. Kikawa, and Y. Itoh, "Crystal growth of nitride-rich GaNP by laser-assisted metalorganic chemical-vapor deposition," J. Cryst. Growth **237–239**, 1037–1041 (2002).

[153]D. J. Chen, B. Shen, Z. X. Bi, K. X. Zhang, S. L. Gu, R. Zhang, Y. Shi, Y. D. Zheng, X. H. Sun, S. K. Wan, and Z. G. Wang, "$GaN_{1-x}P_x$ ternary alloys with high P composition grown by metal-organic chemical vapor deposition," J. Cryst. Growth **255**, 52–56 (2003).

[154]Y. Tsuda, H. Mouri, M. Araki, Y. Ueta, T. Yuasa, and M. Taneya, "Characterization of the GaN-rich side of GaNP grown by metal-organic chemical vapor deposition," Phys. Status Solidi B **240**, 404–407 (2003).

[155]D. J. Chen, B. Shen, Z. X. Bi, K. X. Zhang, S. L. Gu, R. Zhang, Y. Shi, and Y. D. Zheng, "Characterization of $GaN_{1-x}P_x$ alloys grown by metal-organic chemical vapor deposition," Opt. Mater. **23**, 127–132 (2003).

[156]H. D. Li, M. Tsukihara, Y. Naoi, Y. B. Lee, and S. Sakai, "Investigations of V-shaped defects and photoluminescence of thin GaN-rich GaNP layers grown on a GaN epilayer by metalorganic chemical vapor deposition," Appl. Phys. Lett. **84**, 1886 (2004).

[157]L.-W. Lu, T.-J. Chen, B. Shen, J.-N. Wang, and W.-K. Ge, "Optical properties of phase-separated $GaN_{1-x}P_x$ alloys grown by light-radiation heating metal-organic chemical vapour deposition," Chin. Phys. Lett. **22**, 2081 (2005).

[158]D. J. Chen, B. Shen, Z. X. Bi, K. X. Zhang, S. L. Gu, R. Zhang, Y. Shi, Y. D. Zheng, X. H. Sun, S. K. Wan, and Z. G. Wang, "Phase-separation suppression in GaN-rich side of GaNP alloys grown by metal–organic chemical vapor deposition," Appl. Phys. A **80**, 141–144 (2005).

[159]K. Fehse, A. Dadgar, P. Veit, J. Bläsing, and A. Krost, "Metalorganic chemical vapor phase epitaxy and structural properties of $Ga_{1-x}P_xN$ on GaN/Si(111) substrates," Appl. Phys. A **82**, 733–735 (2006).

[160]O. Igarashi and Y. Okada, "Epitaxial growth of $GaN_{1-x}P_x$ ($x \lesssim 0.04$) on sapphire substrates," Jpn. J. Appl. Phys., Part II **24**, L792 (1985).

[161]O. Igarashi, "Heteroepitaxial growth of $GaN_{1-x}P_x$ ($x \lesssim 0.06$) on sapphire substrates," Jpn. J. Appl. Phys., Part I **27**, 790 (1988).

[162]O. Igarashi, "Heteroepitaxial growth of $GaN_{1-x}P_x$ ($x \lesssim 0.09$) on sapphire substrates," Jpn. J. Appl. Phys., Part I **31**, 3791 (1992).

[163]X. S. Wu, Z. Y. Zhai, Y. H. Fan, D. J. Chen, B. Shen, R. Zhang, Y. D. Zheng, and S. S. Jiang, "The solubility of phosphorus in GaN," Appl. Surf. Sci. **250**, 182–187 (2005).

[164]M. P. Polak, M. J. Winiarski, K. Wittek, and P. Scharoch, "Elastic properties and the band gap of semiconductor alloy: A comparative study of various ab initio approaches," Adv. Mater. Sci. Eng. **2016**, 1429023.

[165]D. Borovac, C.-K. Tan, and N. Tansu, "First-principle study of the optical properties of dilute-P $GaN_{1-x}P_x$ alloys," Sci. Rep. **8**, 6025 (2018).

[166]K. Iwata, H. Asahi, K. Asami, R. Kuroiwa, and S. Gonda, "GaN-rich side of GaNAs grown by gas source molecular beam epitaxy," Jpn. J. Appl. Phys., Part I **37**, 1436–1439 (1998).

[167]Y. Zhao, F. Deng, S. S. Lau, and C. W. Tu, "Effects of arsenic in gas-source molecular beam epitaxy," J. Vac. Sci. Technol., B **16**, 1297 (1998).

[168]C. T. Foxon, S. V. Novikov, T. S. Cheng, C. S. Davis, R. P. Campion, A. J. Winser, and I. Harrison, "Arsenic-doped GaN grown by molecular beam epitaxy," J. Cryst. Growth **219**, 327–334 (2000).
[169]A. J. Winser, S. V. Novikov, C. S. Davis, T. S. Cheng, C. T. Foxon, and I. Harrison, "Strong blue emission from As doped GaN grown by molecular beam epitaxy," Appl. Phys. Lett. **77**, 2506 (2000).
[170]S. V. Novikov, A. J. Winser, A. Bell, I. Harrison, T. Lia, R. P. Campion, C. R. Staddon, C. S. Davis, F. A. Ponce, and C. T. Foxon, "The transition from As-doped GaN, showing blue emission, to GaNAs alloys in films grown by molecular beam epitaxy," J. Cryst. Growth **240**, 423–430 (2002).
[171]C. T. Foxon, S. V. Novikov, T. Li, R. P. Campion, C. S. Davis, A. J. Winser, I. Harrison, and Y. Liao, "Strong blue emission from GaN isoelectronically doped with arsenic," Mater. Sci. Eng., B **93**, 35–38 (2002).
[172]C. T. Foxon, S. V. Novikov, T. Li, R. P. Campion, A. J. Winser, I. Harrison, M. J. Kappers, and C. J. Humphreys, "Arsenic incorporation in GaN during growth by molecular beam epitaxy," J. Cryst. Growth **251**, 510–514 (2003).
[173]E. Zdanowicz, P. Ciechanowicz, K. Opolczynska, D. Majchrzak, J.-G. Rousset, E. Piskorska-Hommel, M. Grodzicki, K. Komorowska, J. Serafinczuk, D. Hommel, and R. Kudrawiec, "As-related stability of the band gap temperature dependence in N-rich GaNAs," Appl. Phys. Lett. **115**, 092106 (2019).
[174]H. J. Kim, T. G. Andersson, J.-M. Chauveau, and A. Trampert, "Arsenic incorporation and its influence on microstructure of wurtzite GaN grown by molecular-beam epitaxy," J. Appl. Phys. **94**, 7193 (2003).
[175]H. Na, H. Jin Kim, E. Yoon, C. Sone, and Y. Park, "Arsenic incorporation and growth mode of GaNAs grown by low-pressure metal-organic chemical vapor deposition," J. Cryst. Growth **248**, 437–440 (2003).
[176]A. Kimura, H. F. Tang, and T. F. Kuech, "Growth of GaNAs alloys on the N-rich side with high As content by metalorganic vapor phase epitaxy," J. Cryst. Growth **265**, 71–77 (2004).
[177]A. Kimura, C. A. Paulson, H. F. Tang, and T. F. Kuech, "Epitaxial layers with high As content grown by metalorganic vapor phase epitaxy and their band gap energy," Appl. Phys. Lett. **84**, 1489 (2004).
[178]H. Na, H. J. Kim, S.-Y. Kwon, C. Sone, Y. Park, and E. Yoon, "The formation of cubic GaNAs phase during the growth of thin GaNAs epilayers on GaN at low temperatures by metalorganic chemical vapor deposition," Phys. Status Solidi C **1**, 2462–2465 (2004).
[179]H. Na, "Arsenic incorporation in GaN layers grown by metalorganic chemical vapor deposition," J. Cryst. Growth **312**, 2019–2024 (2010).
[180]C.-K. Tan and N. Tansu, "First-principle natural band alignment of GaN/dilute-As GaNAs alloy," AIP Adv. **5**, 017129 (2015).
[181]C.-K. Tan, D. Borovac, W. Sun, and N. Tansu, "Dilute-As AlNAs alloy for deep-ultraviolet emitter," Sci. Rep. **6**, 22215 (2016).
[182]A. X. Levander, S. V. Novikov, Z. Liliental-Weber, R. dos Reis, O. D. Dubon, J. Wu, C. T. Foxon, K. M. Yu, and W. Walukiewicz, "Doping of $GaN_{1-x}As_x$ with high As content," J. Appl. Phys. **110**, 093702 (2011).
[183]A. X. Levander, Z. Liliental-Weber, R. Broesler, M. E. Hawkridge, S. V. Novikov, C. T. Foxon, O. D. Dubon, J. Wu, W. Walukiewicz, and K. M. Yu, "Thermal stability of amorphous $GaN_{1-x}As_x$ alloys," Appl. Phys. Lett. **98**, 161902 (2011).
[184]Z. Liliental-Weber, R. dos Reis, S. V. Novikov, K. M. Yu, A. X. Levander, O. D. Dubon, J. Wu, W. Walukiewicz, and C. T. Foxon, "Microstructure of Mg doped GaNAs alloys," Phys. Status Solidi C **10**, 453–456 (2013).
[185]A. X. Levander, K. M. Yu, S. V. Novikov, Z. Liliental-Weber, C. T. Foxon, O. D. Dubon, J. Wu, and W. Walukiewicz, "Local structure of amorphous $GaN_{1-x}As_x$ semiconductor alloys across the composition range," J. Appl. Phys. **113**, 243505 (2013).
[186]S. V. Novikov, M. Ting, K. M. Yu, W. L. Sarney, R. W. Martin, S. P. Svensson, W. Walukiewicz, and C. T. Foxon, "Tellurium n-type doping of highly mismatched amorphous $GaN_{1-x}As_x$ alloys in plasma-assisted molecular beam epitaxy," J. Cryst. Growth **404**, 9–13 (2014).
[187]H. Qian, K. B. Lee, S. Hosseini Vajargah, S. V. Novikov, I. Guiney, S. Zhang, Z. H. Zaidi, S. Jiang, D. J. Wallis, C. T. Foxon, C. J. Humphreys, and P. A. Houston, "Characterization of p-$GaN_{1-x}As_x$/n-GaN PN junction diodes," Semicond. Sci. Technol. **31**, 065020 (2016).
[188]C. W. Pei, B. Turk, J. B. Héroux, and W. I. Wang, "GaN grown by molecular beam epitaxy with antimony as surfactant," J. Vac. Sci. Technol., B **19**, 1426 (2001).
[189]L. Zhang, H. F. Tang, and T. F. Kuech, "Effect of Sb as a surfactant during the lateral epitaxial overgrowth of GaN by metalorganic vapor phase epitaxy," Appl. Phys. Lett. **79**, 3059 (2001).
[190]L. Zhang, H. F. Tang, J. Schieke, M. Mavrikakis, and T. F. Kuech, "The addition of Sb as a surfactant to GaN growth by metal organic vapor phase epitaxy," J. Appl. Phys. **92**, 2304 (2002).
[191]A. Kimura, Z. Liu, and T. F. Kuech, "Antimony as a surfactant during the growth of GaN-based GaNAs alloys by metal organic vapor-phase epitaxy," J. Cryst. Growth **272**, 432–437 (2004).
[192]H. Koch, I. Pietzonka, B. Galler, M. Strassburg, H. Kalisch, A. Vescan, and H.-J. Lugauera, "Effect of antimony on growth mode and properties of thick InGaN layers," J. Cryst. Growth **414**, 42–48 (2015).
[193]J. L. Merrell, F. Liu, and G. B. Stringfellow, "Effect of surfactant Sb on In incorporation and thin film morphology of InGaN layers grown by organometallic vapor phase epitaxy," J. Cryst. Growth **375**, 90–94 (2013).
[194]K. G. Sadasivam, J. I. Shim, and J. K. Lee, "Antimony surfactant effect on green emission InGaN/GaN multi quantum wells grown by MOCVD," J. Nanosci. Nanotechnol. **11**, 1787–1790 (2011).
[195]M. Baranowski, M. Latkowska, R. Kudrawiec, M. Syperek, J. Misiewicz, K. Giri Sadasivam, J. Shim, and J. K. Lee, "Time-resolved photoluminescence studies of the optical quality of InGaN/GaN multi-quantum well grown by MOCVD—Antimony surfactant effect," Semicond. Sci. Technol. **27**, 105027 (2012).
[196]X. Yang, J. B. Heroux, M. J. Jurkovic, and W. I. Wang, "High-temperature characteristics of 1.3 μm InGaAsN:Sb/GaAs multiple-quantum-well lasers grown by molecular-beam epitaxy," Appl. Phys. Lett. **76**, 795 (2000).
[197]R. Kudrawiec, M. Gladysiewicz, J. Misiewicz, H. B. Yuen, S. R. Bank, M. A. Wistey, H. P. Bae, and J. S. Harris, Jr., "Interband transitions in $GaN_{0.02}As_{0.98-x}Sb_x$/GaAs ($0<x\leqslant 0.11$) single quantum wells studied by contactless electroreflectance spectroscopy," Phys. Rev. B **73**, 245413 (2006).
[198]R. Kudrawiec, M. Motyka, M. Gladysiewicz, J. Misiewicz, H. B. Yuen, S. R. Bank, H. Bae, M. A. Wistey, and J. S. Harris, "Band gap discontinuity in $Ga_{0.9}In_{0.1}N_{0.027}As_{0.973-x}Sb_x$/GaAs single quantum wells with $0\leqslant x<0.06$ studied by contactless electroreflectance spectroscopy," Appl. Phys. Lett. **88**, 221113 (2006).
[199]M. Shaw, K. M. Yu, M. Ting, R. E. L. Powell, W. L. Sarney, S. P. Svensson, A. J. Kent, W. Walukiewicz, C. T. Foxon, and S. V. Novikov, "Composition and optical properties of dilute-Sb $GaN_{1-x}Sb_x$ highly mismatched alloys grown by MBE," J. Phys. D **47**, 465102 (2014).
[200]W. L. Sarney, S. P. Svensson, S. V. Novikov, K. M. Yu, W. Walukiewicz, M. Ting, and C. T. Foxon, "Exploration of the growth parameter space for MBE-grown $GaN_{1-x}Sb_x$ highly mismatched alloys," J. Cryst. Growth **425**, 255–257 (2015).
[201]N. Segercrantz, Y. Baumgartner, M. Ting, K. M. Yu, S. S. Mao, W. L. Sarney, S. P. Svensson, and W. Walukiewicz, "Undoped p-type $GaN_{1-x}Sb_x$ alloys: Effects of annealing," Appl. Phys. Lett. **109**, 252102 (2016).
[202]F. A. Chowdhury, S. M. Sadaf, Q. Shi, Y.-C. Chen, H. Guo, and Z. Mi, "Optically active dilute-antimonide III-nitride nanostructures for optoelectronic devices," Appl. Phys. Lett. **111**, 061101 (2017).
[203]F. A. Chowdhury and Z. Mi, "Probing the large bandgap-bowing and signature of antimony (Sb) in dilute antimonide III-nitride using micro-Raman scattering," J. Appl. Phys. **126**, 085704 (2019).
[204]S.-H. Moon, H.-A. Do, J. Park, and S.-W. Ryu, "Strong below-band gap absorption of N-rich side GaNSb by metal-organic chemical vapor deposition," J. Mater. Res. **24**, 3569 (2009).
[205]S. Sunkara, V. K. Vendra, J. B. Jasinski, T. Deutsch, A. N. Andriotis, K. Rajan, M. Menon, and M. Sunkara, "New visible light absorbing materials for solar fuels $Ga(Sb_x)N_{1-x}$," Adv. Mater. **26**, 2878–2882 (2014).
[206]D. Komori, K. Takarabe, T. Takeuchi, T. Miyajima, S. Kamiyama, M. Iwaya, and I. Akasaki, "GaNSb alloys grown with H_2 and N_2 carrier gases," Jpn. J. Appl. Phys., Part I **55**, 05FD01 (2016).
[207]A. Belabbes, M. Ferhat, and A. Zaoui, "Giant and composition-dependent optical band gap bowing in dilute alloys," Appl. Phys. Lett. **88**, 152109 (2006).
[208]R. M. Sheetz, E. Richter, A. N. Andriotis, S. Lisenkov, C. Pendyala, M. K. Sunkara, and M. Menon, "Visible-light absorption and large band-gap bowing of $GaN_{1-x}Sb_x$ from first principles," Phys. Rev. B **84**, 075304 (2011).

[209]Q. Shi, Y. Ch. Chen, F. A. Chowdhury, Z. Mi, V. Michaud-Rioux, and H. Guo, "Band engineering of GaSbN alloy for solar fuel applications," Phys. Rev. Mater. **1**, 034602 (2017).
[210]B. Amrani, H. Achour, S. Louhibi, A. Tebboune, and N. Sekkal, "First principles study of AlBi," Solid State Commun. **148**, 59–62 (2008).
[211]A. Janotti, S.-H. Wei, and S. B. Zhang, "Theoretical study of the effects of isovalent coalloying of Bi and N in GaAs," Phys. Rev. B **65**, 115203 (2002).
[212]G. R. Pandya and S. M. Vyas, "Characteristic growth features and etching of InBi single crystals," Cryst. Res. Technol. **28**, 163 (1993).
[213]K. Nishimura, T. Yasukawa, and K. Mori, "Transport properties of In_2Bi and InBi single crystals," Phys. B **329–333**, 1399–1400 (2003).
[214]M. P. Polak, P. Scharoch, and R. Kudrawiec, "First-principles calculations of bismuth induced changes in the band structure of dilute Ga–V–Bi and In–V–Bi alloys: Chemical trends versus experimental data," Semicond. Sci. Technol. **30**, 094001 (2015).
[215]J. Kopaczek, W. M. Linhart, M. Baranowski, R. D. Richards, F. Bastiman, J. P. R. David, and R. Kudrawiec, "Optical properties of GaAsBi/GaAs quantum wells: Photoreflectance, photoluminescence and time-resolved photoluminescence study," Semicond. Sci. Technol. **30**, 094005 (2015).
[216]L. Wang, L. Zhang, L. Yue, D. Liang, X. Chen, Y. Li, P. Lu, J. Shao, and S. Wang, "Novel dilute bismide, epitaxy, physical propertiesand device application," Crystals **7**, 63 (2017).
[217]R. Kudrawiec, J. Kopaczek, O. Delorme, M. P. Polak, M. Gladysiewicz, E. Luna, L. Cerutti, E. Tournié, and J. B. Rodriguez, "Type I $GaSb_{1-x}Bi_x$/GaSb quantum wells dedicated for mid infrared laser applications: Photoreflectance studies of bandgap alignment," J. Appl. Phys. **125**, 205706 (2019).
[218]S. Wang and P. Lu, *Bismuth-Containing Alloys and Nanostructures* (Springer Nature Singapore Pte Ltd., 2019).
[219]A. X. Levander, S. V. Novikov, Z. Liliental-Weber, R. dos Reis, J. D. Denlinger, J. Wu, O. D. Dubon, C. T. Foxon, K. M. Yu, and W. Walukiewicz, "Growth and transport properties of p-type GaNBi alloys," J. Mater. Res. **26**, 2887 (2011).
[220]Z. Liliental-Weber, R. Dos Reis, A. X. Levander, K. M. Yu, W. Walukiewicz, S. V. Novikov, and C. T. Foxon, "Microstructure of $GaN_{1-x}Bi_x$," J. Electron. Mater. **42**, 26–32 (2013).
[221]C. T. Foxon, S. V. Novikov, T. Li, R. P. Campion, A. J. Winser, and I. Harrison, "Bismuth a new surfactant or contact for GaN films grown by molecular beam epitaxy," Phys. Status Solidi A **192**, 441–445 (2002).
[222]S. V. Novikov, A. J. Winser, T. Li, R. Campion, I. Harrison, and C. T. Foxon, "Bismuth a new dopant for GaN films grown by molecular beam epitaxy—Surfactant effects, formation of $GaN_{1-x}Bi_x$ alloys and co-doping with arsenic," J. Cryst. Growth **247**, 35–41 (2003).
[223]J. Ibáñez, D. Pastor, R. Cuscó, L. Artús, M. Avella, J. Jiménez, S. V. Novikov, and C. T. Foxon, "Optical characterisation of Bi-doped GaN films grown by molecular beam epitaxy," Phys. Status Solidi A **202**, 850–853 (2005).
[224]L. Zhang, H. F. Tang, J. Schieke, M. Mavrikakis, and T. F. Kuech, "Influence of Bi impurity as a surfactant during the growth of GaN by metalorganic vapor phase epitaxy," J. Cryst. Growth **242**, 302–308 (2002).
[225]C. Saidi, N. Chaaben, J. Laifi, T. Sekrafi, O. Tottereau, A. Bchetnia, and B. E. Jania, "Effect of TMBi supply on low-temperature MOVPE growth behavior of GaN," J. Alloys Compd. **625**, 271–276 (2015).
[226]F. Bernardini, G. Profeta, and A. Continenza, "Bi incorporation in GaN and $Al_xGa_{1-x}N$ alloys," Phys. Rev. B **68**, 195205 (2003).
[227]A. Belabbes, A. Zaoui, S. Laref, and M. Ferhat, "Imposing changes of band and spin–orbit gaps in GaNBi," Solid State Commun. **152**, 1700–1702 (2012).
[228]M. Mbarki and A. Rebey, "First principles calculations of structural and electronic properties of $GaN_{1-x}Bi_x$ alloys," J. Alloys Compd. **530**, 36–39 (2012).
[229]R. Alaya, M. Mbarki, and A. Rebey, "First principles calculations of structure parameters and transition pressures of $GaN_{1-x}Bi_x$ alloys," Semiconductor **49**, 279–284 (2015).
[230]C. G. Van de Walle and J. Neugebauer, "Universal alignment of hydrogen levels in semiconductors, insulators and solutions," Nature **423**, 626 (2003).
[231]V. Ravindran, M. Boucherit, A. Soltani, S. Gautier, T. Moudakir, J. Dickerson, P. L. Voss, M.-A. di Forte-Poisson, J.-C. De Jaeger, and A. Ougazzaden, "Dual-purpose BGaN layers on performance of nitride-based high electron mobility transistors," Appl. Phys. Lett. **100**, 243503 (2012).
[232]J. R. Dickerson, V. Ravindran, T. Moudakir, S. Gautier, P. L. Voss, and A. Ougazzaden, "A study of BGaN back-barriers for AlGaN/GaN HEMTs," Eur. Phys. J.: Appl. Phys. **60**, 30101 (2012).
[233]L. Guenineche and A. Hamdoune, "Influence of a BGaN back-barrier on DC and dynamic performances of an AlGaN/GaN HEMT: Simulation study," Mater. Res. Express **3**, 055003 (2016).
[234]T.-C. Han, H.-D. Zhao, and X.-C. Peng, "Short-gate AlGaN/GaN high-electron mobility transistors with BGaN buffer," Chin. Phys. B **28**, 047302 (2019).
[235]T. Han, H. Zhao, and X. Peng, "Enhancement of electrons confinement in AlGaN/AlN/GaN heterostructure using BGaN buffer with a small B-content," Superlattices Microstruct. **126**, 57–62 (2019).
[236]K. Atsumi, Y. Inoue, H. Mimura, T. Aoki, and T. Nakano, "Neutron detection using boron gallium nitride semiconductor material," APL Mater. **2**, 032106 (2014).
[237]S. Yoshida, J. Li, and Y. Itoh, "GaInNP MQW structure LED grown by laser-assisted MOCVD," Phys. Status Solidi C **0**, 2236–2239 (2003).
[238]A. J. Bard and M. A. Fox, "Artificial photosynthesis: Solar splitting of water to hydrogen and oxygen," Acc. Chem. Res. **28**, 141–145 (1995).
[239]T. Bak, J. Nowotny, M. Rekas, and C. C. Sorrell, "Photo-electrochemical hydrogen generation from water usingsolar energy. Materials-related aspects," Int. J. Hydrogen Energy **27**, 991–1022 (2002).
[240]M. Ebaid, J.-H. Kang, and S.-W. Ryu, "Controlled synthesis of GaN-based nanowires for photoelectrochemical water splitting applications," Semicond. Sci. Technol. **32**, 013001 (2017).